UNIVERSITÀ DEGLI STUDI DI PADOVA

SEDE AMMINISTRATIVA: UNIVERSITÀ DEGLI STUDI DI PADOVA

DIPARTIMENTO DI BIOLOGIA

SCUOLA DI DOTTORATO DI RICERCA IN: BIOSCIENZE E BIOTECNOLOGIE

INDIRIZZO: GENETTICA E BIOLOGIA MOLECOLARE DELLO SVILUPPO

CICLO XXV

EXPLOITING DROSOPHILA AS A MODEL SYSTEM FOR STUDYING REEP1-LINKED HSP IN VIVO

DIRETTORE DELLA SCUOLA : CH.MO PROF. GIUSEPPE ZANOTTI

COORDINATORE D'INDIRIZZO: CH.MO PROF. PAOLO BONALDO

SUPERVISORE CH.MO PROF. MARIA LUISA MOSTACCIUOLO

CO-SUPERVISORE: DOTT. GENNY ORSO

DOTTORANDO : SENTILJANA GUMENI

ABSTRACT

Hereditary Spastic Paraplegia (HSP) is a genetic group of neurodegenerative disorders characterized by progressive degeneration of corticospinal tracts. Mutations in the SPG31 gene, encoding REEP1, are the third most common cause of autosomal dominant form of HSP. Recent studies have reported that REEP1, an integral ER membrane protein, interacts with the microtubule cytoskeleton to coordinate ER shaping. However it precise molecular function is still unknown.

To better understand the function of REEP1, we generated a model (*Drosophila melanogaster*) for the *in vivo* analysis of the fly REEP1 homolog (D-REEP1). *Drosophila* and human REEP1 proteins display remarkable homology and conservation of domain organization. We analyzed D-REEP1 loss of function and gain of function transgenic lines as well as animals expressing pathological forms of the protein. Our *in vivo* data in *Drosophila* have shown a strong involvement of D-REEP1 in the regulation of lipid droplets (LDs) number and size in neuronal and non neuronal tissues. Loss of D-REEP1 results in larvae leaner and smaller than their wild type counterparts while endoplasmic reticulum membranes are elongated when compared to controls. These ER defects are associated with a decrease in lipid droplets number and low triglycerides content. On the contrary over expression of *wild type* D-REEP1 produces a reduction in the size of lipid droplets. The lack of animal models available for REEP1 studies and experimental data concerning the functional alteration caused by pathological mutations of REEP1 prompted to generate transgenic lines carrying D-REEP1 pathological mutations and to analyse the consequence of their expression in vivo. Two missense mutations (P19R, D56N) affecting the trans-membrane domains of REEP1 and a novel mutation (A132V) located in the C-terminal part of the protein have been assessed.The mutations in the trans membranes domains relocate REEP1 from the ER to the membrane of lipid droplets when expressed in mammalian cells. *In vivo* expression of Drosophila P19R caused oversized LDs in the brain and axons and increased levels of triacylgycerides.

LDs are believed to originate from the endoplasmic reticulum, although the exact molecular mechanisms of their biogenesis is still not known. Based on the findings

described above and the knowledge about REEP family, we hypothesize that REEP1 probably play an important role in membrane remodelling and possibly affects the lipid droplets metabolism. While, pathological forms of REEP1 could perturb the biogenesis and/or turnover of lipid droplets and eventually produce an imbalance in neuronal lipid metabolism.

RIASSUNTO

Le Paraplegie Spastiche Ereditarie (HSP) sono un gruppo eterogeneo di malattie neurodegenerative, caratterizzate da progressiva spasticità degli arti inferiori, e degenerazione del tratto corticospinale. Mutazioni a carico del gene SPG31, codificante per la proteina REEP1, sono la terza causa più comune di forme dominanti di HSP. Studi recenti suggeriscono che REEP1, una proteina integrale della membrana del reticolo endoplasmatico (ER), sia coinvolto nel rimodellamento delle membrane del ER attraverso l'interazione con i microtubuli del citoscheletro. Tuttavia la precisa funzione biologica e il meccanismo patologica di questa proteina sono ancora sconosciuti.

Questa tesi ha come oggetto lo studio *in vivo* della funzione di REEP1 utilizzando come organismo modello *Drosophila melanogaster*. A tale scopo abbiamo identificato l'omologo in *Drosophila* di REEP1 (D-REEP1) e generato delle linee transgeniche per la modulazione dell'espressione genica *in vivo* sia della proteina *wild type* sia di alcune sue varianti patologiche. Analisi *in vivo* suggeriscono che D-REEP1 sia coinvolto nella regolazione del numero e della dimensione dei lipid droplets (LDs) in tessuti neuronali e non neuronali.

L'assenza di D-REEP1 causa una riduzione delle dimensioni larvali e ad un allungamento delle membrane del reticolo endoplasmatico. Le alterazioni morfologiche del reticolo endoplasmatico sono associate ad una diminuzione del numero totale dei LDs e alla riduzione del contenuto dei trigliceridi. Al contrariola sovra-espressione di D-REEP1 *in vivo* induce una riduzione delle dimensioni dei LDs

La mancanza di studi su organismi modelli e dati sperimentali per valutare le possibili alterazioni funzionali causate delle mutazioni patologiche di D-REEP1, ha portato a creare delle linee transgeniche di *Drosophila* per forme mutate di D-REEP1. In tal modo si è voluto valutare gli effetti, sia *in vivo*, che *in vitro*, di due mutazioni missenso (P19R, D56N) localizzate nei domini transmembrana ed una mutazione nuova (A132V), non ancora pubblicata, localizzata nella parte C-terminale di D-REEP1. Le analisi *in vitro* hanno dimostrato che le mutazioni situate nei domini transmembrana determinano una alterata localizzazione subcellulare di REEP1. Inoltre, la

sovrespressione *in vivo* di D-REEP1-P19R determina un aumento delle dimensioni dei LDs nel sistema nervoso di *Drosophila*.

Seppure si ritiene che la biogenesi dei lipidi avviene a livello del reticolo endoplasmatico, appare tuttora sconosciuto l'esatto meccanismo molecolare coinvolto. I dati da noi ottenuti e le conoscenze attuali riguardo la famiglia delle proteine REEP suggeriscono che, agendo sulla curvatura delle membrane del ER o reclutando particolari proteine dei LDs, REEP1 sia probabilmente importante nella generazione dei lipid droplets con possibili effetti sul metabolismo lipidico.

1. INTRODUCTION

1.1 HEREDITARY SPASTIC PARAPLEGIA (HSP)

Hereditary spastic paraplegia (HSP) was first described by Strümpell in 1880 as a neurodegenerative disorder. HSP is a genetically and clinically heterogeneous group of neurodegenerative disorders with predominant feature the progressive spasticity of the lower limbs, associated with mild weakness, and in some cases by urinary urgency and subtle vibratory sense impairment (McDermott et al. 2000). The common pathological feature of these conditions is retrograde degeneration of the distal portions of the corticospinal tracts and the spinocerebellar tracts, which together constitute the longest motor and sensory axons of the central nervous system (CNS) (SCHWARZ and LIU 1956)(Behan and Maia 1974). Clinically these disorders are conventionally subdivided into "pure" (or "uncomplicated") forms, characterized by a progressive spasticity and hyperreflexia of the lower limbs, and "complicated" forms in the presence of additional neurologic or systemic impairments such as mental retardation, cerebellar ataxia, dementia, optic atrophy, retinopathy, extrapyramidal disturbance, epilepsy and motor neuropathy (Harding 1993; E Reid 1997). Age of symptom onset, rate of progression, and degree of disability are often variable between different genetic types of HSP, as well as within individual families. The prevalence of HSP in Europe is estimated at 3–10 cases per 100 000 population (McMonagle, Webb, and M Hutchinson 2002)(Silva et al. 1997). The clinical variability is complicated more by the large genetic heterogeneity. HSPs may have autosomal dominant, recessive and X-linked inheritance (Table1). To date, 52 loci have been mapped on different chromosomes. Autosomal dominant HSP represents about 70% of cases and its mostly characterized by pure forms, whereas complicated forms tend to be autosomal recessive (Harding 1993)(John K Fink 2003).

The large number of genes involved complicates the classification of this disorder. However the availability of more precise and sophisticated neuroradiological investigation techniques, biochemical tests and genetic analysis facilitate the diagnosis of familial and sporadic cases.

NAME	GENE	LOCUS	INHERITANCE	NAME	GENE	LOCUS	INHERITANCE
SPG1	L1CAM	Xq28	X-Linked	**SPG26**	SPG26	12p11.1-q14	Autosomal recessive
SPG2	PLP1	Xq22	X-Linked	**SPG27**	SPG27	10q22.1-q24.1	Autosomal recessive
SPG3A	ATL1	14q11-q21	Autosomal dominant	**SPG28**	SPG28	14q21.3-q22.3	Autosomal recessive
SPG4	SPAST	2p22-p21	Autosomal dominant	**SPG29**	SPG29	1p31.1-p21.1	Autosomal dominant
SPG5A	CYP7B1	8q21.3	Autosomal recessive	**SPG30**	KIF1A	2q37.3	Autosomal recessive
SPG5B	SPG5B	?	Autosomal recessive	**SPG31**	REEP1	2p11.2	Autosomal dominant
SPG6	NIPA1	15q11.1	Autosomal dominant	**SPG32**	SPG32	14q12-q21	Autosomal recessive
SPG7	SPG7	16q24.3	Autosomal recessive	**SPG33**	ZFYVE27	10q24.2	Autosomal dominant
SPG8	KIAA0196	8q24.13	Autosomal dominant	**SPG34**	SPG34	Xq24-q25	X-Linked
SPG9	SPG9	10q23.3-q24.1	Autosomal dominant	**SPG35**	FA2H	16q21-q23.1	Autosomal recessive
SPG10	KIF54	12q13	Autosomal dominant	**SPG36**	SPG36	12q23-q24	Autosomal dominant
SPG11	SPG11	15q21.1	Autosomal recessive	**SPG37**	SPG37	8p21.1-q13.3	Autosomal dominant
SPG12	RTN2	19q13	Autosomal dominant	**SPG38**	SPG38	4p16-p15	Autosomal dominant
SPG13	HSPD1	2q33.1	Autosomal dominant	**SPG39**	PNOLA6	19p13.2	Autosomal recessive
SPG14	SPG14	3q27-q28	Autosomal recessive	**SPG41**	SPG41	11p14.1-p11.2	Autosomal dominant
SPG15	ZFYVE26	14q24.1	Autosomal recessive	**SPG42**	SLC33A1	3q25.31	Autosomal dominant
SPG16	SPG16	Xq11.2	X-Linked	**SPG44**	GJC2	1q42.13	Autosomal recessive
SPG17	BSCL2	11q13	Autosomal dominant	**SPG45**	SPG45	10q24.3-q25.11	Autosomal recessive
SPG18	ERLIN2	8p11.23	Autosomal recessive	**SPG46**	SPG46	9p21.2-q21.12	Autosomal recessive
SPG19	SPG19	9q	Autosomal dominant	**SPG47**	AP4B1	1p13.2	Autosomal recessive
SPG20	SPG20	13q12.3	Autosomal recessive	**SPG48**	AP5Z1	7p22.1	Autosomal recessive
SPG23	SPG223	1q24-q32	Autosomal recessive	**SPG50**	AP4M1	7q22.1	Autosomal recessive
SPG24	SPG24	13q14	Autosomal recessive	**SPG51**	AP4E1	15q21.2	Autosomal recessive
SPG25	SPG25	6q23-q24.1	Autosomal recessive	**SPG52**	AP4S1	14q12	Autosomal recessive

Table 1. HSP genes

Molecular mechanisms underlying axonal degeneration are poorly understood, although the studies and analysis of HSP genes have provide insight into HSP pathogenesis. Proteins codified by genes known to predispose to HSP, have a biological role in

different cellular organelles, this supports the idea that the longest axon of NSC are particularly vulnerable to a number of distinct biochemical disturbances.

At this stage, different molecular processes appear to be involved in different genetic types of HSP:

1) Myelin composition affecting long, central nervous system axons. X-linked SPG2 HSP is due to proteolipid protein gene mutation, an intrinsic myelin protein (Dubé et al. 1997).

2) Embryonic development of corticospinal tracts. X-linked SPG1 is due to mutations in L1 cell adhesion molecule which plays a critical role in the embryonic differentiation of corticospinal tracts guidance of neurite outgrowth during development, neuronal cell migration, and neuronal cell survival (Kenwrick, Watkins, and De Angelis 2000).

3) Oxidative phosphorylation deficit. Two HSP genes (SPG7/paraplegin and SPG13/chaperonin 60) encode mitochondrial proteins (Hansen et al. 2002). Abnormal appearing mitochondria (ragged red fibers) and cytochrome C oxidase deficient fibers are noted in muscle biopsies of some (but not all) subjects with SPG7/parapegin mutation.

4) Axonal transport. SPG10 autosomal dominant HSP is due to mutations in kinesin heavy chain (KIF5A) a molecular motor that participates in the intracellular movement of organelles and macromolecules along microtubules in both anterograde and retrograde directions (Evan Reid et al. 2002).

5) Cytoskeletal disturbance. Spastin (SPG4) is a microtubule severing protein whose mutations are pathogenic through a disturbance in the axonal cytoskeleton (Errico, Ballabio, and Rugarli 2002).

6) Endoplasmic Reticulum network morphology. The three most common autosomal dominant HSPs—SPG3A, SPG4, and SPG31, as well as the less common SPG12 result from mutations in proteins directly implicated in the formation of the tubular ER network (Park et al. 2010)(Montenegro et al. 2012).

7) Lipid Synthesis and Metabolism. These latter three HSP proteins, erlin2 seipin and spartin, have been directly implicated in biogenesis of lipid droplets (Eastman, Yassaee, and Bieniasz 2009; Edwards et al. 2009; Hooper et al. 2010). Although other HSP proteins are not directly implicated in LD biogenesis are involved in related lipid and cholesterol biosynthetic pathways. SLC33A1 gene (SPG42) encodes the acetyl-CoA

transporter that transports acetyl-CoA into the Golgi apparatus lumen. SLC33A1 gene has been directly related to the growth of axons because knock down of *slc33a1* in zebrafish causes defective outgrowth from the spinal cord (Lin et al. 2008). Mutations of PNPLA2 gene (SPG39), that encodes neuropathy target esterase protein (NTE), or chemical inhibition of NTE, modifies membrane composition and causes distal degeneration of long spinal axons in mice and human (Reiter et al. 2001). The cytochrome P450-7B1 (SPG5) is involved in the metabolism of cholesterol (Tsaousidou et al. 2008). There is currently no "cure" for HSP. Treatment for HSP is limited to symptomatic reduction of muscle spasticity through muscle stretching therapy and medication for reduction of urinary urgency. Physical therapy accompanying with a regular exercise do not prevent or reverse the damage to the nerve fibers, it helps HSP patients in maintaining mobility, retaining or improving muscle strength, minimizing atrophy of the muscles due to disuse, increasing endurance (and reducing fatigue), preventing spasms and cramps, maintaining or improving range of motion and providing cardiovascular conditioning.

1.2 RECEPTOR EXPRESSION ENHANCING PROTEIN 1 (REEP1)

1.2.1 The SPG31 gene

Among the loci for pure autosomal dominant HSP (ADHSP) form, three most common genes have been identified: SPG4 on chromosome 2p22, which accounts for approximately 40% of all pure ADHSP, SPG3A on chromosome 14q11-q21, which is responsible for 10% of cases (Zhao et al. 2001) and SPG31 on chromosome 2p11.2 responsible for 6,5% of the cases (Züchner et al. 2006). Missense mutations and little insertions o deletions that cause a reading frameshift, and produce premature stop codons, are the most common SPG31 alterations. Splice site mutations and 3'-URT sequence alterations have been also reported. (Beetz et al. 2008).

The SPG31 gene consists of seven exon and four alternative splicing isoforms:

- Receptor expression enhancing protein 1 (REEP1) isoform 1, is the longest isoform (201 aa) encoded by SPG31 gene. Mutations in REEP1 isoform 1 are responsible for HSP autosomal dominant form.

- REEP1 isoform 2 (181 aa), has a distinct and shorter N-terminus, compared to isoform 1 and differs in the 5' UTR and 5' coding region.
- REEP1 isoform 3 (121 aa), has a shorter N.terminus, and differs in the 5' UTR and 5' coding region compared to isoform 1.
- REEP1 isoform 4 (121aa), differs in the 5' UTR and 5' coding region, and lacks two alternate exons in the central coding region that causes a frameshift, compared to variant 1. The encoded isoform 4 has distinct N- and C-termini and is shorter than isoform 1.

1.2.2 Human REEP1

The REEP1 gene encodes a protein of 201 amino acids that enclose two putative transmembrane domains and a conserved protein domain, TB2/DP1/HVA22, known as "deleted in polyposis" domain, with unknown function (Züchner et al. 2006). REEP1 protein belongs to the REEP/DP1/YOP1 superfamily. Based on the sequence similarity this family includes homologues genes from diverse eukaryote species. Members of this family form higher-order oligomeric structures.

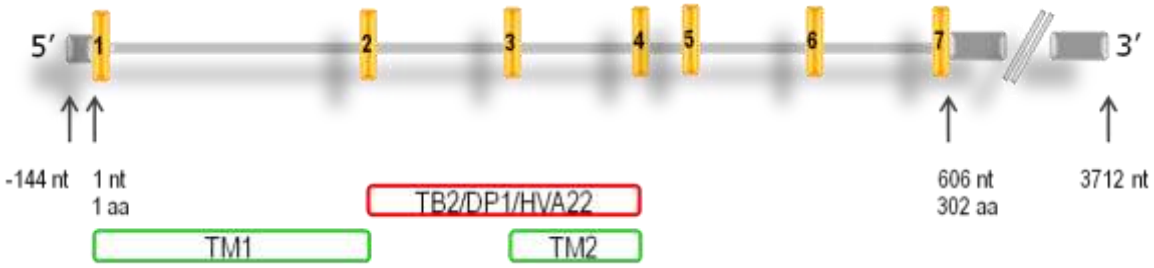

Figure 1. Schematic representation of H-REEP1gene

REEP1 is expressed in various non neuronal and neuronal tissues, including spinal cord. This follows the now-common finding of almost ubiquitous tissue expression for a number of genes that cause distinct neurodegenerative phenotypes. At the subcellular level, REEP1 localize to Endoplasmic reticulum membranes as an integral membrane protein (Park et al. 2010). Immunostaining experiments have suggested that REEP1 C-terminal domain is exposed toward the cytoplasm (H. Saito et al. 2004).

REEP1 was originally identified as a protein that promotes trafficking of olfactory receptors to the plasma membrane surface (H. Saito et al. 2004). Latest studies implies that REEP1 protein, as a member of REEPs subfamily (REEP1–4) is involved in ER shaping (Park et al. 2010). REEP1 protein, upon over-expression in COS cells forms protein complexes with atlasin-1 and spastin, within the tubular ER. Moreover, REEP1, can also bind the microtubules and promote ER alignment along the microtubule cytoskeleton (Park et al. 2010).

1.2.3 REEP/DP1/YOP1 Superfamily

Most species have a number of closely related REEP/DP1/Yop1p superfamily members; there are six members in human and other in mammals (REEP1-6), one member in *S. cerevisia,* Yop1p, and one member in barley, H2AV22, (H. Saito et al. 2004). Systematic analysis of the structure and biochemical properties has shown a clear phylogenetic delineation of REEP proteins into two distinct subfamilies, REEP1–4 and REEP5–6 in higher species. REEP1–4 subfamily are characterized by the presence of a much shorter first hydrophobic segment, the absence of the N-terminal cytoplasmic domain, and the presence of a longer C-terminal region comparing to REEP5–6. Even species such as *Drosophila melanogaster*, *Strongylocentrotus purpuratus*, and *Caenorhabditis elegans* have at least one REEP protein with similarity to each of subfamily REEP1–4 and REEP5–6. Different studies, have established a direct role for mammalian REEP5/DP1 and yeast Yop1p in shaping endoplasmic reticulum (ER) tubules, while the REEP1-4 subfamily is thought to have an important role in ER shaping and ER network formation in vitro (Park et al. 2010).

1.3 THE ENDOPLASMIC RETICULUM

1.3.1 ER structure and organization

The endoplasmic reticulum (ER) is arguably the most complex, multifunctional organelle of eukaryotic cells. Its membrane constitutes more than the half of the total membrane of an average animal cell. The ER has a central role in lipid and protein biosynthesis. Proteins are translocated across the ER membrane, and are folded and

modified before they traverse the secretory pathway. It also plays a central role in other important processes like Ca2+ sequestration and signalling. The ER is a complex structure composed of membrane sheets that enclose the nucleus (the nuclear envelope) and an elaborate interconnected network in the cytosol (the peripheral ER). The nuclear ER, or nuclear envelope (NE), consists of two sheets of membranes with a lumen. The NE surrounds the nucleus, with the inner and outer membranes connecting only at the nuclear pores, and is underlain by a network of lamins. The peripheral ER is extensive network of cisternae and tubules and extends into the cytoplasm all the way to the plasma membrane. ER tubules have a very different shape from ER cisternae . ER tubules have high membrane curvature at their cross-section, whereas cisternae are comprised of extended regions of parallel, flat membrane bilayers that are stacked over each other with regions of membrane curvature found only at their edges. However, there are similarities between ER cisternae and tubules; specifically, the diameter of an ER tubule is similar to the thickness of an ER cistern (38 nm vs 36 nm, respectively, in yeast) (West et al. 2011). The lumenal space of the peripheral ER is continuous with that of the nuclear envelope and together they can comprise >10% of the total cell volume (Terasaki and Jaffe 1991). The ultrastructure of the ER has been visualized by electron microscopy in a number of cell types. The most obvious difference seen is between rough, i.e. ribosome-studded, and smooth regions of the ER (RER and SER, respectively). The RER often has a tubular appearance, whereas the SER is often more dilated and convoluted (Baumann and Walz 2001). The relative abundance of RER and SER found among different cell types correlates with their functions. For example, cells that secrete a large percentage of their synthesized proteins contain mostly RER.

In contrast with every other organelle, the ER does not appear to undergo regulated fragmentation or division. Even during processes like cell division, the ER remains continuous. Several approaches have provided the evidence that the ER is a single membrane system with a continuous intralumenal space. In one experiment, a fluorescent dye that cannot exchange between discontinuous membranes was injected into cells in an oil droplet. The dye diffused throughout the cell in a membrane network that, based on morphological criteria, was the ER. This was observed in a number of different cell types including sea urchin eggs (Terasaki and Jaffe 1991) and Purkinje neurons (Terasaki et al. 1994). Because the dye spread in fixed as well as live cells it

must be diffusing through a continuous network rather than being transported by active trafficking. The continuity of ER membranes network was also proved by fluorescence loss in photobleaching (FLIP). Little is known about how the particular architecture of the ER is formed and maintained. It is known that the cytoskeleton is not necessary for the formation of a tubular network *in vitro*. In *Xenopus* egg extracts, ER networks can form *de novo* and this process is not affected by the addition of inhibitors of microtubule polymerization, by the depletion of tubulin from the extract or by inhibitors of actin polymerization (Dreier and T A Rapoport 2000).

The atlastin proteins (and their yeast homolog Sey1) stimulates homotypic ER fusion. Atlastin are membrane-integral GTPase family proteins components of ER fusion machinery. Atlastin mutation or depletion, leads to unbranched ER tubules in mammalian cells (J. Hu et al. 2009) and ER fragmentation in *Drosophila* neurons whereas its overexpression leads to ER membrane expansion (Orso et al. 2009).

1.3.2 ER dynamics

In interphase cells, the peripheral ER is a dynamic network consisting of cisternal sheets, linear tubules, polygonal reticulum and three-way junctions (Allan and R D Vale 1991). Several basic movements contribute to its dynamics: elongation and retraction of tubules, tubule branching, sliding of tubule junctions and the disappearance of polygons. These movements are constantly rearranging the ER network while maintaining its characteristic structure. The ER fusion machinery and the reticulon proteins play a stabilizing role in maintaining overall ER structure during these dynamics. The dynamics of the ER network depend on the cytoskeleton. In mammalian tissue culture cells, goldfish scale cells, and *Xenopus* and sea urchin embryos the ER tubules often co-align with microtubules. Microtubule-based ER dynamics were studied with time-lapse microscopy and appear to be based on two different mechanisms: via tip attachment complex (TAC) and ER sliding dynamics. During TAC movements, the tip of the ER tubule is bound to the tip of a dynamic microtubule, and the new ER tubule grows in a motor-independent way in concert with the dynamics of the plus-end of the microtubule. TAC events occur through a complex between the integral ER membrane protein STIM1 and a protein that localizes to the tip of a dynamic microtubule,

EB1,(Grigoriev et al. 2008). In ER sliding events, tubules are pulled out of the ER membrane by the motor proteins kinesin-1 and dynein along microtubules that are marked by acetylation (Friedman et al. 2010). ER sliding is the predominant mechanism responsible for dynamic ER rearrangements in interphase cells and is a much is much more common event than tip attachments complex events (Waterman-Storer and Salmon 1998). The differences between TAC and ER sliding mechanisms suggest that they might contribute to very different ER functions.

In yeast and plants, the actin cytoskeleton, rather than the microtubule network, is required for ER dynamics (W A Prinz et al. 2000). The cytoskeleton contributes to ER dynamics, but it is not necessary for the maintenance of the existing ER network. Although depolymerization of microtubules by nocodazole in mammalian tissue culture cells inhibits new tubule growth and causes some retraction of ER tubules from the cell periphery, the basic tubular-cisternal structure of the ER remains intact (Terasaki, L. B. Chen, and Fujiwara 1986). Similarly, actin depolymerization in yeast blocks ER movements but does not disrupt its structure (W A Prinz et al. 2000).

1.3.3 Tubulation of ER membranes and cisternae shaping

The peripheral ER in most cells contains a mixture of interconnected membrane tubules and cisternae Membrane tubules are a structural feature of both the ER and the Golgi complex (Dreier and T A Rapoport 2000; Lee, Ferguson, and L. B. Chen 1989). Both types of tubule have similar diameters (50–100 nm), whether formed *in vitro* or *in vivo*, and in the case of the ER, tubule diameter is conserved from yeast to mammalian cells, suggesting that their formation is a regulated and fundamental process. The relative amount of tubules versus cisternae depends to a large extent on the proteins that regulate ER membrane curvature, the reticulons and DP1/Yop1. These proteins are integral membrane proteins, conserved in all eukaryotes. They localize exclusively in the peripheral regions of the ER that presents a high membrane curvature, which includes the edges of cisternae as well as tubules (Hetzer, Walther, and Mattaj 2005; Kiseleva et al. 2007). Studies *in vitro* and *in vivo* have shown that these proteins are necessary for organizing the ER membrane bilayer into the shape of a tubule (J. Hu et al. 2008), but they also involved in membrane curvature at the edges of cisternae and

fenestrations (West et al. 2011). In contrast, little is known about how the ER cisternae get their shape. These domains are comprised of flat areas of ER membrane that are uniformly spaced around the ER lumen and are connected at highly curved edges. Partitions of Climp63, a rough-ER-specific transmembrane protein, into ER cisternae and its overexpression, propagates the formation of cisternal ER at the expense of tubules (Sparkes et al. 2010).

Climp63 depletion do not lead to a loss of the cisternae, but alterates their intraluminal spacing. These data suggest that, although Climp63 is not required for cisternae formation, it may form intraluminal linker complexes that regulate cisternal dimensions (Sparkes et al. 2010).

1.3.4 ER–organelle contacts

The ER is not an isolated structure but it contacts almost every membrane-bound organelle in the cell, including mitochondria, Golgi, peroxisome, endosomes, lysosome and lipid droplets as well as the plasma membrane.

1) *ER–mitochondria*. The ER and the mitochondria contacts sites have been studied both biochemically and functionally. The interface between the ER and mitochondrial membranes has diverse important roles in cell physiology, like lipid synthesis and Ca^{2+} signalling, the latter of which is crucial for apoptotic regulation (De Brito and Scorrano 2010; Csordás et al. 2006).

2) *ER–peroxisome*. In both yeast and mammalian cells, peroxisomes are derived at least in part from the ER membrane. Some peroxisomal membrane proteins are inserted into the ER and trafficked to peroxisomes in vesicles. These vesicles could also provide the phospholipids required for the growth of peroxisomal membranes, because peroxisomes lack phospholipid biosynthesis enzymes (Raychaudhuri and William A Prinz 2008).

3) *ER–Golgi*. Transport in the ER–Golgi is performed by COPII complex in the anterograde direction and by COPI in the retrograde direction. COPII vesicles are formed at specific sites at the endoplasmic reticulum, the so-called ER exit sites (ERESs), (Castillon, Shen, and Huq 2009). Electron microscopy studies have shown a very close contacts between the ER membrane and the trans-Golgi, which have been proposed to be involved in direct lipid transport (Levine and Loewen 2006).

4) *ER–endosome.* Recent study has establish a relationship between the ER and the endocytic pathway. There is a direct interaction between the ER-localized phosphatase, PTP1B, and the endocytic cargo, EGFR, at ER–endosome contact sites, in animal cells, suggesting that ER proteins might modify endocytosed cargoes, (Eden et al. 2010). Moreover, early endosomes moves in coordination with ER dynamics, and these two organelles can be tightly associated over time (Friedman et al. 2010).

5) *ER–plasma membrane.* The ER makes also an extensive contact with the plasma membrane. Studies in yeast have shown a mixture of interconnected ER tubules and fenestrated cisternea with the cytoplasmic surface of the plasma membrane (West et al. 2011). This contacts are important for the regulation of phosphatidyl inositol metabolism, Ca^{2+} regulation and might be sites of direct non-vesicular sterol transfer (De Stefani et al. 2011).

6) *ER–lipid droplets*. In eukaryotes, lipid droplets may arise primarily from the ER, where the enzymes that synthesize neutral lipids reside (Buhman, H. C. Chen, and R V Farese 2001). In yeast genetically engineered to lack LDs, induction of LD formation has shown that they invariably arise from or close to the ER. Lipid droplets appear to remain in contact with the ER once formed, and there is a continuous movement of the proteins that associate with both compartments (Jacquier et al. 2011).

1.4 LIPID DROPLETS

Lipids are source of energy for the cell. They are critical determinants of membrane integrity, and in some cells substrates for hormones synthesis. Endogenous synthesis of lipid requires a significant energy consume, therefore, coordinated transports processes have been developed to assimilate them from the environment and store them safely. Lipid enter in cytoplasm as free fatty acids or as alcohols (cholesterol). Fatty acid are released from triacylglyercols by lipase and enter in the cell by passive diffusion, facilitated by fatty-acid proteins or fatty-acid translocase (Ehehalt et al. 2006). In contrast to fatty acids, sterols are primarily taken up into cell through endocytosis and lysosomal degradation of lipoproteins. A high concentration of free fatty acid is toxic to the cell, while alcohols, at law concentrations are bioactive as signaling molecules. Thus, efficient systems have evolved to limit the concentrations of acids and alcohols

and to retain their availability by co-esterification into neutral lipids. The majority of neutral lipid synthesis is completed at the endoplasmic reticulum (ER). Due to a limited solubility of lipids in the ER membrane bilayer and the immiscibility with the hydrophilic intracellular environment, the lipid are stored into cytoplasmic lipid droplets, a process that nullifies any impact on the osmolarity of the cytosol (Sturley and Hussain 2012). Lipid droplets (LDs) exist in all kind of living cells, from bacteria, to yeasts, plants and mammals. LDs were identified by light microscopy as cellular organelles in the nineteenth century. For a long time, they were largely ignored in cell biology research, presumably because they were perceived as immobile lipid accumulations with little functional relevance. Recently, they have attracted great interest as dynamic structures at the center of lipid and energy metabolism. Major findings that emphasize the diversity and dynamics of LDs are the identification of key proteins involved in LD biology, the interaction of LDs with other organelles and the different composition in lipids and proteins in different cell types and physiological states. Excessive lipid storage in LDs is central to the pathogenesis of several metabolic diseases such as obesity, diabetes and atherosclerosis, suggesting that LDs have, therefore a crucial role in such disorders.

Despite the acceleration of progresses in LD research and in determining the associations with prominent disorders, most fundamental questions are not yet resolved. How are LDs formed? How proteins and lipids are recruited to LDs? How do they interact with other organelles?

1.4.1 Lipid Droplets characteristics.

A lipid droplet consists of a hydrophobic core of neutral lipids in the form of triacylglycerols, cholesteryl esters, or retinyl esters surrounded by a phospholipid monolayer. In mammalian LDs, phosphatidycholine (PC) is the main surface phospholipid, followed by phosphatidyethanolamine (PE) and phosphatidyinositolo (Bartz et al. 2007). Compared with other membranes, LDs lacks in phosphatidyserine and phosphatidic acid but they are enriched in lyso-PC and lyso-PE. The surface of lipid droplets is also decorated with proteins that provide structural and metabolic functions. The first lipid droplet-associated proteins identified were the perilipins and related

proteins, which have important metabolic roles in the control of triacylglycerol storage and release from lipid droplets (D. L. Brasaemle et al. 2009). Some of the most frequently associated proteins are enzymes involved in triacylglycerol and phospholipid biosynthesis, like acyl-CoA:diacylglycerol acyltransferase 2(DGAT2), acyl-CoA synthetase; phosphocholine cytidylyltransferase, membrane-trafficking proteins (ARF1, Rab5, Rab18), and the adipose tissue triacylglycerol lipase (ATGL) (Guo et al. 2008). However, large scale proteomic studies have identified several other lipids droplets associated proteins, indicating that the protein gathering it's a key feature for the function of a single LD (C. C. Wu et al. 2000).

The mammalian adipocyte is considered the "professional" lipid droplet-storing cell, but lipid droplets are formed nearly by all cell types in eukaryotic organisms as well as in prokaryotes (D J Murphy 2001). Lipid droplets in white adipocytes are probably the most extensively characterized type of lipid droplet. White adipocytes contain, typically, a single, large lipid droplet ranging up to 100 μm in diameter, whereas in most other cell types, LDs, are usually less than 1 μm in size (T. Suzuki et al. 2001). White adipocyte lipid droplets typically occupy the majority of the cytosol, are localized a short distance from the plasma membrane, are associated with intermediate filaments, and have very limited mobility within the cell. By contrast, the multiple small lipid droplets present in nonadipocytes are often observed juxtaposed next to the endoplasmic reticulum, mitochondria, and peroxisomes. These small lipid droplets exhibit directional movement across long distances within the cell through interaction of lipid droplet associated proteins with microtubules (Michael A Welte 2009).

1.4.2 Lipid Droplets formation.

Unlike most other organelles, LDs are not formed by growth and fission of existing droplets, but they are likely formed *de novo*. In bacteria, LDs are formed by lipid synthesis in the cell-delimiting membrane (Wältermann et al. 2005). In yeast genetically engineered to lack LDs, induction of LD formation shows they arise from or close to the ER (Jacquier et al. 2011). In eukaryotes, also, LDs may arise primarily from the ER (Buhman, H. C. Chen, and R V Farese 2001). Observation of a fluorescent LD protein and a fluorescent fatty acid show a concentration of LDs components in the ER or its

direct proximity within 5-15min, followed by rapid formation of lipid droplets (Kuerschner, Moessinger, and Thiele 2008; Turró et al. 2006). Electron microscopy (EM) studies have shown membrane cisternae, which could be connected to the ER, in close proximity to LDs (Soni et al. 2009). Despite these findings, the molecular mechanisms of LD formation are still not understood. How does a monolayer-coated LD arise from a bilayer membrane?

Several hypothesis have been proposed for the process of LD formation. The most prevalent hypothesis postulates that lipids accumulate between the cytoplasmic leaflet of the ER membrane, and as the volume increase the leaflet swell as a globular mass until is pinched off from the membrane to become an independent LD (M. Suzuki et al. 2011). An alternative model support that the LD formation occur at specialized sites of cytoplasmic surface of ER. These sites contain a high concentration of the LD PAT protein, adipophilin, that surround the forming droplets in en egg-cup-like manner in which LD grows through transport of neutral lipids from the ER (H. Robenek et al. 2006). All models hypothesize that LDs are formed toward the cytosolic face of the ER membrane. However, cells, such as hepatocytes, also secrete neutral lipids into the ER lumen, indicating that LDs could be derived also from the luminal origins. Several problems prevent the identification of the correct model. The major reason for the difficulty is likely to be the small size of nascent LDs (12 nm diameter predicted), that is below the resolution of light microscopy. Moreover, most of the cells have LDs, complicating identification of nascent LDs, and there are no systems of induced LD formation in mammals.

1.4.3 Lipid droplets growth.

The size of lipid droplets varies with diameters ranging from 20-40 nm to 100 μm, indicating that LDs can grow in size. To accommodate more triacyglycerols, the cell needs to synthesize new LDs or to grow the existing one. Insertion of neutral lipids to existing LDs requires local synthesis or transfer from the endoplasmic reticulum. Phospholipids and storage lipids synthesized in the ER may be efficiently delivered to growing LDs through LD–ER contact sites or through increased partitioning of neutral

lipids into the LD subdomains or via interorganelle transport by transfer proteins (Moessinger et al. 2011).

An alternative model for LD growth arises from the observations that key enzymes in phospholipid and neutral lipid synthesis are present on the LD surface. Thus LDs may acquire lipids through local synthesis. Several studies have demonstrate the implication o f a number of proteins and lipid factors involved in the growth of lipid size

Cell death-inducing DFF45-like effector (CIDE) family proteins, including Cidea, Cideb, and Fsp27 (fat-specific protein of 27 kDa), are LD-associated proteins that have recently emerged as regulators of lipid storage and energy homeostasis (J. Gong, Sun, and P. Li 2009). Fsp27-deficient white adipocytes lose unilocular LDs, and accumulate many small LDs (Nishino et al. 2008). While the ectopic expression of Cidea or Fsp27 enhances the size and reduces the number of LDs. Furthermore, hepatic Cidea expression is upregulated by saturated fatty acids and plays a crucial role in fatty acid-induced hepatic steatosis in mice and humans (Zhou et al. 2012). Perilipin1 is one of the most widely characterized proteins of the LD surface. Perilipin1 is the founding member of the PAT (perilipin, adipophilin and TIP47) family of LD-coating proteins that regulates lipolysis in adipocyte. Perilipin1 deficient mice exhibit dramatically reduced adipocyte and LD size, suggesting that perilipin1 may induce the formation of giant lipid droplets (Martinez-Botas et al. 2000).

Triacyglycerols (TAG) and sterols (SE) and not other lipids are important not only for the biogenesis of LDs, as demonstrated by the existence of a LD free yeast strain, where the synthesis of TAG and SE is abolished owing to the absence of diacylglycerol (DAG) and sterol acyltransferases, but they are also important for their growth of size (Oelkers et al. 2002). The composition of the phospholipid monolayer coating LD surface may vary from organism to organism, but phosphotidylcholine (PC) and phosphotidylethanolamine (PE) are the major components of most LDs (Bartz et al. 2007). During LD expansion in *Drosophila* S2 and mammalian cells, phosphocholine cytidyltransferase, enzyme of PC synthesis is targeted to the LD surface and activated, thereby providing enough PC to meet the needs of LD growth and proliferation. PC is a cylindrical lipid that has the unique ability to stabilize LDs and prevent LD coalescence. Indeed, when PC synthesis is compromised, giant LDs are readily formed in S2 cells (Krahmer et al. 2011).

Two independent screens of the yeast deletion library have found ‘supersized’ LDs in cells deleted for FLD1. The mammalian orthologue of Fld1p is seipin, mutant forms of which have been linked to Berardinelli-Seip congenital lipodystrophy type 2 (BSCL2), a recessive disorder characterized by an almost complete loss of adipose tissue, severe insulin resistance and fatty liver. Moreover giant LDs have been found in the salivary glands of seipin deficient *Drosophila* (Tian et al. 2011). These results establish seipin as an important factor in regulating LD dynamics, particularly size and distribution.

An additional model proposed for the growth of LDs is the fusion between the existing LDs. LD fusion has been proven to be a rare event under normal conditions, recently has been observed in mutant cells, as well as in 3T3 L1 adipocytes upon insulin and fatty acid treatment.

SNARE proteins (soluble N-ethylmaleimide-sensitive factor attachment receptor proteins) that mediate homotypic fusion of bilayer-bound vesicles during cellular trafficking, have been recently considered as possible candidates of LD fusion. Knockdown of genes SNAP23, syntaxin-5 and VAMP4 in NIH 3T3 cells decrease the rate of LD fusion (Boström et al. 2007). However it is unclear how SNARE proteins would mediate fusion of monolayer-bound vesicles. Other recent studies have identified additional proteins that influence LD size, but the role of these proteins in LD biology requires further analyses

Furthermore, LD fusion can be induced by pharmacological agents like propranolol and other drugs, which may trigger fusion by inserting into and disrupting LD surface monolayer (S. Murphy, Martin, and Parton 2010).

1.4.4 Lipid droplets motility

LDs in non adipocyte cells are capable of rapid, microtubule-dependent movement as shown with live-cell imaging of the *Drosophila* embryos (M A Welte et al. 1998) and mammalian HuH-7 cells (Targett-Adams et al. 2003). The directional movement is driven by minus-end and plus-end motors, dynein and kinesin-1 respectively (S P Gross et al. 2000). LDs move directionally in axons of Aplysia by uncharacterized mechanisms (Savage, D. J. Goldberg, and Schacher 1987). In *Drosophila*, LSD2, a homolog of mammalian perilipin, was shown to regulate LD movement by coordinating

the motors with opposite polarites. Antibodies neutralizing dynein reduce lipid droplet formation and depolymerization of microtubules with nocodazole and inhibits homotypic fusion of lipid droplets (Andersson et al. 2006). Despite the microtubule association, LDs appear to distribute randomly in cultured cells, and patterns suggesting cytoskeletal engagement, such as linear alignment and/or centripetal concentration are not usually seen. This result suggests that LD distribution is not controlled only by microtubules, but is regulated by many factors including association with other organelles (M. Suzuki et al. 2011). These organelle associations might facilitate the exchange of lipids, either for anabolic growth of LDs or for their catabolic breakdown. Instead, LDs might provide a means of transporting lipids between organelles in the cell.

1.4.5 Lipid droplets protein

Like any other organelle, the LD surface monolayer contains a characteristic set of proteins. Mass spectrometry analysis of LD from various cell lines and tissues, has identified two groups of proteins that dominate. The first group is the PAT family, with structural and regulatory function on LD formation (D. L. Brasaemle 2007). The second group consists of enzymes of lipid metabolism that acts on triglyceride and enzymes of sterol biogenesis. From a structural point of view the LD proteome consists of three classes, peripherally associated proteins (like PAT family), lipid anchored proteins of a small GTPase type, and monotopic integral membrane proteins. The monotopic membrane proteins share a typical organization, characterized by a long hydrophobic region that typically extends to 30-40 amminoacids, with flexible regions with many residues that destabilize a regular straight alpha helix (Ostermeyer et al. 2004). The LDs are closely associated with other organelles, in particularly with the ER, thus can confuse the proteomic analysis. For such reasons its often unclear to distinguish between genuine LD protein and other proteins. Moreover, it can be more confusing, because some LD proteins have other well known functions. Histones were unpredictably found by LD proteomics to target LDs in *Drosphila* embryos (Cermelli et al. 2006). Thus LDs may transiently store other proteins that otherwise might aggregate,

like α-synuclein, a Parkinson's disease associated protein prone to self aggregation, localize to LDs (Cole et al. 2002).

1.4.6 Lipid droplets in mammalian physiology and disease

Besides storing lipids, different studies suggest that lipid droplets have other functions in cellular physiology and pathology. LDs are a source of substrates for steroid hormone synthesis, and contain the majority of the body's vitamin A and it's metabolites (Blaner et al. 2009) in retinoid stellate cells in the liver. In hepatocytes, LDs store triacylglycerol and cholesteryl esters that provide up to 70% of the substrate for the assembly of very low-density lipoproteins (Lehner *et al.*, 2009). Moreover, they appear to have important functions in several cell types of the immune system, like macrophages and leukocytes by participating in inflammation and the immune response (Melo et al. 2011). In cardiomyocyte, triacylglyclerol of LDs are hydrolyzed to generate lipid ligands that activate the nuclear receptor peroxisome proliferator-activated receptor α and mitochondrial function. Therefore, suggesting that lipids of LDs might act as signaling molecules or ligand for the transcription factors (Haemmerle et al. 2002). Lipid droplet can serve as temporary storage site for hydrophobic proteins to prevent their degradation or/and they aggregation. One example is the accumulation of protein α-synuclein, dysfunction of which is associated with Parkinson's disease (Cole et al. 2002).

An excessive or defective storage of lipid in LDs can lead to many metabolic diseases, or diabetes and atherosclerosis. Accumulation of triacylglyclerol in LDs in liver and pancreatic β-cells and skeletal muscule can lead to lipotoxicity and determine insulin resistance, obesity and nonalcoholic steatohepatits (Lusis *et al.*, 2010). Macrophage excessive storage of lipid in LDs is a characteristic of foam cell formation in atherosclerosis. Dysfunction of LDs hydrolysis is associated with accumulation of lipids in skeletal and cardiac muscle. Mutations in adipose triglyceride lipase (ATGL) cause myopathy, whereas mutations in the activator of ATGL (CGI-58) cause Chanarin – Dorfman syndrome, that present the same symptoms caused by ATGL deficiency (Fischer et al. 2007; Schweiger et al. 2009).

Lipid droplets play an important role in the pathogenesis of bacteria and virus. The viral genome of hepatitis C virus, after replication, is recruited to the ER surrounding lipid droplets and is encapsulated by the viral nucleocapisd core to produce progeny virions.
Recent studies have shown also a correlation between cancer and LDs. In most cancer cells there is an upregulation of synthesis of fatty acid, presumably to provide the lipid necessary for the membrane proliferation. Some of this cells present large LDs (Patricia T Bozza and Viola n.d.). However the mechanism for the LD accumulation in cancer cells is unclear.

1.5 *DROSOPHILA* IN THE STUDY OF NEURODEGENERATIVE DISEASES

A growing number of neurodegenerative diseases, as well as other human diseases, are being modelled in *Drosophila*.
Drosophila is used as a platform to identify and validate cellular pathways that contribute to neurodegeneration and to identify promising therapeutic targets by using a variety of approaches from screens to target validation. The unique properties and tools available in the *Drosophila* system, coupled with the fact that testing *in vivo* has proven highly productive, have accelerated the progress of testing therapeutic strategies in mice and, ultimately, humans.

1.5.1 How fly models can complement other systems

In studying human neurodegenerative diseases, one typically employs multiple systems, including cell-based models in which one can generate stably expressing lines and phenocopy cellular aspects of disease. However, in many cases, the response of the intact organism is not fully recapitulated in cell lines. *In vitro*, intersecting physiological pathways and responses (e.g., neurotransmitter circuitry and interactions with support cells, etc.) are eliminated, nonautonomous cellular influences are removed, and new parameters such as those used to immortalize cells, are often introduced, thus reducing the ability of cultured cells to mirror *in vivo* pathology. It can also be very difficult to obtain a functional measure of the impact of pathogenic proteins in *in vitro* systems.

In contrast, although mice and other mammalian model systems offer *in vivo* opportunities and extensive similarity to the human brain, the length of time and cost required to perform experiments comparable to those possible in flies can be prohibitive.

Flies, on the other hand, are a minuscule system model with a rapid generation time, inexpensive culture requirements, large progeny numbers produced in a single cross and a small highly annotated genome devoid of genetic redundancy. Flies allow excellent genetic manipulation and the pathways are considered generally highly conserved with vertebrates.

A comparative genome analysis reveals that approximately 75% of all human disease genes have a *Drosophila* ortholog (Fortini et al. 2000; Reiter et al. 2001). *Drosophila* has homologues of genes that, when disrupted, cause a broad spectrum of human diseases such as neurological disorders, cancer, developmental disorders, metabolic and storage disorders and cardiovascular disease, as well as homologues of genes required for the visual, auditory and immune systems. This and other bioinformatic analyses indicate that *Drosophila* can serve as a complex multicellular assay system for analysing the function of a wide array of gene functions involved in human diseases .

The anatomy and development of *Drosophila* nervous system has been extensively characterized and many tools are available to identify specific neuronal subtypes. Neuronal functions (i.e. synaptic transmission) and survival can been measured in flies, as can learning and memory.

Drosophila has been used to model neurodegenerative diseases ranging from tauopathy, Alzheimer's disease (AD), and Parkinson's disease (PD) to fragile X syndrome as well as several polyglutamine–repeat diseases such as Spinocerabellar ataxia and Huntington's disease (Marsh and Thompson 2004; Muqit and Feany 2002).

1.5.2 Diseases can be modelled in flies

There are three main approaches to modelling human diseases, including neurodegenerative disorders, in *Drosophila*.

Traditionally, forward-genetic approaches have been used. Mutations are selected on the basis of a neurodegenerative phenotype, and human homologues of the identified

Drosophila gene products are plausible candidates for involvement in neurodegenerative diseases. Alternatively, 'reverse genetics' can be used. In this case, the *Drosophila* homologue of a specific gene that is implicated in a human disease is targeted, and phenotypes that result from altered expression of the gene are studied. Useful phenotypes can emerge by reducing or eliminating (knocking out) gene expression, or by overexpressing the gene product.

An even more direct path from human disease to invertebrate model is possible with certain human disorders: those caused by a toxic dominant gain-of-function mechanism. If disease is produced in humans by the action of a toxic protein, it might not be necessary, or even desirable, to manipulate the invertebrate homologue of the human disease-related gene. Instead, simple expression of the toxic human protein in the model organism might accurately model the disease. Toxic dominant mechanisms almost certainly operate in neurodegenerative disorders such as Huntington's disease and amyotrophic lateral sclerosis (ALS).

Nearly all of the current fly models of neurodegenerative diseases have been made using the GAL4/UAS (upstream activating sequence) system which allows the ectopic expression of a transgene in a specific tissue or cell type (Brand and Perrimon 1993).

In this system, a human disease-related transgene is placed under the control of the yeast transcriptional activator GAL4. In the absence of GAL4, the transgene is inactive. When flies that carry the human disease-related transgene are crossed to flies that express GAL4 in a specific tissue or cell type, the transgenic protein is made only in the tissues that have GAL4 (Figure 2).

Many cell-type and developmentally regulated GAL4 ('driver') lines exist at present, and are readily available from public stock centres. So, the effect of expressing a human disease-related transgene in many different tissues and at various developmental times can be assayed without creating many independent transgenic fly strains. This system provides a particular advantage for studying neurodegenerative disease, because the issue of cell-type specificity can be readily addressed.

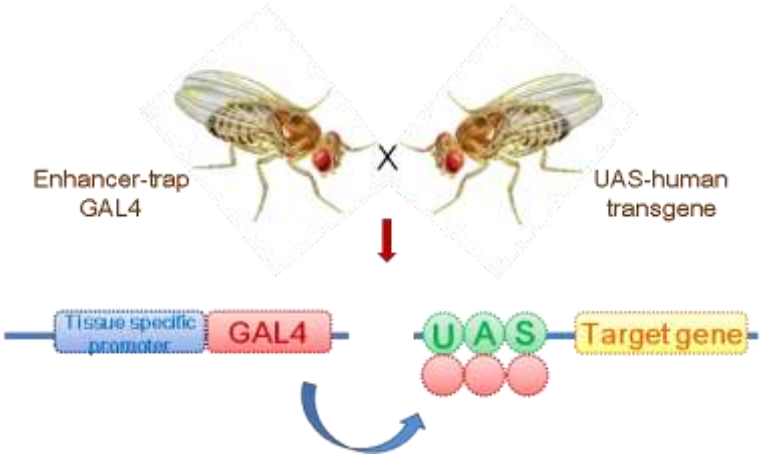

Figure 2. GAL4/UAS (upstream activating sequence) system allows the ectopic expression of a human transgene in a specific tissue or cell type.

Once relevant *Drosophila* models of neurodegenerative disease have been created, the genetic potential of the system can be exploited. Second-site modifier analysis identifies unlinked mutations that either suppress or enhance neurodegeneration. Such modifier genes encode proteins that are involved in the pathogenesis of the neurodegenerative process in flies, and potentially in the human disease as well. One strength of genetic analysis in *Drosophila* is that the whole cellular cascade that mediates neurodegeneration, including both specific interactors and downstream elements, can be defined. In practical terms, the phenotype that is used to select genetic modifiers should be externally visible, easily scored and involve structures that are not essential for viability. Abnormalities of the *Drosophila* eye have therefore been the phenotypes of choice in modifier screens.

Modifier identification can follow both biased and non-biased strategies. In the biased 'candidate' approach, mutations are selected on the basis of pre-existing hypotheses, and these mutations are tested for their ability to suppress or enhance neurodegeneration. Candidate testing can rapidly confirm the role of suspected mediators, but is limited by preformed hypotheses. The second approach is to do an unbiased forward-genetic screen. A forward-genetic screen interrogates the genome for mutations that modify a neurodegenerative phenotype, without bias as to possible function. Random mutations are produced by chemical or insertional mutagenesis, and the ability of these mutations to suppress or enhance the phenotype of interest is tested. The unbiased approach has

the potential to identify new proteins, or to implicate previously defined cellular pathways that were not suspected to be important in neurodegenerative disease (Muqit and Feany 2002).

2. AIMS

Hereditary Spastic Paraplegia (HSP) is a complex and heterogeneous group of genetic disorders clinically characterized by progressive spasticity and weakness of lower limbs. To date over 54 loci have been recognized but only 27 genes have been molecularly characterized. The genetic complexity of the disease and the lack of information concerning the pathways of most of the genes involved, prevent the development of valid therapeutic approaches. Mutations of the SPG31 gene, which encodes for REEP1 protein, are responsible for autosomal dominant form of HSP. Recently, *in vitro* experiments conducted in mammalian cell systems have shown that REEP1 interacts with other two HSP related genes, Spastin and Atlastin-1, within the tubular ER membrane to coordinate ER shaping and microtubule dynamics. However, the exact function of REEP1 and the mechanism which lead to axonophaty in HSP remain to date unresolved.

The aim of this project was to try to understand the biological role of REEP1 by *in vivo* analysis of loss and gain of function transgenic lines of the *Drosophila* homologue D-REEP1. This approach is based on the high degree of evolutionary conservation of genes structure and function between *Drosophila* and human. The analysis of the cellular phenotype generated by down regulation and over-expression of REEP1 through biochemical, molecular and Confocal imaging techniques have represented the strategy for the aim of this thesis.

Moreover, we wanted to evaluate the *in vivo* effects produced by pathological form of D-REEP1 protein. To gain insight into the pathological mechanism underlying HSP neurodegeneration we generated transgenic animals expressing D-REEP1 protein with missense mutation.

3. METHODS

3.1 MOLECULAR BIOLOGY TECHNIQUES: GENERATION OF CONSTRUCTS

The H-REEP1 cDNA was previously obtained from *HeLa cells* RNA extract followed by RT reaction and cloned in the pcDNA3.1/Zeo(+) cloning vector (Qiagen).
The D-REEP1 cDNA was obtained from *Drosophila* RNA extract and cloned in the pDrive cloning vector (Qiagen): D-REEP1/pDrive.

3.1.1 Amplification of H-REEP1 and D-REEP1 cDNA

Full-length H-REEP1 cDNA (606 pb) D-REEP1 cDNA (867 pb) were obtained by RT-PCR from, respectively, HeLa cells total RNA extract and *Drosophila total* RNA.
RT-PCR is short for Reverse Transcription-Polymerase Chain Reaction. RT-PCR, is a technique in which a RNA strand is "reverse" transcribed into its DNA complement, followed by amplification of the resulting DNA using a polymerase chain reaction (PCR).
Transcribing a RNA strand into its DNA complement is termed reverse transcription (RT), and is accomplished through the use of a RNA-dependent DNA polymerase (reverse transcriptase). Afterwards, a second strand of DNA is synthesized through the use of a deoxyoligonucleotide primer and a DNA-dependent DNA polymerase. The complementary DNA and its anti-sense counterpart are then exponentially amplified via a polymerase chain reaction (PCR). The original RNA template is degraded by RNase H treatment.

3.2 RT-PCR

The complementary strand from RNA template was obtained using the ThermoScript ™ RNase H^- Reverse Transcriptase (Invitrogen); for PCR reaction we used Phusion High-Fidelity DNA polymerase (Finnzymes). The entire procedure is described below.

Component	Volume/ 12 ul reaction
Oligo$(dT)_{20}$ (50μM)	1 ul
Total RNA	1 ug
10mM dNTP mix (10 mM each dATP, dGTP, dCTP and dTTP at neutral pH)	1 ul
H_2O	add to 12 ul

The misture was incubated at 65°C for 5 minutes and then placed on ice. The contents of the tube was collected by brief centrifugation and to the tube were added:

Component	Volume/ 20 ul reaction
RTBuffer (5X)	4 ul
DTT 0.1M	1 ul
primer Oligo(dT)	1 ul
RNaseOUTTM	1 μl
Superscript III (retrotrascriptase)	200U

Contents of the tube were mixed gently and incubated at 50°C for 60 minutes. The reaction was terminated by heating at 75°C for 5 minutes. To remove the original RNA template, 1μl (2 units) of *E. coli* RNase H was added and incubated at 37°C for 20 minutes.

3.2.1 Cloning of the H-REEP1 cDNA fragment in pcDNA3.1/Zeo(+) plasmid: H-REEP1-HA/pcDNA3.1/Zeo(+), H-REEP1-Myc/ pcDNA3.1/Zeo(+) and HA/H-REEP1-Myc/ pcDNA3.1/Zeo(+)

pcDNA3.1/Zeo(+) is a plasmid designed for high level expression in a variety of mammalian cell lines (see Appendix C). Three differently tagged REEP1 forms were cloned in the pcDNA3.1/Zeo(+) plasmid: REEP1-HA, REEP1-Myc and HA-REEP1-Myc.

To insert the HA epitope in the N-terminus of REEP1, cDNA was amplified from total extract using the following primers:

Forward

FHAREEP1EcorI 5’GAATTCATGTACCCATACGATGTTCCTGACTA TGCGGGCGTGTCATGGATCATCTCCAGGC3’

Reverse

RREEP1XhoIStop 5’CTCGAGCTAGGCGGTGCCTGAGCTGCTAGCG CT3’

To insert the Myc epitope in the C-terminus of H-REEP1, cDNA was amplified using the following primers:

Forward

FREEP1EcorI 5’GAATTCATGGTGTCATGGATCATCTCCAGGC3’

Reverse

RREEP11XhoIMyc 5’CTCGAGTTACAGATCTTCTTCAGAAATAAGTTT TTGTTCGGCGGTGCCTGAGCTGCTAGCGCT3’

To insert the HA epitope in the N-terminal and Myc epitope in the C-terminal of REEP1, cDNA was amplified using the following primers:

Forward

FHAREEP1EcorI 5’GAATTCATGTACCCATACGATGTTCCTGACTAT GCGGGCGTGTCATGGATCATCTCCAGGC3’

Reverse

RREEP1XhoIMyc 5’CTCGAGTTACAGATCTTCTTCAGAAATAAGTTT TTGTTCGGCGGTGCCTGAGCTGCTAGCGCT3’

3.2.2 Cloning of the D-REEP1 cDNA fragment in pcDNA3.1/Zeo(+) plasmid: D-REEP1-HA/pcDNA3.1/Zeo(+), D-REEP1-Myc/ pcDNA3.1/Zeo(+) and HA-D-REEP1-Myc/ pcDNA3.1/Zeo(+)

To insert the HA epitope in the N-terminus of D-REEP1, cDNA was amplified from total RNA extract using the following primers:

Forward

FHAEcoRI D-REEP1 GAATTCATGTACCCATACGATGTTCCTGACTAT

	GCGGGCATCAGCAGCCTGTTTTC
Reverse	
RXbaI D-REEP1 stop	TCTAGATTAGTAGTTTTCCACATCCACATC

To insert the Myc epitope in the C-terminus of D-REEP1, cDNA was amplified using the following primers:

Forward	
FNotI D-REEP1	GCGGCCGCATGATCAGCAGCCTGTTTTC
Reverse	
RXbaI D-REEP1myc	TCTAGATTACAGATCTTCTTCAGAAATAAGTTT TTGTTCGTAGTTTTCCACATCCACATC

To insert both epitopes, HA at N-terminus and c-myc at C-terminus, in D-REEP1, cDNA was amplified using the following primers:

Forward	
FHA EcoRI D-REEP1	GAATTCATGTACCCATACGATGTTCCTGACTA TGCGGGCATCAGCAGCCTGTTTTC
Reverse	
RXbaI D-REEP1myc	TCTAGATTACAGATCTTCTTCAGAAATAAGTT TTTGTTCGTAGTTTTCCACATCCACATC

To generate each of these constructs the protocol used was the following:

PCR

Component	Volume/ 50 ul reaction
H-REEP1/D-REEP1cDNA (20 μg/ul)	1 ul
Buffer 10X	2 ul
MgCl2 (50mM)	2 μl
dNTPs (10 mM)	0.5 ul
Forward (10 uM)	1 ul
Reverse (10 uM)	1 ul
Taq DNA polymerase (2 U/μl)	0.4 ul
H_2O	add to 50 ul

PCR cycle

Cycle step	Temperature	Time	
Initial denaturation	94°C	5 minutes	
Denaturation	94°C	30 seconds	33 cycles
Annealing	58°C	30 seconds	
Extension	72°C	1 minute	
Final extension	72°C	10 minutes	

Restriction reactions

pcDNA3.1/Zeo(+) plasmid, D-REEP1and H-REEP1 PCR fragments, containing HA and/or c-myc epitops, were digested with restriction enzymes in the following reactions:

Component	Volume/ 50 ul reaction	Component	Volume/ 50 ul reaction
H-REEP1 PCR fragment (50ng/ul)	20 ul	pcDNA3.1/Zeo(+) plasmid (100ng/μl)	5 ul
EcoRI (10U/ul)	2 ul	EcoRI (10U/ul)	2 ul
XhoI (10U/ul)	2 ul	XhoI (10U/ul)	2 ul
10X L buffer	5 ul	10X L buffer	5 ul
H_2O	to 50 ul	H_2O	to 50 ul

D-REEP1 PCR fragment (50ng/ul)		pcDNA3.1/Zeo(+) plasmid (100ng/□l)	
EcoRI (10U/ul)	2 ul	EcoRI (10U/ul)	2 ul
XBaI (10U/ul)	2 ul	XBaI (10U/ul)	2 ul
10X L buffer	5 ul	10X L buffer	5 ul
H2O	to 50 ul	H2O	to 50 ul

Mixed products were incubated at 37°C for 1 hour and successively separated by electrophoresis through a 1% agarose gel. The bands corresponding to the H-REEP1 PCR fragment and pcDNA3.1/Zeo(+) plasmid were cut from gel and purified using the

QIAquick Gel Extraction Kit Qiagen). Purified DNA products were eluted in 10 µl of elution buffer.

The purified DNA fragments were ligated as follows:

Ligation

Component	Volume/ 10 ul reaction
Purified pcDNA3.1/Zeo(+) plasmid (100ng/ul)	3 ul
Purified H-REEP1 fragment (50 ng/ul)	6 ul
5X Buffer	3 ul
T4 DNA ligase (1U/ ul) Invitrogen	2 ul
H_2O	to 20 ul

The mixture was incubated at 16°C for 1 hour.

Transformation

Ligation mixture was used for transformation of chemically competent DH5alpha cells (Invitogen). Transformed bacteria were plated on LB–ampicillin agar plates and incubated overnight at 37°C. 10 colonies for each construct were grown in LB medium with ampicillin. Plasmid DNA was successively purified by minipreparation protocol and tested by restriction analysis for the right insertion.

Purification of H-REEP1 and D-REEP1 plasmids

Plasmid DNA were purified from an overnight culture using a "Midi" plasmid purification kit, according to Qiagen Plasmid Midi purification protocols. The final pellets were re-suspended in 50 ul of TE buffer.

3.2.3 Cloning of the H-REEP1 and D-REEP1 cDNA fragment in pcDNA3.1/Zeo(+) with GFP at N-terminus

To insert GFP sequence at N-terminus of H-REEP1 and D-REEP1, the GFP sequence was amplified from pEGFP-N1 vector using the following primers:

F GFPXhoI	CTCGAGGGTACCATGATCAGCAGCCTGTTTTC
R GFPEcoRI	GAATCCTCTAGAGTAGTTTTCCACATCCACATC

After blunt-end ligation GFP sequence was cloned in pBLUESCRIPT II KS/SK (+). pBLUESCRIPT II KS/SK (+) plasmid (Appendix C) and GFP sequence were digested with restriction enzymes in the following reactions:

Component	Volume/ 50 ul reaction	Component	Volume/ 50 ul reaction
GFP sequence (50ng/ul)	20 ul	pBLUESCRIPT II KS/SK (+) (100ng/μl)	5 ul
EcoRI (10U/ul)	2 ul	EcoRI (10U/ul)	2 ul
XhoI (10U/ul)	2 ul	XhoI (10U/ul)	2 ul
10X L buffer	5 ul	10X L buffer	5 ul
Add H_2O	to 50 ul	Add H_2O	to 50 ul

Mixed products were incubated at 37°C for 1 hour and successively separated by electrophoresis through a 1% agarose gel. The bands corresponding to the GFP sequence and pBLUESCRIPT II KS/SK (+) plasmid were cut from gel and purified using the QIAquick Gel Extraction Kit (Qiagen). Purified DNA products were eluted in 10 μl of elution buffer.

The two purified DNA fragments were ligated as follows:

Component	Volume/ 10 ul reaction
Purified pBLUESCRIPT II KS/SK (+) plasmid (100ng/ul)	1 ul
Purified GFP fragment (50 ng/ul)	4 ul
10X Ligation buffer	1 ul
Ligase enzyme (Invitrogen)	2 ul
H_2O	to 10 ul

The mixture was incubated at 16°C for 1 hour.

pcDNA3.1/Zeo(+) plasmid was digested with XhoI and XbaI restriction enzymes, GFP sequence was digested with EcoRI and XhoI restriction enzyme and H-REEP1 and D-REEP1 cDNA were digested with EcoRI and XbaI restriction enzyme**.** The bands corresponding to each of this sequence were cut from gel and purified using the QIAquick Gel Extraction Kit (Qiagen) and eluted in 10 μl of elution buffer. The

purified DNA fragments were ligated as described above. Ligation mixture was used for transformation of chemically competent DH5 alpha cells (Invitogen). Transformed bacteria were plated on LB–ampicillin agar plates and incubated overnight at 37°C.

3.2.4 Site specific mutagenesis

To introduce specific nucleotide substitutions in REEP1 cDNA, site-directed mutagenesis was performed using Pfu Ultra HF DNA polymerase (Startagene).
The basic procedure utilizes a supercoiled double-stranded DNA (dsDNA) vector with an insert of interest and two synthetic oligonucleotide primers containing the desired mutation. The oligonucleotide primers, each complementary to opposite strands of the vector, are extended during temperature cycling by the Pfu Ultra DNA polymerase polymerase. Pfu Ultra DNA polymerase replicates both plasmid strands with high fidelity and without displacing the mutant oligonucleotide primers. Incorporation of the oligonucleotide primers generates a mutated plasmid containing staggered nicks. Following temperature cycling, the product is treated with DpnI. The DpnI endonuclease (target sequence: 5´-Gm6ATC-3´) is specific for methylated and hemimethylated DNA and is used to digest the parental DNA template and to select for mutation-containing synthesized DNA. DNA isolated from almost all *E. coli* strains is dam methylated and therefore susceptible to DpnI digestion. The nicked vector DNA containing the desired mutations is then transformed into XL1-Blue chemiocompetent cells.

PCR reaction

Component	Volume/ 50 ul reaction
H-REEP1-HA/pcDNA3.1/Zeo(+) (50 ng/ul) or H-REEP1-Myc/pcDNA3.1/Zeo(+) (50 ng/ul)	1 ul
Forward (10 uM)	1 ul
Reverse (10 uM)	1 ul
10 mM dNTPs	1 ul
10X PfuUltra HF reaction buffer	5 ul
Pfu Ultra HF DNA polymerase (2.5 U/ ul)	1 ul
H_2O	to 50 ul

HD-REEP1-HA/pcDNA3.1/Zeo(+) (50 ng/ul) or HD-REEP1-Myc/pcDNA3.1/Zeo(+) (50 ng/ul)	1 ul
Forward (10 uM)	1 ul
Reverse (10 uM)	1 ul
10 mM dNTPs	1 ul
10X PfuUltra HF reaction buffer	5 ul
Pfu Ultra HF DNA polymerase (2.5 U/ ul)	1 ul
H2O	to 50 ul

PCR cycle

Cycle step	Temperature	Time	
Initial denaturation	95°C	1 minute	
Denaturation	95°C	50 seconds	18 cycles
Annealing	52°C	50 seconds	
Extension	68°C	10 minutes	
Final extension	68°C	30 minutes	

Following temperature cycling, the reaction was placed on ice for 2 minutes.
1 µl of the DpnI restriction enzyme (10 U/µl) was added directly to the amplification.
The reaction was mixed by pipetting the solution up and down several times, and immediately incubated at 37°C for 1 hour to digest the parental (i.e., the non mutated) supercoiled dsDNA.

Specific primers used for single and multiple substitutions

Aminoacidic Substitutions		Primers for H-REEP1 cDNA In small letters are indicated the substituted nucleotides
P19R	Forward	5'TATTTGGCACCCTTTAC**CGT**GCGTATTA TTCCTAC3'
	Reverse	5'GTAGGAATAATACGC**ACG**GTAAAGGGT GCCAAATA3'

A20E	Forward	5'TGGCACCCTTTACCCT**GAG**TATTATTCC TACAAG3'
	Reverse	5'CTTGTAGGAATAATA**CTC**AGGGTAAAG GGTGCCA3'
A132V	Forward	5'TTGAACGTGGCCG**T**CACAGCGGCTGTGA TG3'
	Reverse	5'CATCACAGCCGCTGTG**A**CGGCCACGTTC AA3'
D56N	Forward	5' GAGACATTCACA**AAC**ATCTTCCTTTG 3'
	Reverse	5' CAAAGGAAGATGT**TTG**TGAATGTCTC 3'

Aminoacidic Substitutions		Primers for D-REEP1 cDNA
P19R	Forward	5'TGCGGCACCCTGTAC**CGG**GCATATGCCT CATAC 3'
	Reverse	5'GTATGAGGCATATGC**CCG**GTACAGGGT GCCGCA3'
A20E	Forward	5'GGCACCCTGTAC**C**GGG**A**ATATGCCTCAT ACTCC3'
	Reverse	5'GGAGTATGAGGCATAT**T**CCCGGTACAG GGTGCCGCA 3'

Transformation

10 µl of each reaction mixture was used for transformation of chemically competent XL1-blue bacteria. Transformed bacteria were plated on LB–ampicillin agar plates and incubated overnight at 37°C.

10 colonies were grown in LB medium with ampicillin. Plasmid DNA was successively purified by minipreparation protocol (see Appendix A for procedure).

Plasmid purification

Plasmids were purified from an overnight culture using a "Midi" plasmid purification kit, according to Qiagen Plasmid Midi purification protocols. The final pellets were re-suspended in 50 ul of TE buffer.

Sequencing of mutated REEP1 cDNA

Two clones of each construct have been sequenced to verify the presence of the specific mutations. The DNA clones were sequenced by Bio-Fab Research (http://www.biofabresearch.it/index2.html) using the following primers:

T3 universal primer 5'AGCACCTGCAGCTCTTCACT3'

T7 universal primer 5'TAATACGACTCACTATAGGG3'

3.2.5 Cloning the D-REEP1 wt cDNA, and P19R D-REEP1 cDNA in pUAST plasmid

pUAST plasmid (Appendix C), D-REEP1 wt cDNA and D-REEP1 cDNA carrying the P19R mutation in pcDNA3.1/Zeo(+) were digested with EcoRI and XbaI restriction enzymes in the following reactions:

Component	Volume/ 50 ul reaction	Component	Volume/ 50 ul reaction
D-REEP1cDNA/ pcDNA3.1/Zeo(+) (50ng/ul)	20 ul	pUAST plasmid (100ng/μl)	5 ul
EcoRI (10U/ul)	2 ul	EcoRI (10U/ul)	2 ul
XbaI (10U/ul)	2 ul	XhoI (10U/ul)	2 ul
10X L buffer	5 ul	10X L buffer	5 ul
H_2O	to 50 ul	H_2O	to 50 ul

Mixed products were incubated at 37°C for 1 hour and successively separated by electrophoresis through a 1% agarose gel. The bands corresponding to the D-REEP1 cDNA and pUAST plasmid were cut from gel and purified using the QIAquick Gel Extraction Kit (Qiagen). Purified DNA products were eluted in 10 μl of elution buffer.
The two purified DNA fragments were ligated as follows:

Component	Volume/ 10 ul reaction
Purified pUAST plasmid (100ng/ul)	1 ul
PurifiedD-REEP1 cDNA fragment (50 ng/ul)	4 ul
10X Ligation buffer	1 ul
Ligase enzyme (Invitrogen)	2 ul
H_2O	to 10 ul

The mixture was incubated at 16°C for 1 hour.

3.2.6 Cloning the H-REEP1 wt cDNA, A132V H-REEP1 cDNA and P19R H-REEP1 cDNA in pUAST plasmid

pUAST plasmid (Appendix C), H-REEP1 wt cDNA and H-REEP1 cDNA carrying P19R and A132V mutations, in pcDNA3.1/Zeo(+) were digested with EcoRI and XhoI restriction enzymes in the following reactions

Component	Volume/ 50 ul reaction	Component	Volume/ 50 ul reaction
D-REEP1cDNA/ pcDNA3.1/Zeo(+) (50ng/ul)	20 ul	pUAST plasmid (100ng/μl)	5 ul
EcoRI (10U/ul)	2 ul	EcoRI (10U/ul)	2 ul
XbaI (10U/ul)	2 ul	XhoI (10U/ul)	2 ul
10X L buffer	5 ul	10X L buffer	5 ul
H_2O	to 50 ul	H_2O	to 50 ul

Mixed products were incubated at 37°C for 1 hour and successively separated by electrophoresis through a 1% agarose gel. The bands corresponding to the H-REEP1 cDNA and pUAST plasmid were cut from gel and purified using the QIAquick Gel Extraction Kit (Qiagen). Purified DNA products were eluted in 10 μl of elution buffer.

Transformation

Ligation mixture was used for transformation of chemically competent DH5 alpha cells (Invitogen). Transformed bacteria were plated on LB–ampicillin agar plates and incubated overnight at 37°C.
10 colonies were grown in LB medium with ampicillin. Plasmid DNA was successively purified by minipreparation protocol (Appendix A 3.8) and tested by restriction analysis for the right insertion.

Plasmid purification

D-REEP1/pUAST, P19R D-REEP1/pUAST, H-REEP1/pUAST, P19R H-REEP1/pUAST, A132V H-REEP1/pUAST plasmids were purified from an overnight culture using a "Midi" plasmid purification kit, according to Qiagen Plasmid Midi purification protocols. The final pellet was re-suspended in 50 ul of TE buffer.

3.3 REAL TIME PCR

Set up reactions on ice. Volumes for a single 50-µl reaction are listed below.
For multiple reactions, prepare a master mix of common components, add the appropriate volume to each tube or plate well on ice, and then add the unique reaction components. Preparation of a master mix is crucial in qRT-PCR to reduce pipetting errors.

Component	**Single reaction**
SuperScript® III RT/Platinum® *Taq* Mix (includes RNaseOUT™)	1 µl
2X SYBR® Green Reaction Mix	25 µl
Forward primer, 10 µM	1 µl
Reverse primer, 10 µM	1 µl
ROX Reference Dye (optional)	1 µl/0.1 µl
Template (1 pg to 1 µg total RNA)	≤ 10 µl
DEPC-treated water to	50 µl

To test for genomic DNA contamination of the RNA template, prepare a control reaction containing 2 units of Platinum® *Taq* DNA Polymerase (catalog no. 10966-018) instead of the SuperScript® III RT/Platinum® *Taq* Mix.

Cap or seal the reaction tube/PCR plate, and gently mix. Make sure that all components are at the bottom of the tube/plate; centrifuge briefly if needed.

Place reactions in a preheated real-time instrument programmed as described above. Collect data and analyze results.

Primers for D-REEP1 amplification:

Forward primer	GCGGCCGCATGATCAGCAGCCTGTTTTC
Reverse primer	CCAGTACATCATTCATTTAACATATTC

Primers for rp49 housekeeping gene amplification:

Forward primer	AGGCCCAAGATCGTGAAGAA
Reverse primer	TCGATACCCTTGGGCTTGC

3.4 CELLULAR BIOLOGY

3.4.1 Cells culture

HeLa cell culture was derived from a cervical carcinoma of a 31 years old african-american woman. This was the first aneuploid line derived from human tissue maintained in continuous cell culture.

COS7 cell line was obtained by immortalizing a CV-1 cell line derived from kidney cells of the African green monkey with a version of the SV40 genome that can produce large T antigen but has a defect in genomic replication.

Propagation and subculturing

HeLa and Cos7 cells were grown in complete DMEM medium (see Appendix B) with 10% FBS serum and antibiotics, at 37°C in a CO_2 incubator.

Cells were passaged when growing logarithmically (at 70 to 80 % confluency) as follows:

- The cell layer was briefly washed twice with PBS to remove all traces of serum, then trypsin solution (see Appendix B) was added to flask and cells were observed under an inverted microscope until cell layer was dispersed (usually within 5 minutes).
- Complete growth medium was added to stop trypsin action, cells were aspirated by gently pipetting and diluted 1:10 into a new flask with new complete medium.
- For cell count, an aliquot of the cell suspension, before plating, was mixed 1:1 with a solution of 0.1% Trypan blue (Sigma) in PBS. Trypan blue is a vital stain used to selectively colour dead cells. In a viable cell Trypan blue is not absorbed, however it traverses the membrane in a dead one. Hence, dead cells are shown as a distinctive blue colour under a microscope. 10 ul of the above mixture was charged on a counting chamber and viable cells in the "counting squares" were counted. The cells density was calculated as follows: average of counted cells/ counting square X 10^4 X dilution factor (=2) = number of cells/ml.

3.4.2 Plasmid DNA Transfection

To introduce expression plasmids into HeLa and Cos7 cells *TransIT-LT1*® Transfection Reagent (Mirus) was used. Transfection Reagent is a mix of cationic lipids. The basic structure of cationic lipids consists of a positively charged head group and one or two hydrocarbon chains. The charged head group governs the interaction between the lipid and the phosphate backbone of the nucleic acid, and facilitates DNA condensation. The positive surface charge of the liposomes also mediates the interaction of the nucleic acid and the cell membrane, allowing for fusion of the liposome/nucleic acid ("transfection complex") with the negatively charged cell membrane. The transfection complex is thought to enter the cell through endocytosis. Once inside the cell, the complex must escape the endosomal pathway, diffuse through the cytoplasm, and enter the nucleus for gene expression.

Protocol

In a six-well, one day before transfection, 2 x 10^5 cells were plated in 1,5 ml of DMEM medium without antibiotics so that cells were 90-95% confluent at the time of transfection.

For each transfection sample, the complexes were prepared as follows:

- ✓ DNA (2-3ug) was diluted in 250 µl of DMEM medium without antibiotics and serum and mixed gently.
- ✓ *TransIT-LT1* was mixed gently before use, then 8ul were diluted in 250 µl of DMEM medium without antibiotics and serum. The sample was incubated for 5 minutes at room temperature.
- ✓ After the 5 minute incubation, the diluted DNA was combine with the diluted *TransIT-LT1* (total volume = 500 µl), mixed gently and incubated for 20 minutes at room temperature.

The 500 µl of complexes were added to each well containing cells and medium.

Cells were incubated at 37°C in a CO_2 incubator for 24 hours prior to testing for transgene expression.

3.4.3 Immunocytochemestry (ICC)

For immunocytochemistry, the day before transfection cells were plated on a glass coverslip previously sterilized with ethanol.

The procedure used is divided into the below steps:

Fixation

One day after transfection, the cells were fixed in 4% paraformaldehyde in PBS pH 7.4 for 10 minutes at room temperature. The cells were then washed tree times with PBS to eliminate paraformaldehyde.

Permeabilization

To permeabilize cell membranes and improving the penetration of the antibody, the cells were incubated for 10 minutes with PBS containing 0.1% Triton X-100 (Applichem).

Blocking and Incubation

Cells were incubated with 10% serum in PBS for 10 minutes to block non specific binding of the antibodies.

Primary antibodies, diluted in PBS with 5% serum, were applied for 1 hour in a humidified chamber at 37°C. Cells were washed three times with PBS and then secondary antibodies, diluted in PBS, were applied for 1 hour in a humidified chamber at 37°C.

Mounting and analysis

Coverslips were mounted with a drop of the mounting medium Mowiol (Sigma). Images were collected with a Nikon C1 confocal microscope and analysed using either Nikon EZ-C1 (version 2.1) or NIH ImageJ (version 1.32J) softwares.

Primary antibodies used	**Dilution**
Anti REEP1 rabbit (Proteintech Europe)	1:200
Anti c-Myc rabbit (Sigma)	1:200
Anti HA rabbit (Sigma)	1:200
Anti c-Myc mouse (Sigma)	1:200
Anti HA mouse (Sigma)	1:200
Anti calnexin rabbit (Santa Cruz Biotechnology)	1:200
Anti PDI mouse (BD biosciences)	1:100
Anti GM130 mouse (BD biosciences)	1:200
Anti-ubiquitin rabbit (Chemicon)	1:200
Anti GM130 mouse (BD biosciences)	1:200
Anti apo-B100 rabbit (Calbiochem)	1:100
Anti-GFP mouse (Sigma A*ldrich*)	1:200
Anti LAMP2 rabbit (Sigma A*ldrich*)	1:100
Anti-ALDI rabbit (Acris Antibody)	1:100

Secondary antibodies used	**Dilution**
DyLight™488 anti rabbit (Jackson Immuno Research	1:1000
DyLight™488 anti mouse (Jackson Immuno Researcl	1:1000
Cy™3 anti mouse (Jackson Immuno Research)	1:1000
DyLight™549 anti rabbit (Jackson Immuno Research	1:1000
DyLight™649 anti mouse (Jackson Immuno Researcl	1:1000
DyLight™649 anti rabbit (Jackson Immuno Research	1:1000

Markers	**Dilution**
BODIPY 493/503 (Invitrogen)	1:1000
Mito Tracker Orange CMTMRos (Invitrogen)	1:1000

3.4.4 Selective membrane permeabilization

In order to determine the right topology of REEP1 protein, cells were selectively permeabilized for the plasma membrane and subsequently treated with protease. This assay is based on the accessibility of proteases to exposed polypeptides versus their inaccessibility to polypeptides that are located in protected intracellular regions such as the lumen of organelles. We use the cholesterol binding drug digitonin, a toxin derived from the plant *Digitalis purpurea* for the selective permeabilzation. The selectivity of this cell surface permeabilization results from the fact that the plasma membrane has the highest concentration of cholesterol, which renders the cell surface the prime target for digitonin intercalation with very few effects on intracellular membranes

- Cells were transfected with pcDNA3.1 expressing GFP-REEP1 protein (GFP tag located at the N-terminal).
- One day after transfection, the cells were washed cells three times for 1 min each in KHM buffer and fixed in 4% paraformaldehyde in PBS pH 7.4 for 10 minutes at room temperature
- To permeabilize the plasma membrane, the same volume of KHM buffer containing digitonin 20 mM was added to the cells for 10–60 s.
- Cells were washed in KHM buffer (optional) and then 4–8 mM of the protease trypsin (in KHM buffer) was directly added on to the cells.
- Primary antibodies, diluted in PBS with 5% serum, were applied for 1 hour in a humidified chamber at 37°C. Cells were washed three times with PBS and then secondary antibodies, diluted in PBS, were applied for 1 hour in a humidified chamber at 37°C

3.5 BIOCHEMICAL TECHNIQUES

3.5.1 Co-Immunoprecipitation (co-IP)

Co-immunoprecipitation (Co-IP) is a common technique for protein interaction discovery.

An antibody for the protein of interest, linked to a support matrix, is incubated with a cell extract so that the antibody will bind the protein in solution. The antibody/antigen complex will then be pulled out of the sample: this physically isolate, from the rest of the sample, the protein of interest and other proteins potentially bound to it. The sample can then be separated by SDS-PAGE for Western blot analysis.

In Co-IP experiments, anti-Myc agarose conjugate (Sigma) was used. Anti-c-Myc agarose conjugate is prepared with an affinity purified anti-c-Myc antibody coupled to cyanogen bromide-activated agarose. The purified antibody is immobilized at 1.0 to 1.5 mg antibody per ml agarose. Anti-c-Myc antibody is developed in rabbit using a peptide corresponding to amino acid residues 408-425 of human c-Myc as the immunogen.

Anti-c-Myc antibody recognizes the epitope located on c-Myc tagged fusion proteins and it reacts specifically with N- and C terminal c-Myc-tagged fusion proteins.

The co-immunoprecipitation procedure used the following:

- 10^6 cells, plated on a six wells plate, were harvested using 0.5% Triton X-100 (Applichem) in PBS, incubated in ice for 15 minutes and then centrifuged at 16000g for 15 minutes.
- 30 ul of anti-c-Myc agarose conjugate suspension was added to a microcentrifuge tube and washed 5 times with PBS by a short spin.
- Cell extract (lysate) was added to the resin and incubated for 2 hours on an orbital shaker at room temperature.
- At the end of incubation time, the supernatant was recovered and the resin was washed 5 times with PBS.
- After the final wash, 70 ul of 1X Laemmli buffer (see Appendix B) were added to the resin and incubated at 95°C for 5 minutes.
- After boiling, the sample was vortexed and then centrifugated for 5 seconds (pellet).
- The presence of the c-Myc tagged protein and of other proteins potentially bound to it was detected in lysate, supernatant and pellet by Western blotting.

3.5.2 Immunoisolation of membrane vesicles and membrane fractionation

To obtain harbouring vesicles, the sample were prepared as follows:

- 10^6 transfected cells, plated on a six wells plate, were suspended in homogenization buffer (10 mM HEPES-KOH buffer pH 7.4 containing 0.22 M mannitol, 0.07 M sucrose and protease inhibitors) and homogenized using a syringe with a 26-gauge needle.
- Homogenate was sonicated and the supernatant containing vesiculated membranes recovered by centrifugation at 4000g for 5 minutes at 4°C in order to remove unbroken organelles.
- When required, the vesiculated membranes were mixed with another pool of harbouring vesiscles and incubated at 30°C for 1 hour.
- After incubation, immunoprecipitation of the harbouring vesicles was performed as described above (3.5.1).
- The remaining supernatants containing vesiculated membranes were centrifugated at 120000 g for 60 minutes to separate a membrane fraction (pellet) and a soluble fraction (supernatant).
- Supernatant and pellet derived from the immunoprecipitation and 100000 g centrifugation were analysed by western blotting.

3.5.3 REEP1 Membrane topology by membrane fractionation

To determine the right membrane topology of REEP1 protein, membrane vesicles were isolated as above (chapter 1.3.2) and the sample was prepared as follow:
The membrane fraction (pellet) was resuspended in homogenization buffer. The sample was divided into two parts: in one part of which 250 uM of protease K were added and incubated at 37°C for 15 minutes. The samples were analysed by western blotting.

3.5.4 SDS PAGE

SDS-PAGE stands for Sodium dodecyl sulfate (SDS) polyacrylamide gel electrophoresis (PAGE) and is a method used to separate proteins according to their size. Since different proteins with similar molecular weights may migrate differently due to their differences in secondary, tertiary or quaternary structure, SDS, an anionic detergent, is used in SDS-PAGE to reduce proteins to their primary (linearized)

structure and coat them with uniform negative charges: proteins having identical charge to mass ratios are fractionated by size.

Gel making

The resolving gel was prepared with a 10% polyacrylamide content, while the stacking gel had a 5% acrylamide concentration.

Components	Resolving gel	Stacking gel
Acrylamide solution (Fluka)	10% (v/v)	5% (v/v)
Tris-HCl pH 8.8	0.37M	
Tris-HCl pH 6.8		0.125M
Ammonium persulphate	0.1% (w/v)	0.1% (w/v)
SDS	0.1% (w/v)	0.1% (w/v)
TEMED	0.02% (v/v)	0.02% (v/v)

Sample preparation

Samples were diluted in Laemli buffer (Appendix B) and then boiled at 95°C for 5 minutes.

Running the electrophoresis

The amperage applied was 15mA/gel until the proteins reached the resolving gel, and then it was increased to 25mA/gel.

Western blotting

After the electrophoresis, the proteins were transferred from gel to PVDF membrane (Amersham Biosciences).
The membrane was blocked with a solution of 10% milk in TBS-T (Appendix B) for 15 minutes at room temperature on a shaking platform.
The membrane was then incubated with the primary antibody diluted to the appropriate concentration in TBS-T and milk 2%, at 4°C O/N.

The secondary antibody diluted to the appropriate concentration in TBS-T was added and incubated for 1 hour at room temperature.
The membrane detection was performed by ECL plus kit (Amersham Biosciences).

Primary antibodies used	Dilution
Anti c-Myc mouse (Sigma)	1:1000
Anti HA mouse (Cell Signalling)	1:1000
Anti PDI mouse (BD biosciences)	1:500
Anti calnexin rabbit (Millipore)	1:1000
Anti caveoline rabbit (Abcam)	1:1000
Anti-α-actin mouse (sigma)	1:1000

Secondary antibodies used	Dilution
Anti mouse-HRP (Dako)	1:10000
Anti rabbit-HRP (Dako)	1:10000

3.6 DROSOPHILA *MELANOGASTER* LIFE CYCLE

Fruit flies begin their lives as an embryo in an egg. This stage lasts for about one day. During this time, the embryo develops into a larva. The first instar larva hatches out of the egg, crawls into a food source, and eats. After a day, the first instar larva molts and becomes the second instar larva. After two days in this stage, the larva molts again to become the third instar larva. After three days of eating in this stage, the larva crawls out of the food source and molts again. Following this molt, the larva stops moving and forms a pupa. *Drosophila* stays in the pupa for about five days. During this time, the metamorphosis, or change, from larva to adult is occurring. Adult structures like wings, legs, and eyes develop. When the adults emerge from the pupa they are fully formed. They become fertile after about ten hours, copulate, the females lay eggs, and the cycle begins again. The whole life cycle takes about 12-14 days (Figure 3).

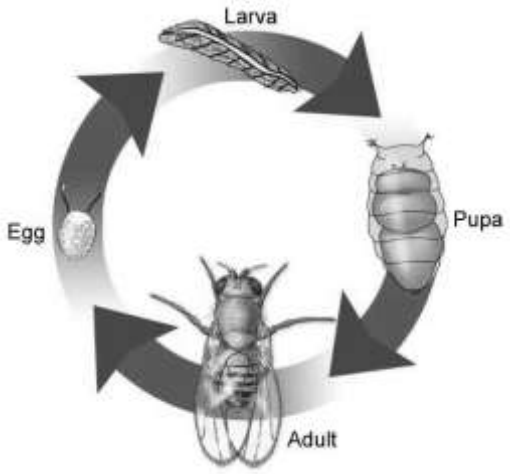

Figure 3. *Drosophila melanogaster* life cycle

3.6.1 Microinjection

Preparing the DNA for microinjection

Injection mix	Final concentration
Construct plasmid	3 μg/μl
Helper plasmid	1 μg/μl
10XMicroinjecting buffer	1X

(Appendix B 3.9)

The mix is filtered through a 0.2 μm filter.

The helper plasmid is a source of P-element transposase that allows the insertion of DNA construct into the fly genome.

Fly strains

A white mutant strain, w1118 (phenotype white eyes) was used in this protocol to allow detection of transgenic flies carrying white gene (phenotype red/orange eye). These flies were used both as a source of embryos for the injection and as a backcross stock to amplify the transformants.

Needles Preparation

The quality of the needles is critical for high through-put. Needles should be pulled on any horizontal puller of the Sutter brand series using 1.0 mm OD borosilicate capillaries with omega dot fiber (WPI). The settings will be different for each machine and will need to be updated each time the heating filament is replaced or re-shaped, or a new type of capillaries is used. Several parameters influence the shape and properties of the needle and the effect produced by changing any of them (heat, velocity of pull, pressure of gas flow, number of steps) is difficult to predict. However, a paper by (Miller, Holtzman et al. 2002) is a very useful guideline for designing suitable needles. The needle should be progressively but shortly tapered and have no discontinuity or step. Needles that are too elongated will bend and brake when impaling the chorion. The condition used for our contruct microinjection are: Heat=414 Pull=200 Vell=250 Time=150

Embryo collection

Embryos must be injected before blastoderm cellularization, a developmental stage that begins 45-50 minutes after eggs are laid at 22°C. Cellularization is easily visible at the microscope, and such old embryos should not be injected. They should be killed by piercing them with the injection needle. Injections should be performed during the first 45 minutes after egg laying.

Preparing the embryos

Clean embryos were transferred in a small quantity of water to the centre of the coverslip with a clean thin pointed brush. 100 moist embryos were lined up with the dissection needle, one at a time, near one edge of the coverslip, with the posterior pole pointing to the edge. Embryos were let to dry for a few minutes to attach them firmly to the coverslip and then covered with as little halocarbon oil mix as possible. After 5-10 min the oil has penetrated between the chorion and the vitelline membrane clearing the embryo and allowing a rough staging under the dissecting scope.

Microinjection

The injection set-up consists of two parts: an inverted microscope (Nikon) equipped with a 20X lens and a micromanipulator InjectMan (Eppendorf) linked to the FemtoJet air-pressure injecting device (Eppendorf) connected to the needle holder. A set-up was installed in a cool room (18˚/20°C) to give more time flexibility as the embryos develop more slowly and the appropriate stage for injection lasts longer. The microinjection of the embryos was completely automatic, the needle was inserted quickly in the centre of the posterior pole were the germ cells will form, and pulled out quickly to avoid any leakage.

After the injection

Most of oil was drained off the coverslip and it was transferred to a food vial, placing the edge with the embryos against the food. The vials were kept at 18° C for two days then larvae were collected and transferred in vials of standard food and maintained at room temperature until adults hatched.

Back-crossing the injected flies

Hatching adults (F0) were separated by sex. Each male was crossed to 2 virgin w1118 females and each female, even if obviously not virgin, to 2 or more w1118 males. Crosses were performed in separate vials of standard food. When at least 20-50 adult F1 flies hatched in each vial they were screened to look for transformants individual. Transgenic flies (red eyes individuals) were crossed again with w1118 flies and with balancer lines.

Characterization of transgenic lines

F1 individuals may bear one transgene insertion on any of the chromosomes: X, II or III. Transgenes inserted on the fourth chromosome are very rare as this chromosome is rather small and essentially heterochromatic.
The transgene should be immediately placed in front of a balancer chromosome, to avoid its loss.

If the insertion lays on the second chromosome the fly is crossed with the Sm6/TfT balancer stock (carrying the dominant morphological marker curly wing) as the schema reported below.

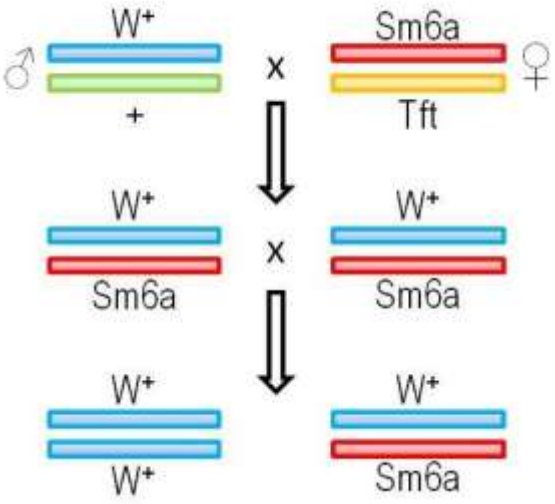

Figure 4. Cross with II chromosome balancer

If in F2 progeny there are individuals with white eyes the insertion is localized on another chromosome.

If the insertion lays on the third chromosome, the fly is crossed with the TM3/TM6 balancer stock (carrying the dominant morphological marker stubble hairs) as the schema reported below.

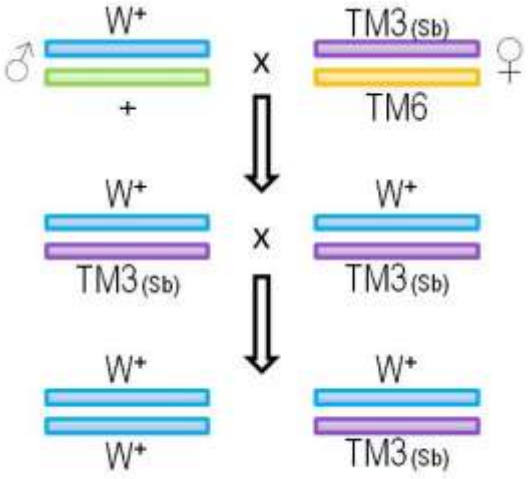

Figure 5. Cross with III chromosome balancer

If in F2 progeny there are individuals with white eyes the insertion is localized on another chromosome.

If the insertion lies on the X chromosome the fly is crossed with the Fm7/Sno balancer stock (carrying the dominant morphological marker heart- shaped eyes) as the schema reported below.

If the insertion is occurred in the X chromosome, all the F1 females have w^{+}/FM7 phenotype.

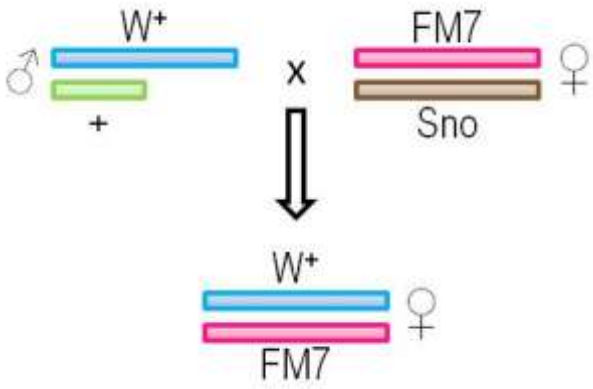

Figure 6. Cross with X chromosome balancer

Drosophila genetics

Drosophila strains used: elav-Gal4, D42-Gal4, GMR-Gal4, tubulin-Gal4, nanos-Gal4:VP16, UAS-mCD8-GFP (Bloomington); UAS-aCOP-RNAi, UAS-Sar1- RNAi (VDRC); MHC-Gal4; Mef2-Gal4; armadillo-Gal4; pUASp:Lys-GFPKDEL, pUASp:GalT-GFP and Sar1-GFP. Control genotypes varied depending on individual experiments, but always included promoter-Gal4/+ and UAS-transgene/+ individuals.

3.7 TECHNIQUES FOR PHENOTYPIC ANALYSIS

3.7.1 Immunohistochemistry

Immunostaining was performed on wandering third instar larvae reared at 25°C.

Larvae dissection

Wandering third instar larvae were raised at 25°C. After harvesting larvae, they were dissected dorsally in standard saline and fixed in 4% paraformaldeyde for 45 min. Preparations were subsequently washed in phosphate-buffered saline (PBS) containing 0.5% bovine serum albumin.

Antibodies

The following antibodies were used: mouse anti-Myc (1:500, Cell Signaling), rabbit anti-Myc (1:200, Santa Cruz Biotechnology), mouse anti-HA (1:1,000, Cell
ignaling), rat anti-BiP (1:50, Babraham), mouse anti-p120 (1:600, Calbiochem), mouse anti-GFP (1:500, Roche), mouse anti-Dlg (1:100, DSHB), mouse anti-PDI (1:500, Stressgen), rabbit anti-calnexin (1:1,000, Millipore). Secondary antibodies for immunofluorescence (Cy5 and Cy3 conjugates from Jackson laboratories, Alexa Fluor 488 conjugates from Invitrogen) were used at 1:1,000. Anti-mouse, anti-guinea pig and anti-rabbit

Image analysis

Confocal images were acquired through x40 or x60 CFI Plan Apochromat Nikon objectives with a Nikon C1 confocal microscope and analysed using the NIS 2. METHODS 44.
Elements software (Nikon). Figure panels were assembled using Adobe
Photoshop CS4.

3.7.2 Electron microscopy

Drosophila third instar larva brains were fixed in 4% paraformaldehyde and 2% glutaraldehyde and embedded as described. EM images were acquired from thin sections under a FEI Tecnai-12 electron microscope. EM images of individual neurons for the measurement of the length of ER profiles were collected from three brains for each genotype. At least 20 neurons were analyzed for each genotype. Quantitative analyses were performed with ImageJ software

HRP conjugates from DACO were used at 1:10,000 Image analysis

Images were collected with a Nikon C1 confocal microscope and analyzed using either Nikon EZ-C1 (version 2.10) or NIH ImageJ (version 1.32J) softwares.

3.7.3 *Drosophila* Driver lines

D-REEP1 and H-REEP1 transgenic lines were tested using different Gal4 driver lines. The Gal4 activator lines used in this study were GMR-Gal4, Tubulin-Gal4, Elav-Gal4, MEF2-Gal4 and D42-Gal4 (Bloomington Stock Center, Indiana University). All experimental crosses were performed at 25°C.

3.8 APPENDIX A: GENERAL PROTOCOLS

Transformation of chemiocompetent cells

- Gently thaw the chemiocompetent cells on ice.
- Add ligation mixture to 50 µl of competent cells and mix gently. Do not mix by pipetting up and down.
- Incubate on ice for 30 minutes.
- Heat-shock the cells for 30 seconds at 42°C without shaking.
- Immediately transfer the tube to ice.
- Add 450 µl of room temperature S.O.C. medium.
- Cap the tube tightly and shake the tube horizontally (200 rpm) at 37°C for 1 hour.
- Spread 20 µl and 100 µl from each transformation on prewarmed selective plates and incubate overnight at 37°C.

Preparation of plasmid DNA by alkaline lysis with SDS: minipreparation

Plasmid DNA may be isolated from small-scale (1-3 ml) bacterial cultures by treatment with alkali and SDS.

- Inoculate 3 ml of LB medium (Appendix B) containing the appropriate antibiotic with a single colony of transformed bacteria. Incubate the culture overnight at 37°C with vigorous shaking.
- Pour 1.5 ml of the culture into a microfuge tube. Centrifuge at maximum speed for 30 seconds in a microfuge. Store the unused portion of the original culture at 4°C.
- When centrifugation is complete, remove the medium by aspiration, leaving the bacterial pellet as dry as possible.
- Resuspend the bacterial in 100 µl of ice-cold Alkaline lysis solution I (Appendix B) by vigorous vortexing.
- Add 200 µl of freashly prepared Alkaline lysis solution II (Appendix B) to each bacterial suspension. Close the tube tightly, and mix the contents by inverting the tube rapidly five time. Do not vortex. Store the tube on ice.
- Add 150 µl of ice-cold Alkaline lysis solution III (Appendix B). Close the tube and disperse Alkaline lysis solution III through the viscous bacterial lysate by inverting the tube several times. Store the tube on ice 3-5 minutes.
- Centrifuge the bacterial lysate at maximum speed for 5 minutes at 4°C in a microfuge. Transfer the supernatant to a fresh tube.
- Precipitate nucleic acids from the supernatant by adding 2 volumes of ethanol at room temperature. Mix the solution by vortexing and then allow the mixture to stand 2 minutes at room temperature.
- Collect the precipitate of nucleic acid by centrifugation at maximum speed for 10 minutes at 4°C in a microfuge.
- Remove the supernatant by gentle aspiration. Stand the tube in an inverted position on a paper towel to allow all of the fluid to drain away. Use a pipette tip to remove any drops of fluid adhering to the walls of the tube
- Add 2 volumes of 70% ethanol to the pellet and invert the closed tube several times. Recover the DNA by centrifugation at maximum speed for 5 minutes at 4°C in a microfuge.
- Again remove all the supernatant by gentle aspiration.
- Dissolve the nucleic acids in 50 ul of TE buffer (pH 8.0) or distillated autoclavated water containing 20 ug/ml DNase-free RNase A (pancreatic

RNase). Vortex the solution gently for a few seconds. Store the DNA solution at -20°C.

3.9 APPENDIX B: STOCKS AND SOLUTIONS

LB Medium (Luria-Bertani Medium)

Bacto-tryptone	10g
Yeast extract	5g
NaCl	10g
H_2O	to 1 Liter

Autoclave.

LB Agar

Bacto-tryptone	10g
Yeast extract	5 g
NaCl	10 g
Agar	20g
H_2O	to 1 Liter

Adjust pH to 7.0 with 5 N NaOH. Autoclave.

LB–Ampicillin Agar

Cool 1 Liter of autoclaved LB agar to 55° and then add 10 ml of 10 mg/ml filter-sterilized Ampicillin. Pour into petri dishes (~25 ml/100 mm plate).

SOC medium

Bacto-tryptone	20g
Yeast extract	5 g
NaCl	0,5 g
KCl 1M	2,5 ml
H_2O	to 1 Liter

Adjust pH to 7.0 with 10N NaOH, autoclave to sterilize, add 20 ml of sterile 1 M glucose immediately before use.

Alkaline lysis solution I

Glucose 50 mM
Tris HCl 25 mM (pH 8.0)

EDTA 10 mM (pH 8.0)
Solution I can be prepared in batches of approximately 100 ml, autoclaved for 15 minutes and stored at 4 °C.

Alkaline lysis solution II

NaOH 0.2 N (freshly diluted from a 10 N stock)
SDS 1% (w/v)

Alkaline lysis solution III

Potassium acetate 3 M
Glacial acetic acid 11.5% (v/v)

TE Buffer

Tris-HCl 10 mM (pH 7.5)
EDTA 1 mM

DMEM complete medium

DMEM 4.5g/L Glucose with L-Glutamine (Lonza)
FBS 10% (v/v)
Penicillin-Streptomycin mixture 100X (Lonza, contains 5000 units potassium penicillin and 5000 ug streptomycin sulfate)

Phoshate Buffered Saline (PBS)

KH_2PO_4	1444 mg/L
NaCl	9000 mg/L
Na_2HPO_4	795 mg/L

Trypsin solution

Trypsin 2,5% 10X (Lonza)

Running buffer 1X

Tris 25mM
Glycine 250mM
SDS 0.1%

In deionized H_2O

Transfer buffer 1X

Tris 25mM
Glycine 192mM

In deionized H_2O

TBS-T buffer 1X

Tris 100mM
NaCl 1,5M
Tween-20 1%

In deionized H_2O

Laemmli buffer 2X

SDS 4%
Glycerol 20%
2-mercaptoethanol 10%
Bromphenol blue 0,004%
Tris HCl 125mM

The solution has a pH of approximately 6.8

10X injection buffer:

Sodium Phosphate Buffer pH 6.8 0.1M
KCl 5Mm

Drosophila's food

Agar	15 g
Yeast extract	46.3 g
Sucrose	46.3 g
H_2O	to 1 Liter

Autoclave and then add 2 g of Nipagine dissolved in 90% ethanol.

Egg laying food

Agar	6 g
Sucrose	6.6 g
Fruit juice	66 ml
H_2O	to 200ml

3.10 APPENDIX C: PLASMIDS

pDrive cloning vector (Qiagen)

The pDrive Cloning Vector provides superior performance through UA-based ligation and allows easy analysis of cloned PCR products.
This vector allows ampicillin and kanamycin selection, as well as blue/white colony screening. The vector contains several unique restriction endonuclease recognition sites around the cloning site, allowing easy restriction analysis of recombinant plasmids.
The vector also contains a T7 and SP6 promoter on either side of the cloning site, allowing *in vitro* transcription of cloned PCR products as well as sequence analysis using standard sequencing primers. In addition, the pDrive Cloning Vector has a phage f1 origin to allow preparation of single-stranded DNA

pcDNA3.1/Zeo(+) (Invitrogen)

pcDNA3.1/Zeo (+) is an expression vector, derived from pcDNA3.1, designed for high-level stable and transient expression in a variety of mammalian cell lines.
To this aim, it contains Cytomegalovirus (CMV) enhancer-promoter for high-level expression; large multiple cloning site; Bovine Growth Hormone (BGH) polyadenylation signal; transcription termination sequence for enhanced mRNA stability and Zeocin resistance coding region.

pUAST vector

pUAST is a P-element based vector that allows one to place the gene of interest under GAL4. pUASt consists of five tandemly arrayed optimized GAL4 binding sites followed by the hsp70 TATA box and transcriptional start, a polylinker containing unique restriction sites and the SV40 small T intron and polyadenylation site. These features are included in a P-element vector (pCaSpeR3) containing the P-element ends (P3' and P5') and the white gene which acts as a marker for successful incorporation into the *Drosophila* genome

3.11 APPENDIX D: CLINICAL PHENOTYPES OF HSP MUTATIONS CONSIDERED IN THIS STUDY

Patients carrying REEP1 p.P19R mutation presented an HSP pure, autosomal dominant form, with an early onset age. Clinical features of this patients are: severe spasticity, moderate weakness.

Patients carrying REEP1 p.D56N mutation presented an HSP pure, autosomal dominant form, with an early onset age. Clinical features of this patients are: moderate spasticity and weakness.

Patients carrying REEP1 p.A132V mutation presented an HSP pure, autosomal dominant form, with an late onset age. Clinical features of this patients are: slightly spasticity and weakness

4. RESULTS

4.1 4.1 CHARACTERIZATION OF THE *DROSOPHILA* HOMOLOG OF *SPG31 (H-REEP1)*

Using the amino acid sequence of human REEP1 protein isoform 1, we searched the whole *Drosophila* genomic sequence to identify homologous proteins employing the Blast software in the Flybase website (**flybase**.bio.indiana.edu/blast/). The blast search produced a highly significant alignment of human REEP1 to the protein encoded by the CG42678 gene (Figure 7). Similar to the human homolog, CG42678 consists of more than one alternative splicing isoform. It encodes nine annotated transcripts, CG42678-PD (435 aa), CG42678-PE (288 aa), CG42678-PG (288 aa), CG42678-PH (569 aa), CG42678-PI (716 aa), CG42678-PJ (570 aa), CG42678-PK (408 aa), CG42678-PL (151 aa), CG42678-PO (291 aa). The CG42678 gene (D-REEP1) localizes on the second chromosome. As reported in *Drosophila* data base, CG42678 gene has an expression peak observed within 12-18 embryonic stages and throughout the pupal period.

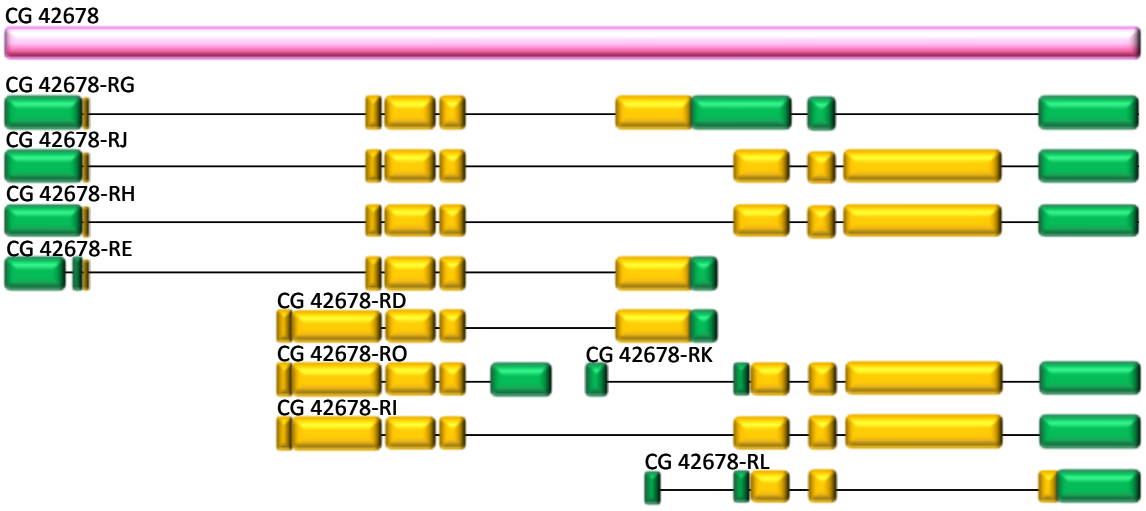

Figure 7. Schematic representation of D-REEP1 gene. The *Drosophila* homolog of H-REEP1 gene, localize on the second chromosome and codifies nine transcript isoformes**.**

Based on protein sequence alignment the CG42678-PG and the CG42678-PE are translated into the same polypeptide. This two isoforms show the highest homology with human REEP1, displaying a 67% of identity and 81% of similarity. Human REEP1 consists of two putative transmembrane domains and a conserved protein domain, TB2/DP1/HVA22 of unknown function. Domain sequence analysis showed that all of these domains are conserved in the *Drosophila* homolog (Figure 8). In order to alter the expression of D-REEP1 in a targeted manner in different tissue of *Drosphila*, we generated multiple, independent transgenic lines for the overexpression of the *wild-type* protein. Based on the existing genomic sequence, we have designed oligonucleotide primers to amplify the *D-REEP1* transcript CG42678-PG, the most similar form to H-REEP1 and generated the corresponding cDNA. For this purpose reverse transcription experiments were carried out on total RNA isolated from heads of *wild type* adults and subsequently D-REEP1 was cloned into pUAST plasmid for P-element mediated transgenic insertion.

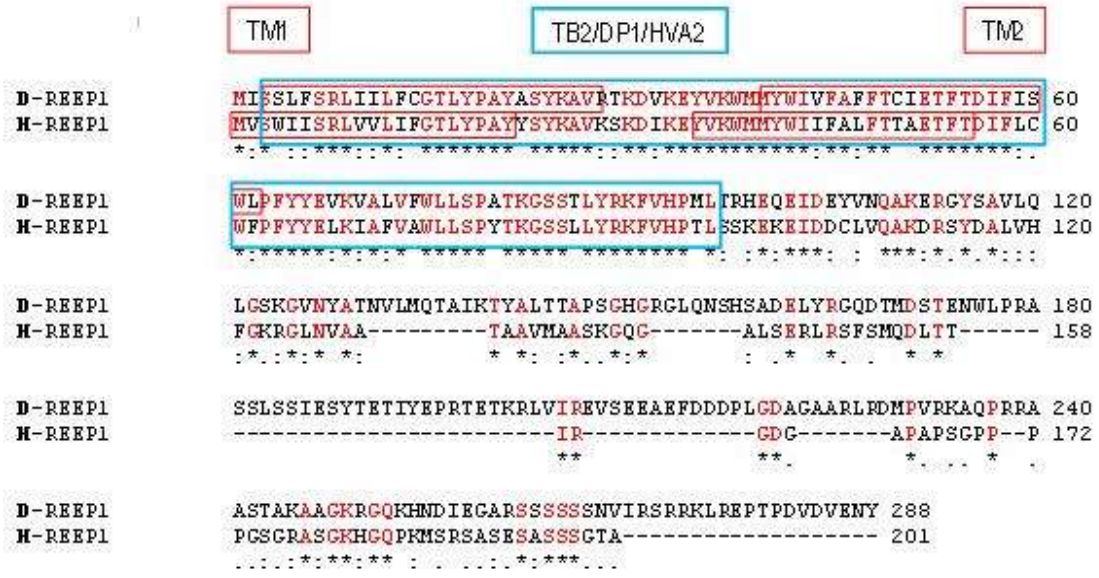

Figure 8. Alignment of human and *Drosophila* REEP1 protein sequence. The conserved amino acids are in red, blu and red boxes are the conserved domain of the protein**.**

4.2 D-REEP1 LOCALIZES TO THE ER

To determine D-REEP1 subcellular localization we generated transgenic *Drosophila* lines for expression of D-REEP1 fused with c-Myc tag at the C-terminal of the protein. We used an antibody against Myc tag for the immunolocalization of D-REEP1 protein. Immunohistochemistry experiments performed on third instar larva expressing ubiquitously UAS-D-REEP1 under the control of the tubulin-Gal4 driver showed that D-REEP1 signal overlapped the ER specific marker GPF-KDEL (Figure 9). To further confirm the D-REEP1 localization to the ER, we isolated the membrane fraction from cell homogenate. For this purpose the D-REEP1 cDNA was cloned in pcDNA3.1 for expression in mammal cell culture. We expressed D-REEP1 in HeLa cells. Transfected cells were homogenized in the absence of detergent and fragmented membranes were vesiculated by sonication. Fractionation of cleared cell homogenates showed that D-REEP1 and the ER integral membrane protein calnexin partitioned exclusively to the membrane fraction (Figure 9). These data demonstrates that *D-REEP1*, like the Human homolog, is an integral ER membrane protein.

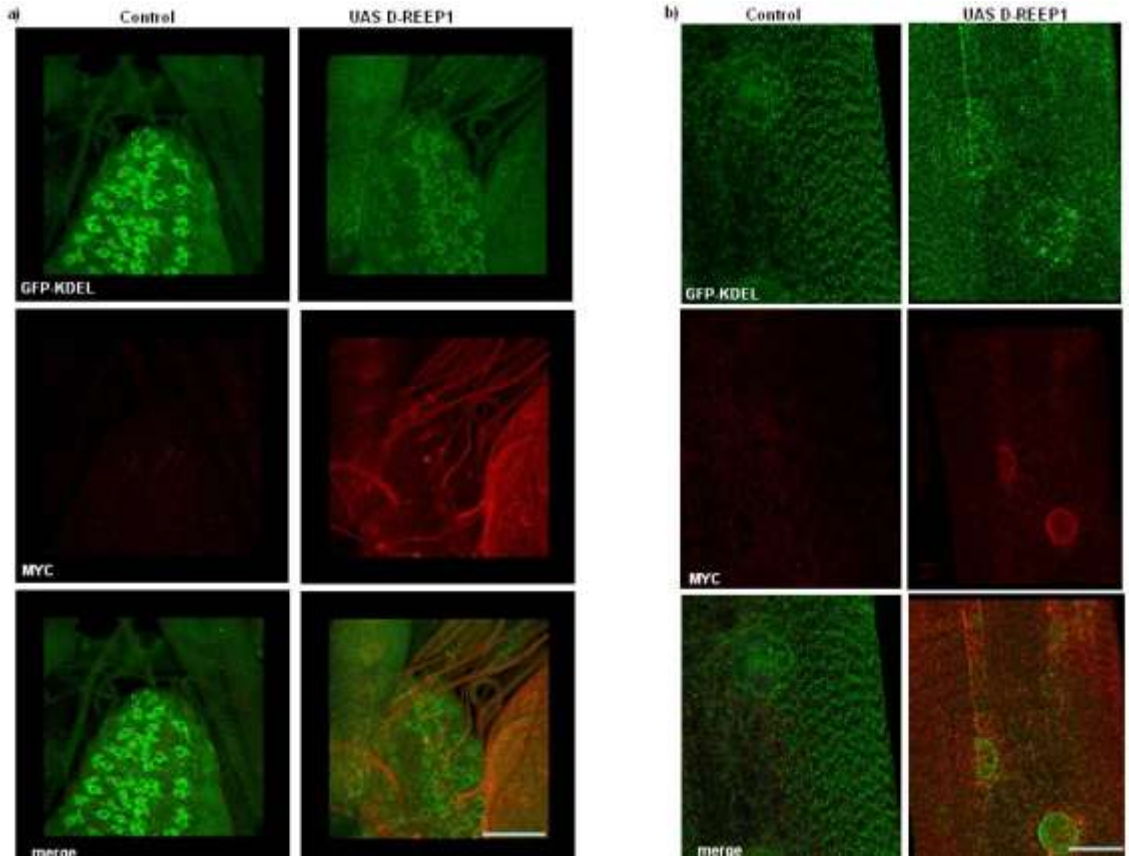

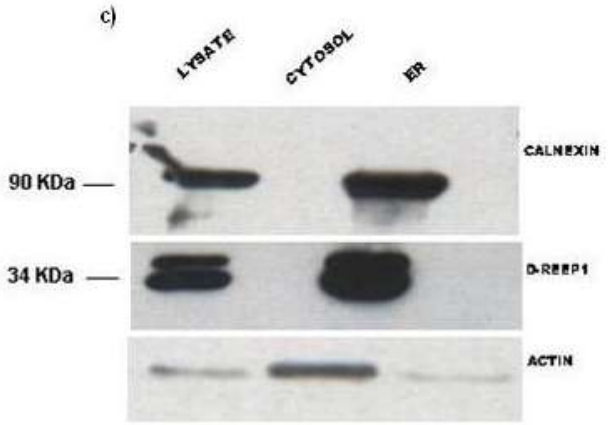

Figure 9. D-REEP1 localizes on ER membranes. (a)) Immunocytochemistry of third instar larval ventral ganglion (NSC) with anti Myc to label D-REEP1 expression GFP-KDEL to label the ER marker (b) Immunocytochemistry on third instar larva body wall muscles. D-REEP1 localizes with the ER marker KDEL. (c) Western blot analysis of the soluble and membrane fractions from HeLa homogenates over-expressing D-REEP1 protein. D-REEP1 band was detected at membrane fraction corresponding to ER together with ER membrane protein calnexin. Scale bar 20 µm.

4.3 CHARACTERIZATION OF D-REEP1 LOSS OF FUNCTION MUTANT

In order to study the biological role of D-REEP1 we analyzed a transgenic line, CG42678 ^{EP2014}, containing a transposable P-element insertion in the first intron of the *D-REEP1* gene. Insertions of P-elements in introns could affect transcription rates, alternative transcription start or stop sites, or the frequencies of different splicing patterns. Various *P*-element insertions have been reported to increase or decrease transcription rates or to change the timing or the location of expression. (Leland Hartwell et al. 2004). To verify the genomic insertion of the P-element, we extracted the genomic DNA from CG42678 ^{EP2014} flies and effectuated a direct sequencing (Figure 10). This analysis confirmed the P element insertion in the first intron of CG42678 gene, in the genomic DNA.

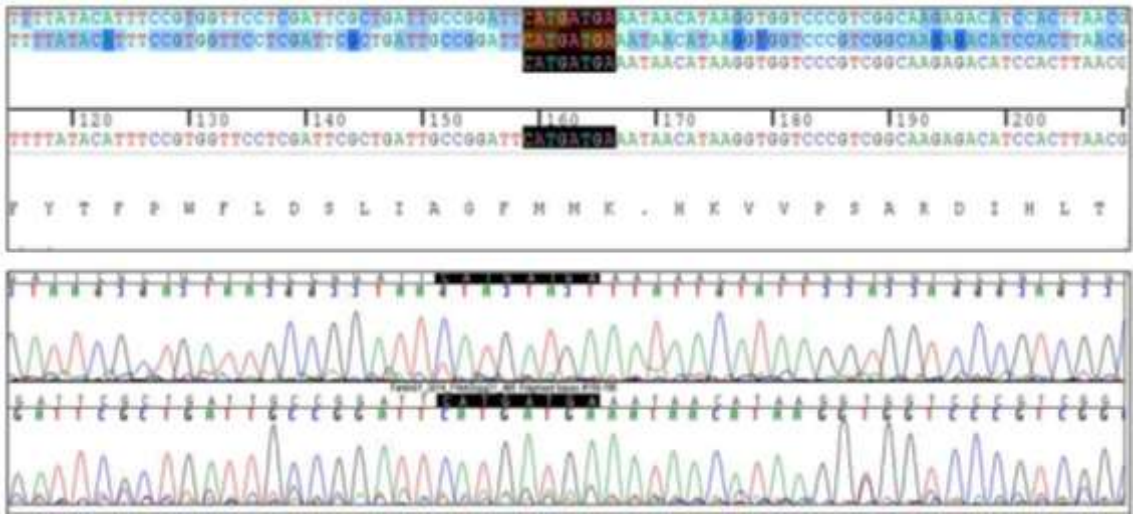

Figure 10. DNA chromatogram sequence of P element insertion site. Black boxes show the P element insertion in to the genome DNA of CG42678^{EP2014} flies.

In order to determine whether the presence of this P element could affect the CG24678 transcripts expression levels we performed a semi-quantitative RT PCR analysis from CG42678 ^{EP2014} flies. In a semi-quantitative PCR the PCR product is measured within the exponential phase of the PCR reaction, where the amount of amplified target is directly proportional to the input amount of target. Therefore the PCR must be carried out during the exponential phase (between cycles 25 and 30) of the PCR reaction and the plateau phase (>30 cycles) must be avoided. Total RNA was extracted from CG42678^{EP2014} and *wild type* flies, and semi-quantitative PCR was performed for target gene, *D-REEP1* and a housekeeping gene, D-GDPH. The amplified product were resolved in agarose gel and the band intensity signal was analyzed with ImageJ software (Java based program for image analysis, developed at the National Institute of Health). After RT-PCR of 35 cycles a band detectable in agarose gel, corresponding to D-REEP1 cDNA was amplified from both mutant and *wild type* RNA extract. However, after RT-PCR of 25 cycles D-REEP1 cDNA corresponding band, was not amplified from total RNA extracted from CG42678 ^{EP2014} flies. We analysed the band intensity signal of D-REEP1 cDNA PCR product compared to D-GDPH cDNA levels (Figure 11). This analysis showed that CG42678^{EP2014} have a significantly lower D-REEP1 cDNA levels that *wild type* flies.

To further confirm this result we performed a Real Time PCR analysis. Total RNA was extracted from adults CG42678 ^{EP2014} and *wild type* flies and analyzed. Real Time PCR was performed for *D-REEP1* gene and rp49 as housekeeping gene. The result obtained, confirmed the semi-quantitative PCR data. CG42678^{EP2014} flies showed a reduction of D-REEP1 mRNA levels to about 2% of its endogenous levels. (Figure 11). These data indicate that the P-element insertion in the first intron reduces the expression level of the D-REEP1 mRNA.

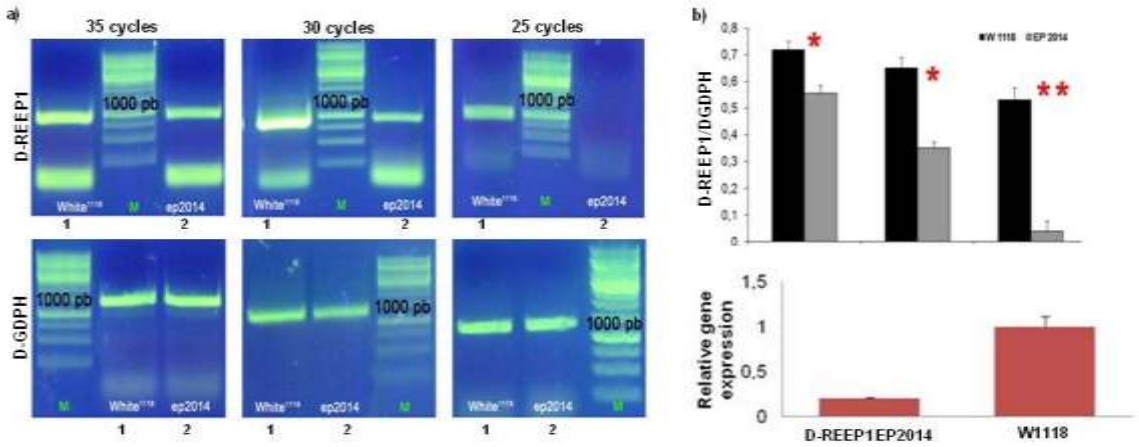

Figure 11. D-REEP1 expression levels. (a) Semiquantitative RT-PCR analysis of 35 cycles, 30 cycles and 25 cycles of amplification for D-REEP1 and D-GDPH as control, in *wild type* (1) and CG42678^{EP2014} flies (2). (b) D-REEP cDNA expression compared to D-GDPH, based on PCR band intensity. (c) Bar graph illustrating real time PCR, data demonstrating a reduction of D-REEP1 mRNA in CG42678^{EP2014} flies compared to the host gene rp49. Assays were performed in triplicate and results shown are representative of two independent experiments.

Phenotypic analysis of D-REEP1^{EP2014} flies showed that these mutants, though viable, display a developmental delay and exhibit morphological alterations of the wings. We compared the wings area of D-REEP1 mutant flies to the wings area *wild type.* As shown in figure 12, D-REEP1 mutant flies presented oversized wings. Measurement of wing area showed that D-REEP1 mutant flies wings are about 20% larger of wings of *wild type* flies. To demonstrate that the oversized wing phenotype was due to loss of D-REEP1 we performed rescue experiments by expressing *wild type* D-REEP1 in the D-REEP1 mutant background. In 90% of the cases, the presence of D-REEP1 rescued the phenotype, indicating that oversized wings of mutant flies is caused by loss of D-REEP1 (Figure 12).

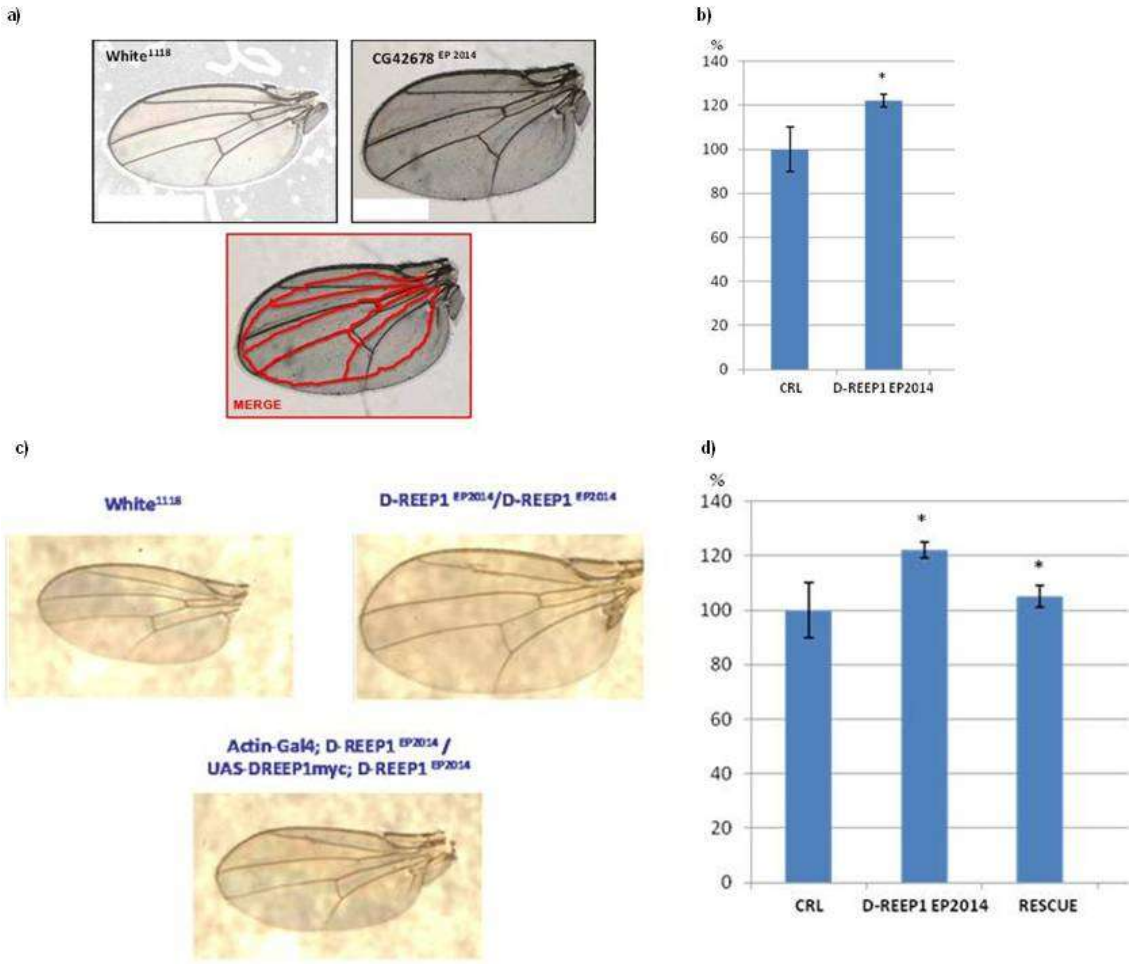

Figure 12. Mutants CG42678^{EP2014} wings phenotype. (a) In this panel are shown wings of *wilde type* fly (W1118), and wings of D-REEP1 mutant flies. (b) Graph analysis of the area of the wings of *wild type* flies and D-REEP1 mutant flies. D-REEP1 mutant flies displayed oversize wings of 20% compared to control. (c) Expression of *wild type* D-REEP1 protein rescued wings phenotype in D-REEP1 mutant background. *Wild type* D-REEP1 was expressed at 25°C using ubiquitous driver actin-Gal4. (d) Graph analysis of rescue wings area phenotype. Error bars represent s.d.; * $p<0.000001$

4.4 LOSS OF D-REEP1 FUNCTION INDUCES ER MORPHOLOGY ALTERATION

H-REEP1 is an ER protein structurally related to the DP1/ Yop1 family of proteins involved in ER shaping. It forms molecular complexes with other two HSP related proteins, spastin and atlastin-1, to coordinate ER shaping in corticospinal neurons.

Therefore we wanted to define in more detail the morphology of the ER membrane in the nervous system of D-REEP1^{EP2014} mutant flies. We performed electron microscopy (EM) and visualized the neuronal ER in third instar larva brains. Ultra structural analysis of the ER revealed significant morphological variations of the ER in neurons of D-REEP1 mutant flies (Figure 13). ER profiles of D-REEP1 loss of function neurons display an alteration of ER length compared to ER profiles of *wild type* neurons (Figure 13). Control neurons displayed ER profiles with average length 742±54 nm, whereas neurons lacking D-REEP1 showed elongated ER profiles, 1334±71 nm. Moreover, ER profile size distribution analysis, in *wild type* neuron, revealed that most representative class of ER profiles length is between 500-1000 nm, whereas in neurons lacking D-REEP1 three classes of long ER profiles were observed (1000 nm-1500 nm, 1500-2000 nm, >2000 nm. The two last classes of ER length profiles (1500-2000 nm, >2000 nm) were virtually absent in control neurons (Figure 13). In addition, in about 20% of D-REEP1 loss of function neuronal cells, a modification of normal luminal width of the ER was observed (Figure 13).

To demonstrate that the alteration of ER morphology was due to loss of D-REEP1 we performed rescue experiments by expressing *wild type* D-REEP1 in the D-REEP1 mutant background. The presence of D-REEP1 rescued ER profile length, indicating that loss of D-REEP1 alters ER morphology (Figure 14).

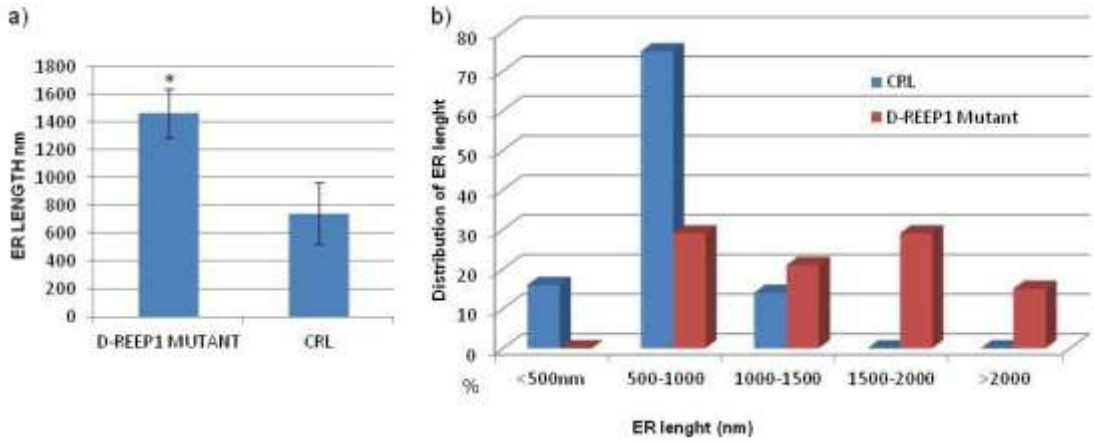

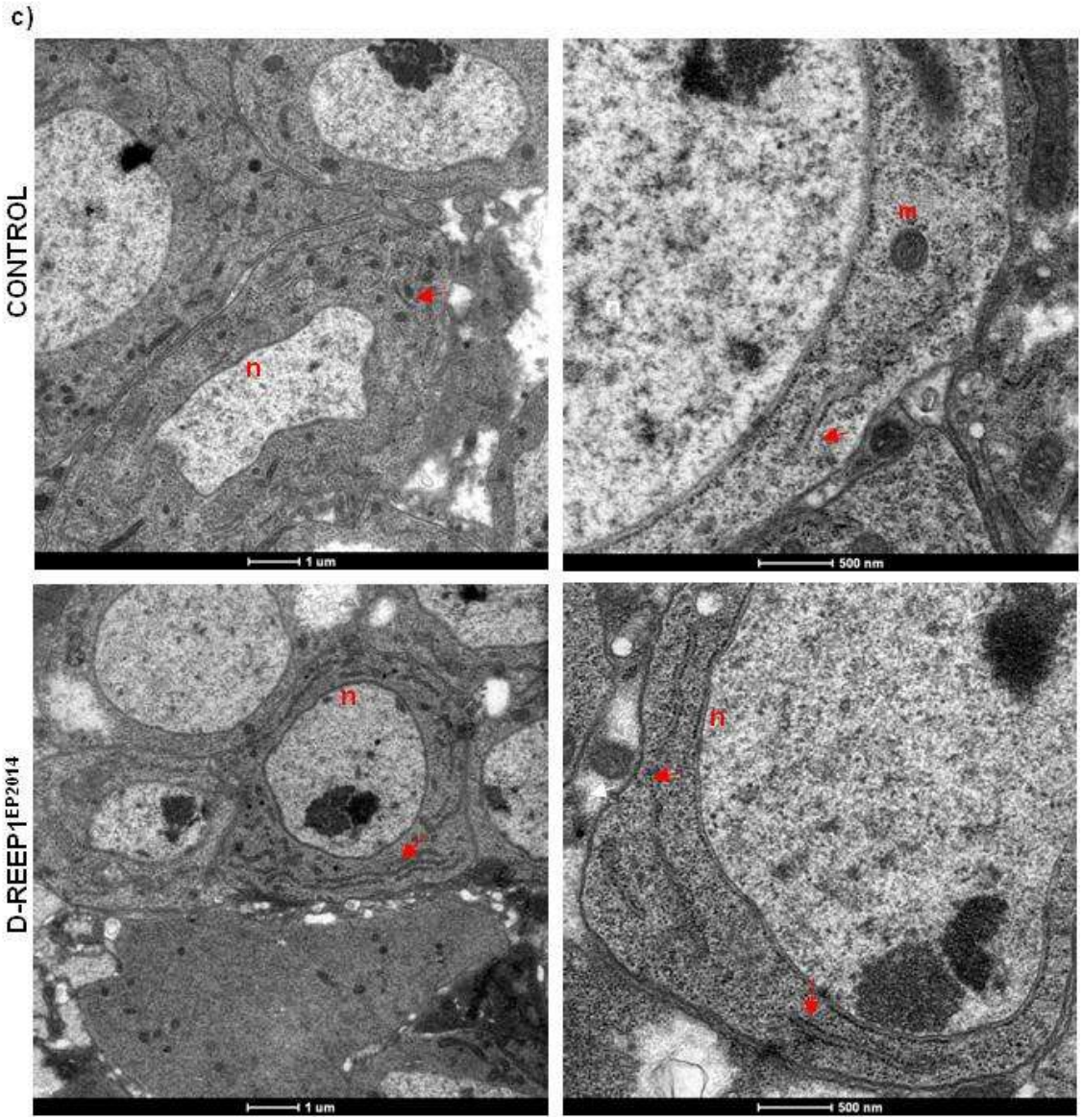

Figure 13. Loss of D-REEP1 cause ER length modification. a) Graph analysis of ER average length of ER profiles. Error bars represent s.d.; * $p<0.000001$. b) Difference in size distribution of ER profiles c). Electron microscopy images of third instar larva brains, show ER with typical tubular structure in control neurons and D-REEP1 loss of function neurons (n, nucleus; m, mitochondria, white arrows indicate ER).

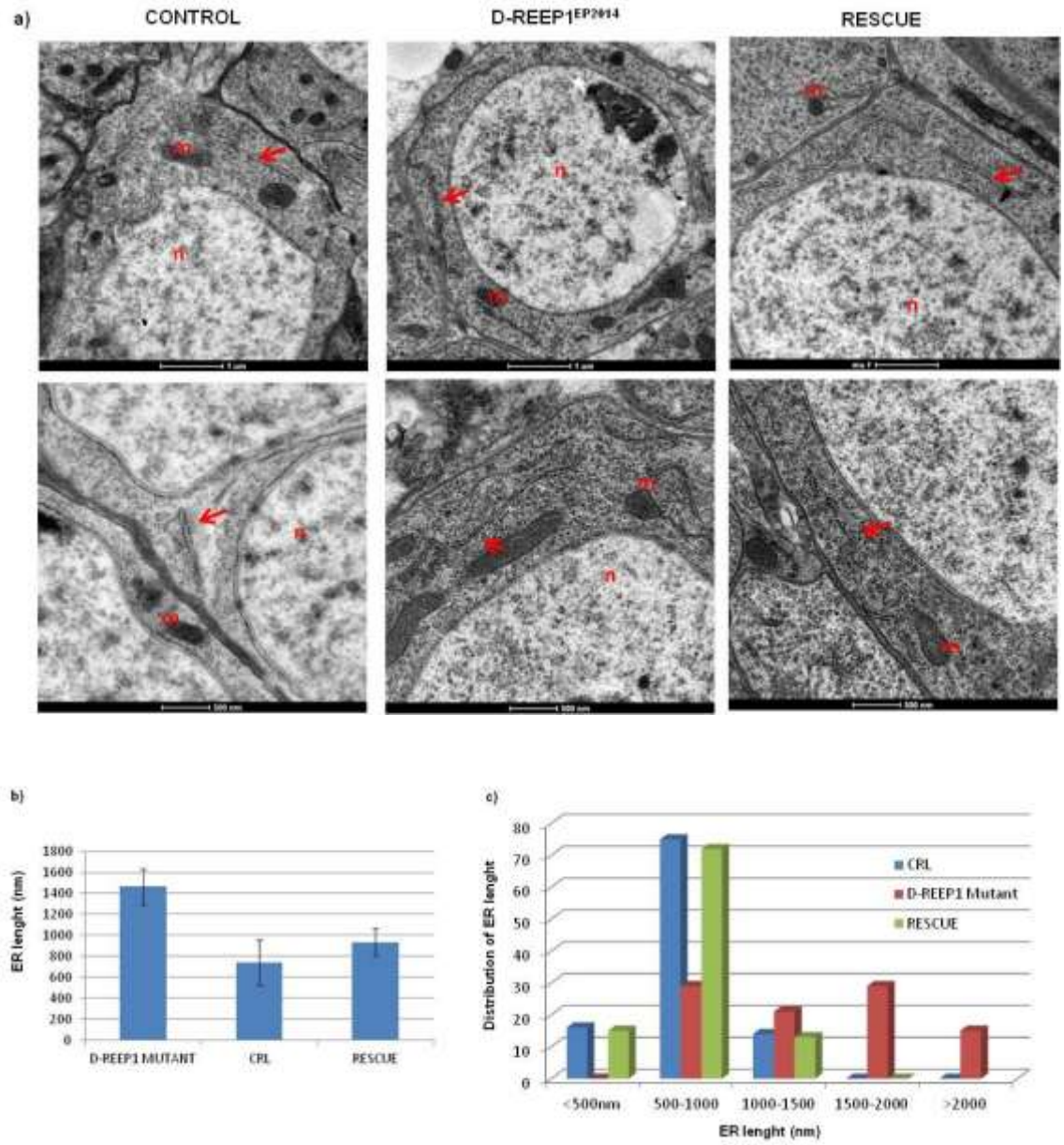

Figure 14. Expression of *wild type* D-REEP1 rescues ER length profiles in the *D-REEP1* mutant null background. *Wild type* D-REEP1 was expressed at 25°C using the ubiquitous driver actin-Gal4. (a) representative EM images of third instar larva brains (n,nucleus; m, mitochondria; white arrows indicate ER). (b) Average ER profile length. Error bars represent s.d; * p<0,000001. (c) Difference in size distribution of ER profiles

4.5 D-REEP1 LOSS OF FUNCTION MUTANT HAS REDUCED LIPID STORAGE.

Animals homozygous for D-REEP1^{EP2014} are viable but homozygous mutant larvae display a growth delay and reach pupation with a delay by one day compared to wild

type controls. This resulted in pupa about 17% smaller than controls. In addition during larvae dissection we noticed that D-REEP1 mutant larvae show a reduction of total fat compared to the *wild type* (Figure 15). We decided to focus our attention on the fat body, which is the adipose tissue of insects and also has liver-like activity due to its detoxification function since it plays an important role in larva growth regulation (Colombani et al.2003). Moreover, fat body is shown to act as an endocrine tissue that controls the growth of imaginal discs (structure that store precursor cells of adult structures such as eyes, antennae, legs, wings, halteres and genitalia) by releasing growth hormones (Kawamura et al.1999). Therefore, we systematically investigated if in D-REEP1 mutants there were alterations in lipid storage. Within the cells lipid are stored in specific organelle, the lipid droplets (LDs). We used BODIPY 493/503 dye to stain the lipid droplets in the fat body of wandering third instar larvae. Dissection of the larval fat body of D-REEP1 mutant and staining with a lipid droplet marker, BODIPY 493/503, revealed that the number of lipid droplets in fat body cells is significantly reduced, in contrast to *wild type* fat bodies which have many large lipid droplets (Figure 15). We than decided to perform lipid staining in other tissues of D-REEP1 mutants, including wing disc and muscle. Similar to the fat body, D-REEP1 mutants have reduced lipid storage in the imaginal wing disc.

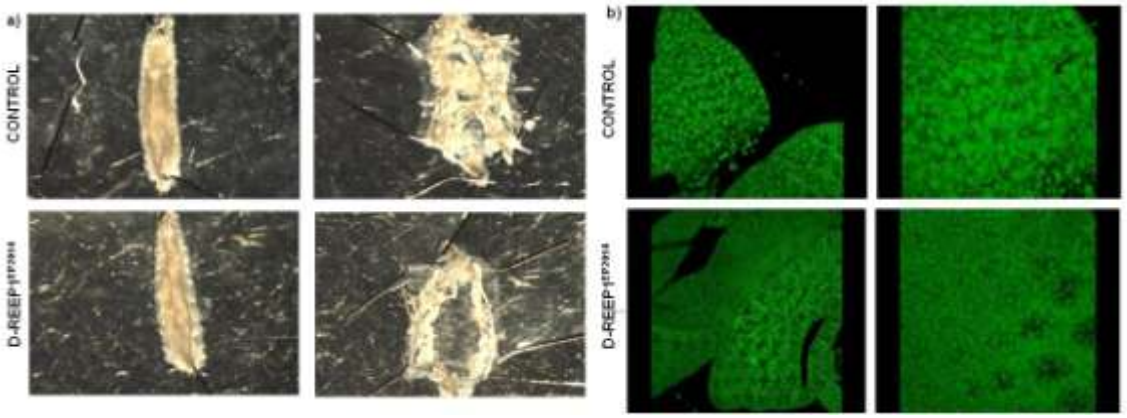

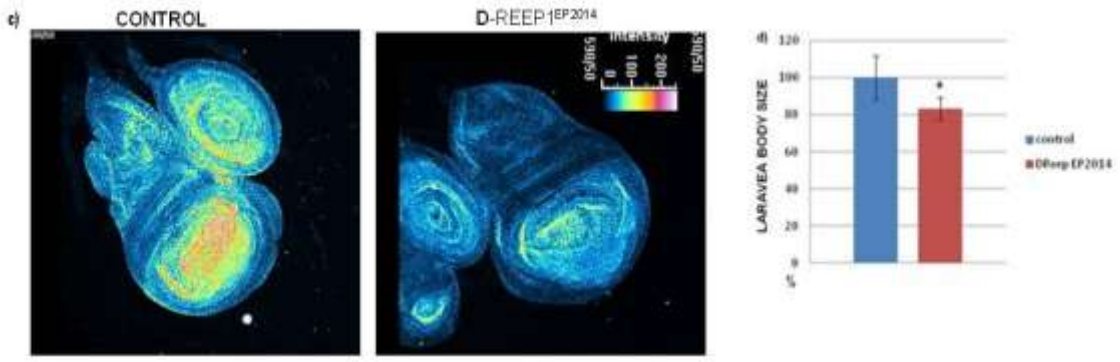

Figure 15. D-REEP1 loss of function mutants show a reduce lipid storage. (a) Third instar larvae dissection of *wild type* and D-REEP1 loss of function mutant. D-REEP1 mutants display a less fat quantity. (b) BODIPY 493/503 staing of lipid storage in fat body cells of *wild type* and D-REEP1 loss of function mutant. (c) Intensity analysis of BODIPY 493/503 staining for lipid droplets of imaginal disc. (d) Graph analysis of third instar larvae body size of D-REEP1 loss of function mutant and *wild type* flies. Scale bar: 20 µm. Error bars represent s.d, * p<0,0001

Several proteins implicated in neurodegenerative diseases have recently been linked to the regulation of neutral lipid storage. For instance HSP related protein like seipin and spartin are involved in lipid droplets biogenesis and LDs turnover. Neutral lipid deposition and lipid droplet formation seems to have a role in neuronal functions, and it may be particularly important under stress conditions. Therefore, we wanted to analyze in greater detail if in the nervous system of D-REEP1 loss of function mutants there were variations in LDs storage. After dissection and lipid staining we observed that, unexpectedly, even in nervous system, D-REEP1 mutants, presented a reduced number of lipid droplets. (Figure 16). We measured the reduction of LDs number in the nervous system of D-REEP1 mutants, by counting the LDs number in the axon of muscle 4 neuromuscular junction (NMJs) of segments A2. In a *wild type* larvae the average number of LDs in the axons is 0,1 LDs/µm^2 while in D-REEP1 mutant there is a significant decrease to 0,04 LDs/µm^2. Changes in LDs size in D-REEP1 mutants may reflect changes in lipid levels. Moreover, we examined the total triglyceride (TAG) content and found that the triglycerides level in D-REEP1 mutants is greatly reduced compared to control animals (Figure 16). The TAG level in D-REEP1 mutants turned out to be 70% that of wild type. Under starved conditions animals can mobilize stored lipid from LDs. Animals with high levels of TAG are resistant to starvation, while animals with low levels of TAG may be sensitive to starvation. We than starved flies adult of D-REEP1 mutants and *wild type*. We found that D-REEP1 mutants died after

48 hours of starvation while about 60% of *wild type* were still alive after the same period of time. These results further confirm a reduction of lipid droplets levels in D-REEP1 mutants (Figure 16)

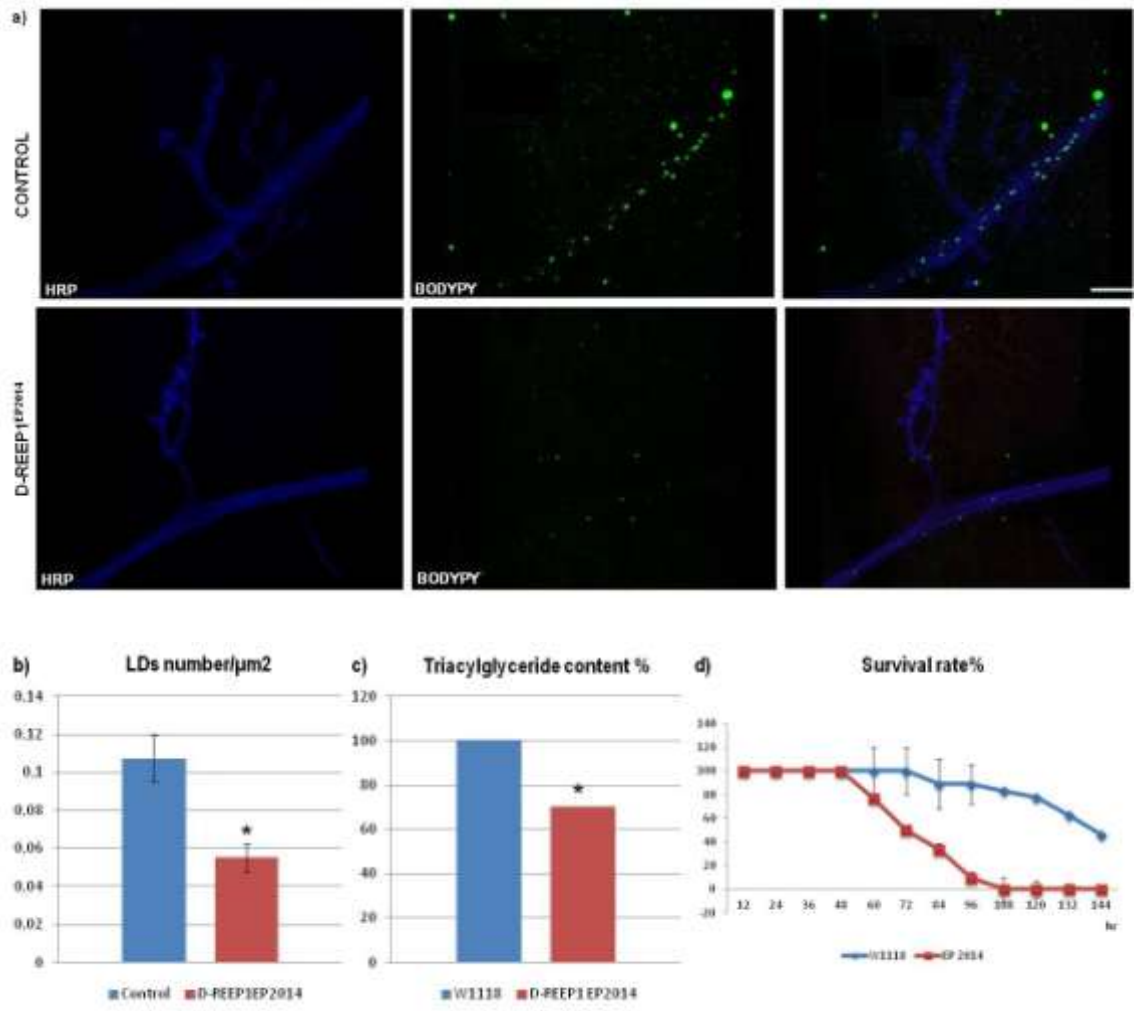

Figure 16. D-REEP1 loss of function mutant have a reduced lipid storage. (a) Representative muscle 4 NMJs of segments A2 of third instar larvae immunostained with anti-HRP to label the axon and the NMJ, and BODIPY 493/503 for LDs staining. (b) Bar graph analysis of lipid droplets number in the axons muscle 4 of NMJs of segments A2 of third instar larvae for D-REEP1 loss of function mutant and control. (c) Bar graph showing total triglycerides levels of wild type and D-REEP1 loss of function mutant. (d) Adult starvation assay. The x-axis shows the hours of starvation and the y-axis shows the survival rate. Scale bar: 10 µm. Error bars represent s.d, * p<0,0001

To evaluate whether this alteration of lipid droplets number in the neuromuscular junction of D-REEP1 mutant larvae was due to loss of D-REEP1, we over expressed

wild type D-REEP1 in the mutant background. The presence of the *wild type* protein increased the number of LDs in D-REEP1 mutant background, suggesting that loss of D-REEP1 alters the quantity of LDs in *Drosophila* axons (Figure 17).

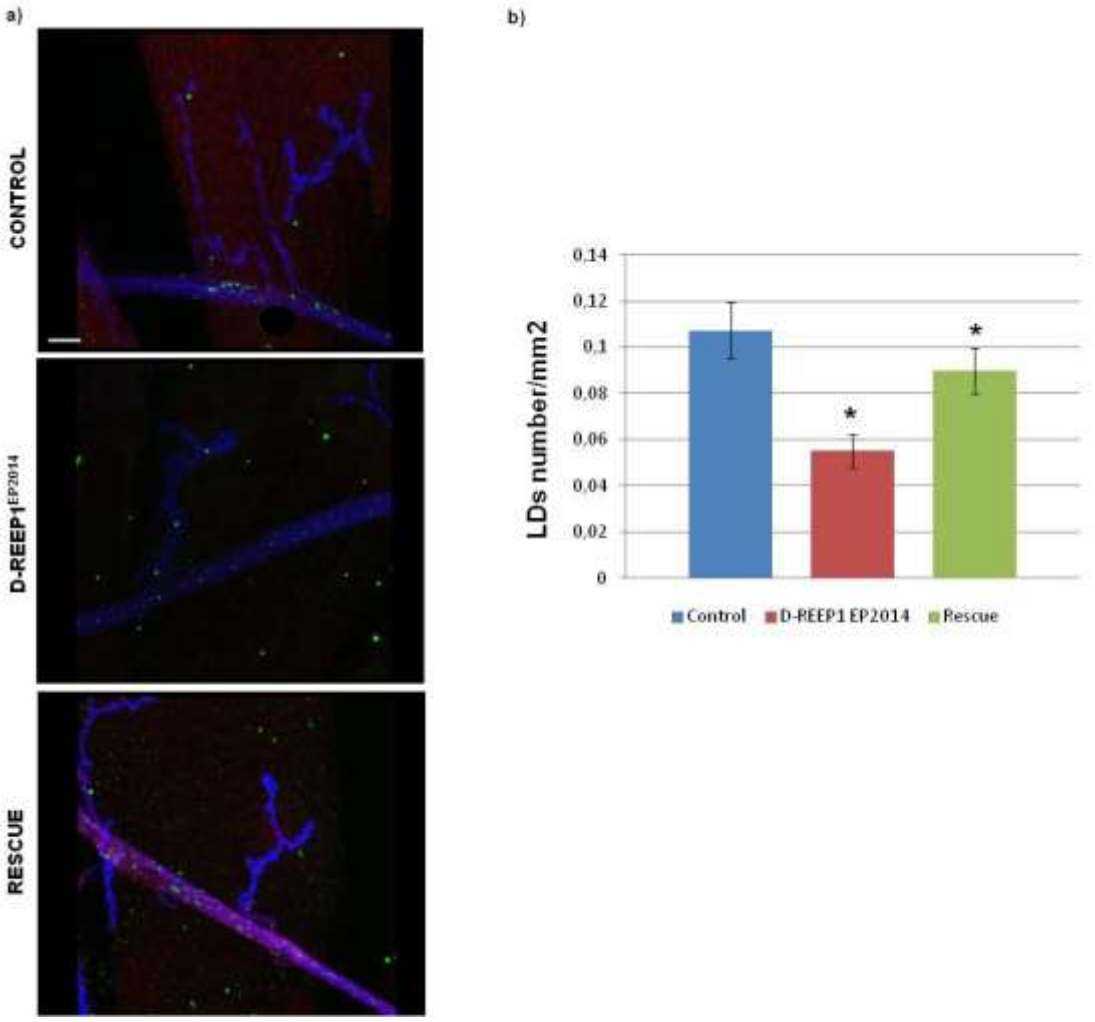

Figure 17. Expression of *wild type* D-REEP1 rescue the reduced lipid droplets number phenotype in D-REEP1 mutant background. *Wild type* D-REEP1 was expressed at 25°C using ubiquitous driver actin-Gal4. (a) Representative muscle 4 NMJs of segments A2 of third instar larvae immunostained with anti-HRP to label the axon and the NMJ, and BODIPY 493/503 for LDs staining. (d) Graph analysis of lipid droplets number in the axon of muscle 4 of NMJs of segments A2 of third instar larvae. Error bars represent s.d.; * $p<0.0001$. Scale bar: 10 µm

4.6 D-REEP1 OVEREXPRESSION RESULTS IN REDUCED SIZE OF LIPID DROPLETS

We overexpressed in Gal4-mediated manner UAS-*D-REEP1*-Myc with a number of ubiquitous and tissue specific promoters. Flies overexpressing D-REEP1 are viable, fertile and without any visible morphological phenotype. Since loss of D-REEP1 protein led to an increase of ER length and altered the ER morphology, we wanted to analyze in more detail the ER in flies overexpressing D-REEP1. Confocal microscopy analysis of third instar larvae expressing ubiquitously D-REEP1 under the control of tubulin-Gal4/GFP-KDEL driver shows a morphologically normal ER in the nervous system. In the muscle of these larvae we observed an accumulation of the ER marker GFP-KDEL (Figure 18). To investigate in more detail the ER morphology and to analyze these accumulation we used electron microscopy (EM) and visualized the neuronal ER in third instar larva brains overxpressing D-REEP1. However, ultrastructural analysis did not show any significant changes of ER length profiles or ER morphology of neurons overexpressing D-REEP1 (Figure 18).

Because of the reported lipid droplets D-REEP1 loss of function phenotype, we asked whether overexpression of D-REEP1 could also influence lipid droplet number. Our analysis focused on the lipid droplets in neuronal cells. To examine the effects on lipid droplets we expressed D-REEP1 ubiquitously using the actin-Gal4 driver. The expression of D-REEP1 did not change the number of LDs number in the axons, but unexpectedly we observed a modification of LDs size. In *wild type* larvae the lipid droplet display an average diameter of 0.76 nm while in larvae expressing D-REEP1 the average diameter of lipid droplets is decreased to 0,56 nm

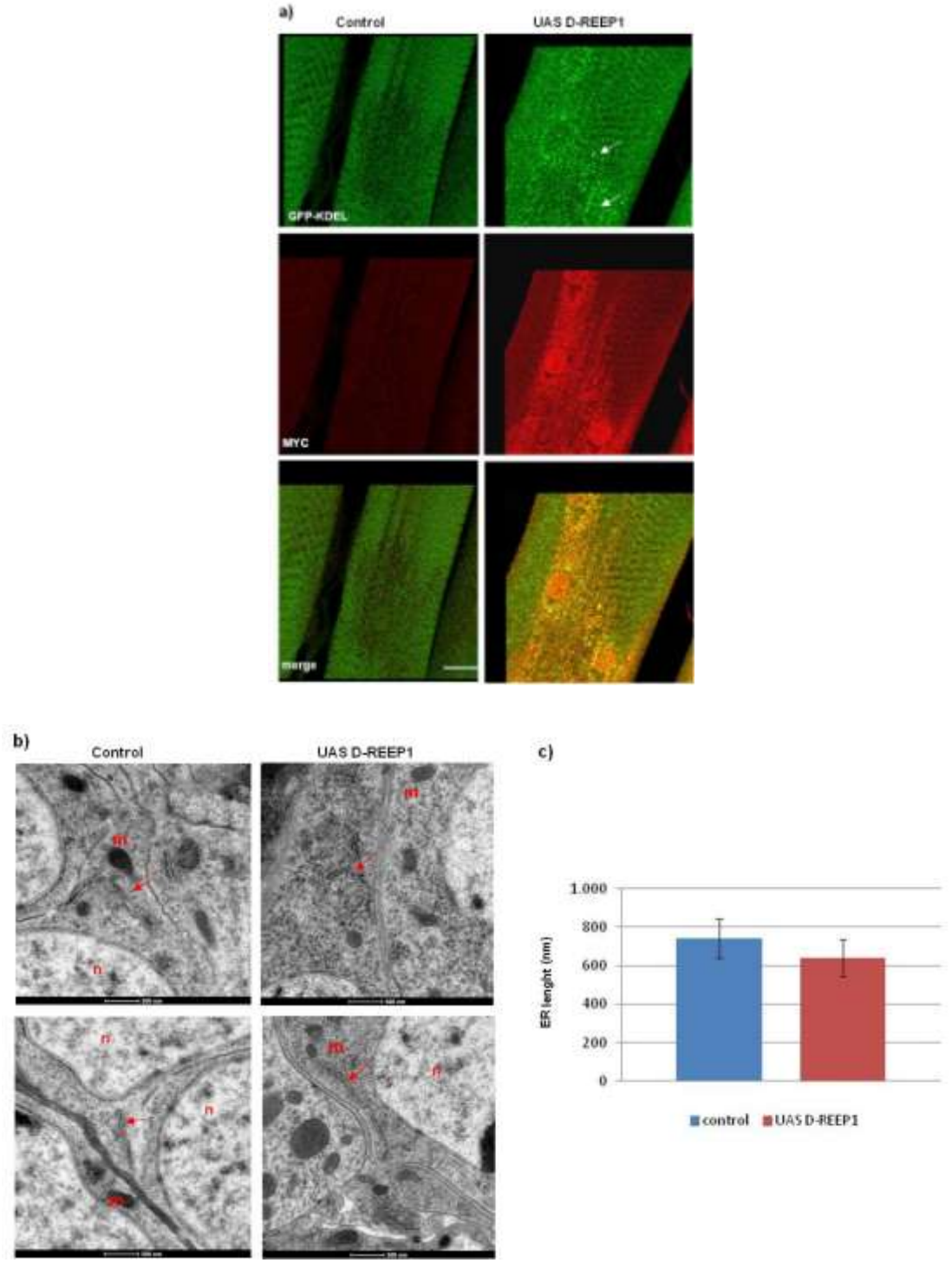

Figure 18. Expression of *wild type* D-REEP1 *in vivo*. (a) Immunocytochemistry of third instar wall muscle with anti Myc to label D-REEP1 expression GFP-KDEL to label the ER marker. Expression of *wild type* D-REEP1 induce accumulation of ER marker GFP-KDEL in wall muscle of third instar larvae. (b) Electron microscopy images of third instar larva brains, show ER with typical tubular structure in both control neurons and in neurons expressing D-REEP1, (n, nucleus; m, mitochondria, white arrows indicate ER. c) Graph analysis of ER average length of ER profiles. No significant changes were observed. Error bars represent s.d. n>100. Scale bar 20µm.

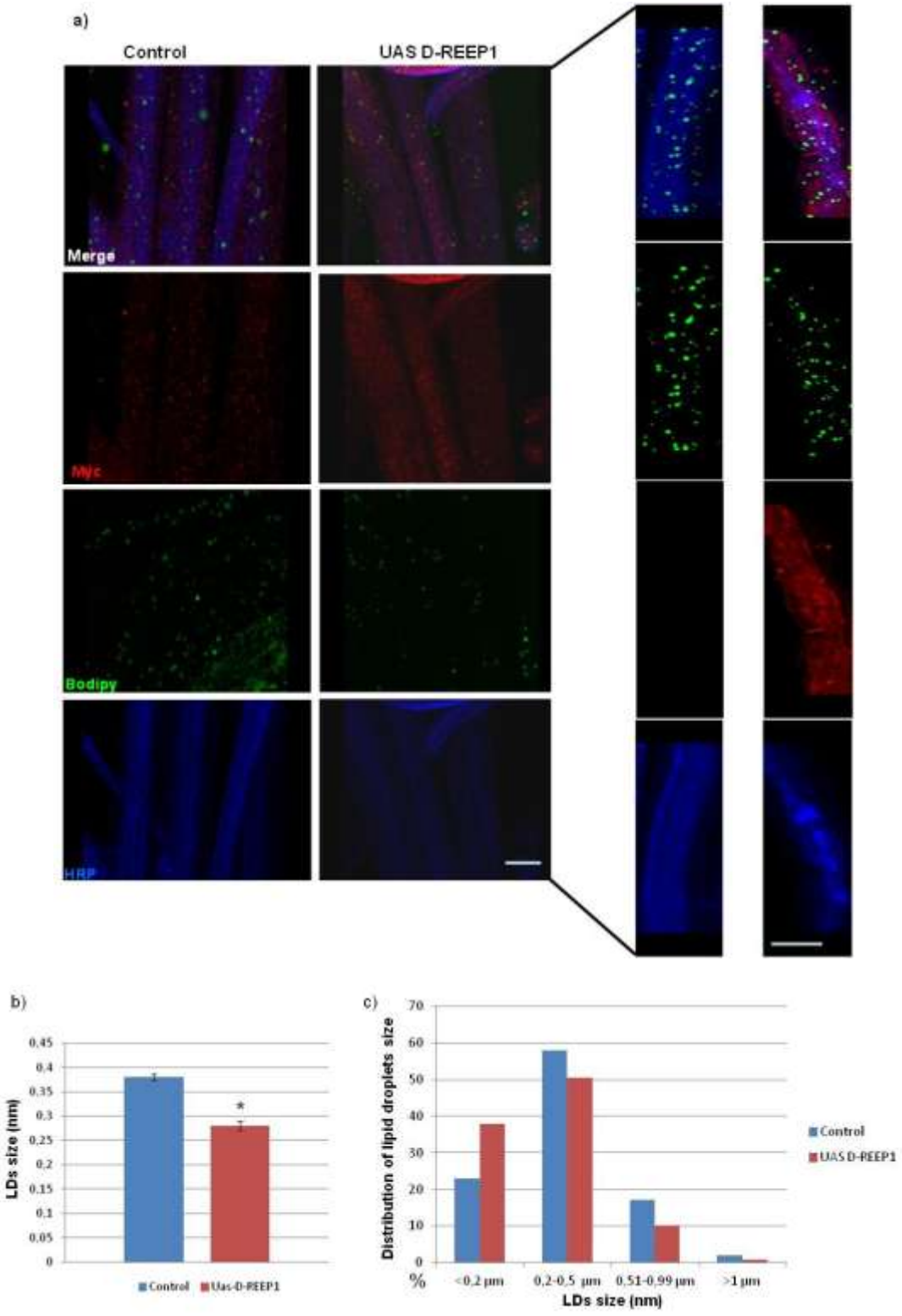

Figure 19. Expression of D-REEP1 *wild type* reduces the lipid droplets size. (a) Immunocytochemistry of third instar larval neurons with HRP to label the neuronal membranes, anti Myc to label D-REEP1 expression and BODIPY 493/503 to label lipid droplets. (b) Graph analysis of LDs radius in neurons of *wild type* and neuron expressing D-REEP1. (c) Distribution of lipid droplets size profiles. Error bars represent s.d.; * $p<0.0001$. Scale bar: 10 µm

4.7 D-REEP1 P19R PATHOLOGICAL MUTATION LOCALIZE ON LDS

To establish *Drosophila* as a model system for H-REEP1 linked spastic paraplegia and try to understand the pathogenic mechanism underlying H-REEP1 mutations, we have introduced by site-directed mutagenesis a disease mutation, P19R, in the *D-REEP1* cDNA. H-REEP1 p.P19R (c.56C>G) is a missense mutation localized at the first transmembrane domain of H-REEP1 protein (Beetz et al. 2008). The degree of homology of D-REEP1 with the human protein is so remarkable that the great majority of disease causing missense mutations occur in conserved aminoacid residues. We generated transgenic *Drosophila* lines for the expression of D-REEP1-P19R under the control of the ubiquitous and tissue specific Gal4 drivers lines. The P19R substitution was introduced in the D-REEP1 cDNA and its presence was confirmed by sequence analysis. To generate *Drosophila* transgenic lines, the mutated cDNA was introduced in the pUAST vector, in frame at the 3' terminal with a Myc tag. To study the effects of *in vivo* of D-REEP1-P19R we expressed the protein under the control of the ubiquitous driver line tubulin-Gal4. Confocal microscopy analysis of third instar larvae showed that while the *wild type* protein D-REEP1 is an ER protein, D-REEP1-P19R co-localized predominantly with the LDs marker BODIPY 493/503 (Figure 20). In addition, quantification analysis of LDs in the axons revealed that expression of D-REEP1-P19R reduced significantly the number of lipid droplets. In *wild type* larvae axons the number of lipid droplets was about 0,10 LDs/μm^2 , while in larvae expressing D-REEP1-P19R, the number of lipid droplets in the axons was about 0,03 LDs/μm^2. The LDs number in the nervous system of larvae expressing D-REEP-P19R mutant form was even lower that LDs number of D-REEP1 loss of function mutant. In contrast, in larvae expressing D-REEP-P19R, we observed an increase in the size of lipid droplets. In larvae expressing D-REEP1-P19R the average diameter of lipid droplets was increased to 1,16 nm (Figure 20)

Even thought D-REEP1-P19R localized predominantly in LDs, we decided to analyze also ER morphology by electron microscopy. This analysis reveled that there were no

alterations of ER length profiles in the neuron expressing D-REEP1-P19R. However some morphological changes in luminal width were observed as shown in figure 21.

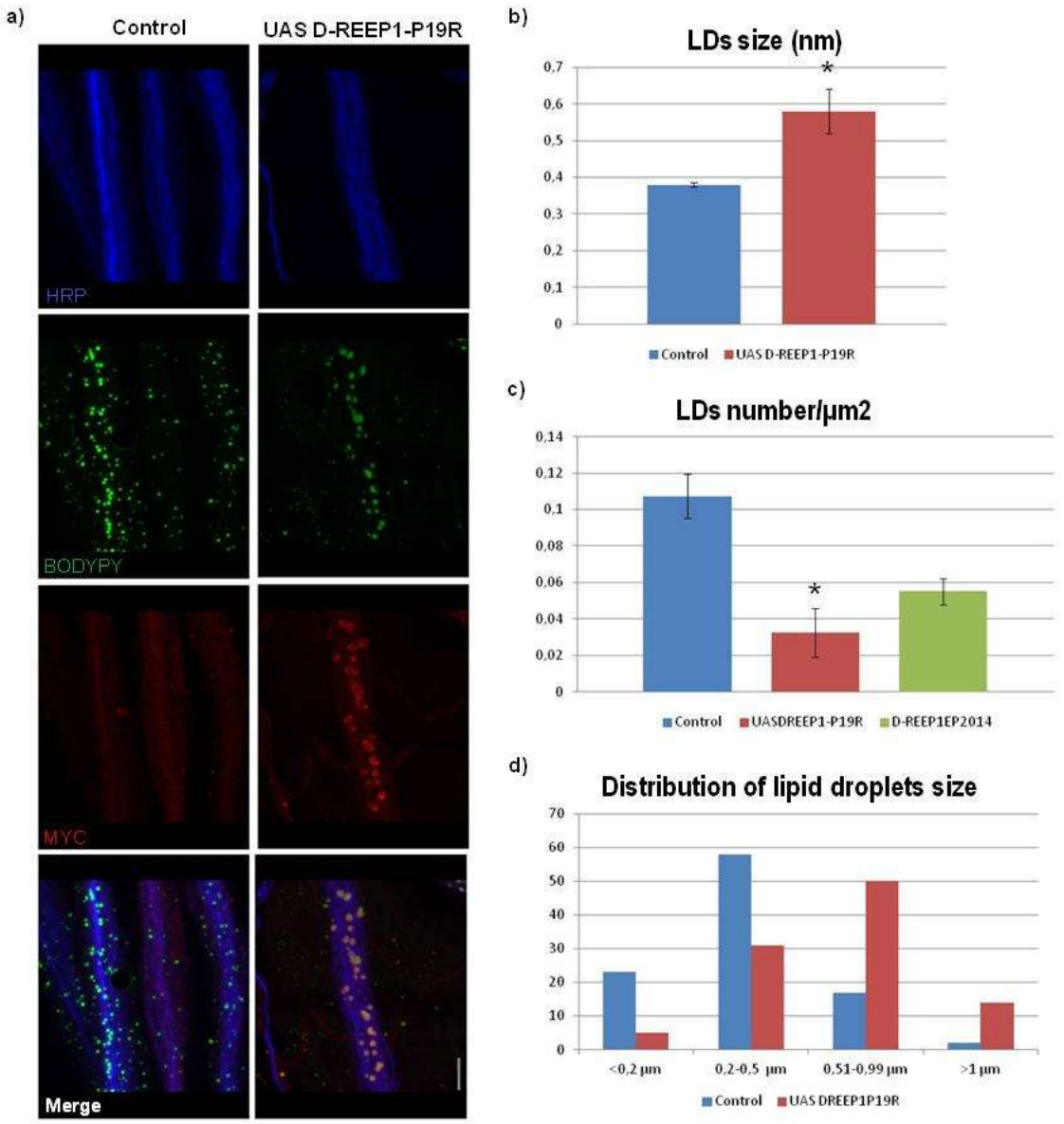

Figure 20. Expression of D-REEP1-P19R increases the size of lipid droplets reduces their number in *Drosphila* nervous system. (a) Immunocytochemistry of third instar larval neurons with HRP to label the neuronal membranes, anti Myc to label D-REEP1-P19R expression and BODIPY 493/503 to label lipid droplets. (b) Graph analysis of LDs radius in neurons of *wild type* and neurons expressing D-REEP1-P19R mutated form. (c) Graph bar showing the average number of LDs in *wild type* and in neuron expressing D-REEP1-P19R muted form. (d) Distribution of lipid droplets size profiles. Error bars represent s.d.; * $p<0.0001$. Scale bar: 10 µm

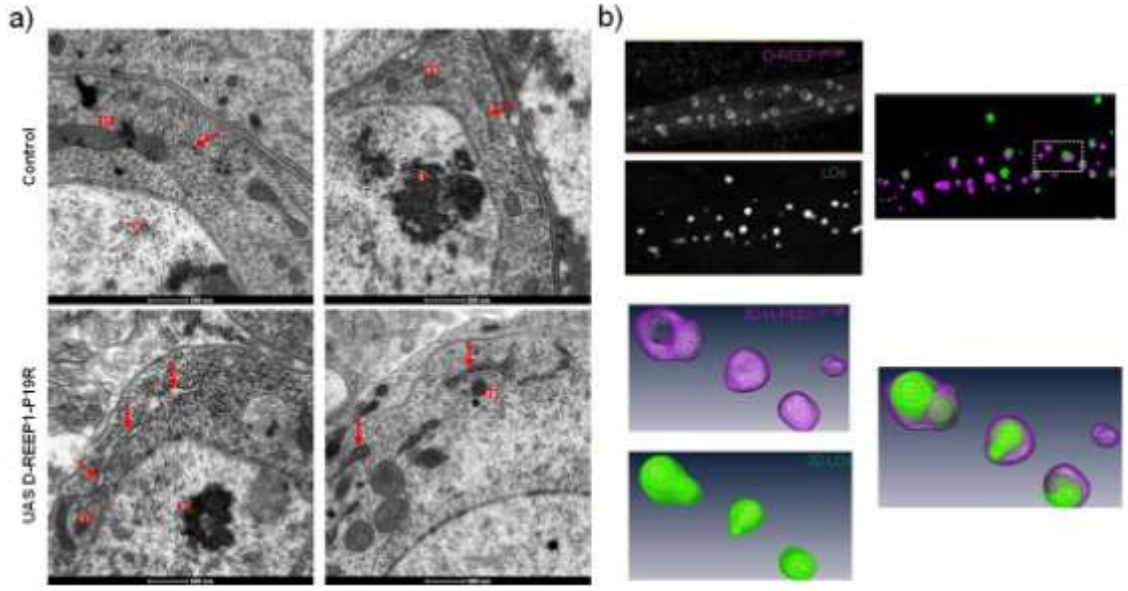

Figure 21. Ultrastructural analysis of ER morphology in neurons expressing D-REEP1-P19R mutated form. (a) representative EM images of third instar larva brains (n,nucleus; m, mitochondria; white arrows indicate ER). (b) 3D rendering of D-REEP1-P19R localization in lipid droplets labeled with BODIPY 493/503 in *Drosophila* nervous system. Inset shows higher-magnification images

4.8 EXPRESSION IN *DROSOPHILA* OF H-REEP1-A132V PATHOLOGICAL MUTATION

H-REEP1 p.A132V (c.C395T) is an unpublished missense mutation (M. L. Mostacciuolo group), localized at the C-terminal part of the protein. We generated transgenic lines for tissue specific expression of H-REEP1-A132V in *Drosophila.* The A132V substitution was introduced in the H-REEP1 cDNA by site directed mutagenesis and its presence was confirmed by sequence analysis. To generate *Drosophila* transgenic lines, the mutated cDNA was introduced in the pUAST vector, in frame at the 5' terminal with a HA tag.

To study the effects of *in vivo* H-REEP1-A132V we expressed the mutant protein under the control of the ubiquitous driver line tubulin-Gal4. Confocal microscopy analysis of third instar larvae showed a different subcellular localization of H-REEP1-A132V compared to D-REEP1-P19R. Surprisingly, H-REEP1-A132V, co-localized predominantly with the ER marker KDEL-GFP, as the *wild type* protein.

Immunocytochemistry analysis did not show any alteration of ER morphology. (Figure 22). However, because resolution of confocal analysis is limited we decided to analyze in more detail the ultrastructure of the ER by electron microscopy. We performed electron microscopy and visualized the neuronal ER in the brains of third instar larvae expressing H-REEP1-A132V. EM analysis did not show any significant alteration of ER length profiles or morphology (Figure 23).

Our ongoing work is focused on understanding if H-REEP1-A132V pathological mutation can affect the lipid metabolism in the nervous system as the expression of D-REEP1-P19R mutated form. Moreover, we will try to study if H-REEP1-A132V can perturb the cytoskeleton dynamics *in vivo*, since this mutation is located at the C-terminal part of H-REEP1, a domain important for microtubule binding.

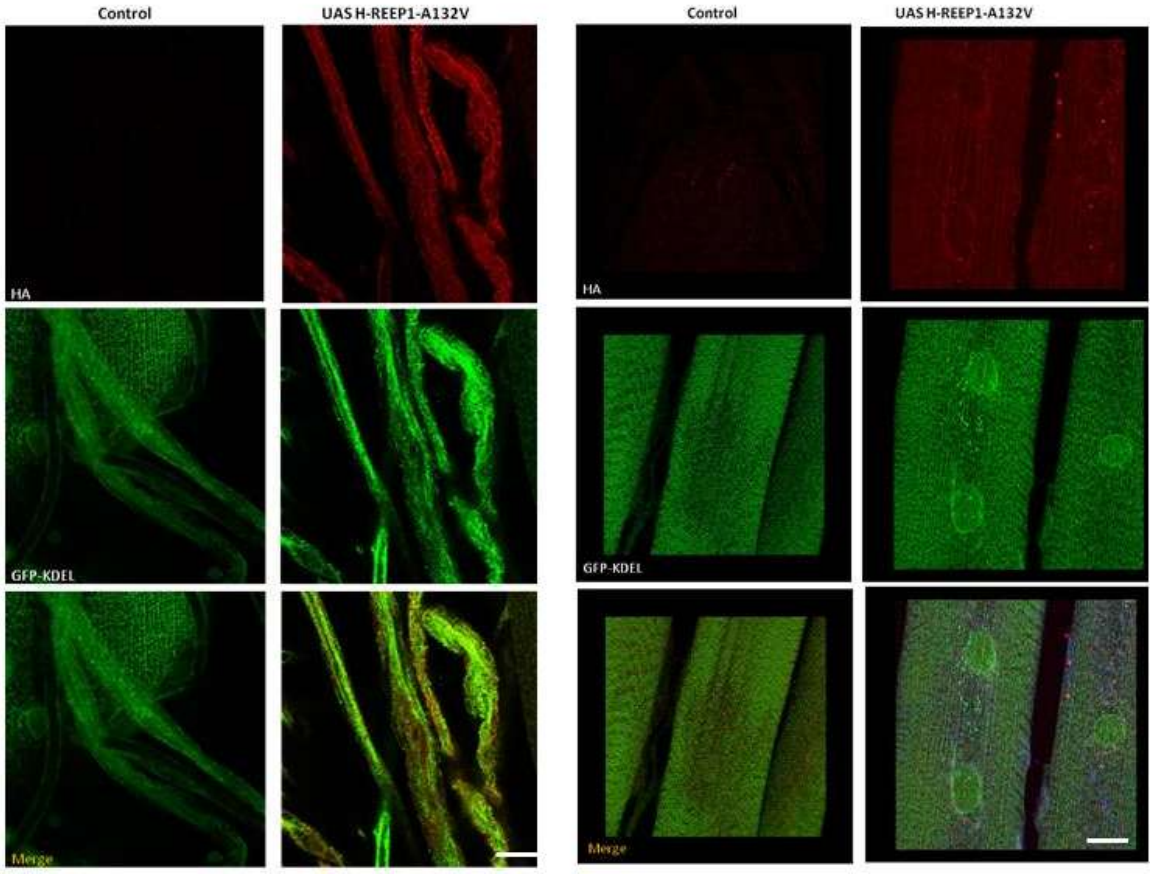

Figure 22. *In vivo* expression of H-REEP-A132V. Immunocytochemistry of wall muscle and nervous system axons of third instar larvae expressing H-REEP-A132V with anti HAto label H-REEP1-A132V expression GFP-KDEL to label the ER marker. The mutated form of H-REEP1 co-localize with ER marker GFP-KDEL. Scale bar 20µm

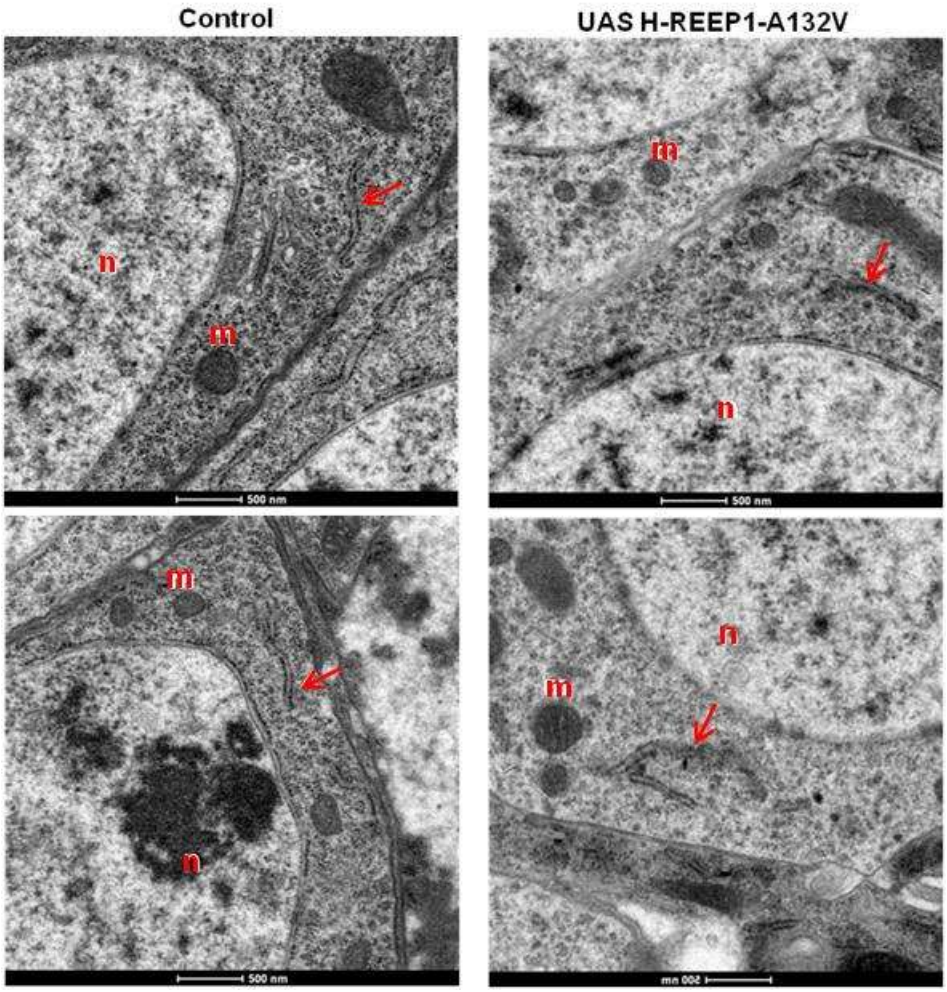

Figure 23. Ultrastructural analysis of ER morphology in neurons expressing H-REEP1-A132V mutated form. Representative EM images of third instar larva brains (n,nucleus; m, mitochondria; white arrows indicate ER)

4.9 HUMAN AND *DROSOPHILA* REEP1 EXPRESSION IN MAMMALIAN CELL CULTURE

We generated different construct for expression in cell system of *wild type* and pathological mutant forms of human and *Drosophila* REEP1, for *in vitro* studies. cDNA of H-REEP1 and D-REEP1 were cloned in the pcDNA3.1 plasmid in frame with HA tag and/or Myc tag. This constructs were expressed in HeLa cells, mammalian cell line

derived from a cervical carcinoma. As *in vivo*, D-REEP1 protein localized with ER marker PDI while the mutated form D-REEP1-P19R localized principally with lipid droplets marker BODIPY (Figure 25). Expression of H-REEP1 protein in HeLa cells showed a reticular pattern and partially co-localized with the microtubule marker, acetylated tubulin. The data obtained for H-REEP1 are in accordance with previous studies. The expression in HeLa cells of the mutated form H-REEP1-A132V displayed a phenotype very similar to the *wild type* form, confirming the reticular localization observed *in vivo* (Figure 24).

In addition, we generated another pathological mutation H-REEP1 p.D56N (Goizet et al. 2011) at the second trans-membrane domain. H-REEP1 p.D56N was inserted in H-REEP1 cDNA by site-directed mutagenesis and its presence was confirmed by sequence analysis. We expressed H-REEP1-D56N in HeLa cells. Surprisingly we observed that H-REEP1-D56N displayed the same phenotype as H-REEP1-P19R, it co-localized predominantly with the LDs marker BODIPY (Figure 24).

Using a bio-informatics approach, we analyzed how this pathological mutation could affect the REEP1 protein. We used two different software: *Membrane topology software*, available on the European Molecular Biology Laboratory (EMBL) protein prediction web site, that evaluates the hydrophobicity of the amino acid sequence and compares it with the hydrophobicity of polytopic proteins whose membrane topologies have been solved (Rost, Fariselli, and Casadio 1996); Hidden Markov Model for Topology Prediction (HMMTOP) based on the principle that membrane topology of trans-membrane proteins is determined by the divergence of amino acid composition of sequence segments (Tusnády and Simon 1998). Based on these studies, these software confirmed the presence of two transmembrane domain for wild type REEP1 protein and suggested that in REEP1 p.P19R, the substitution of the proline with arginine leads to a total loss of the first trans-membrane domain.,while for the REEP1 p.D56N, substitution of aspartic acid with asparagine could increase the loop between the two trans-membranes.

Therefore pathological mutations of H-REEP1 localized in the trans-membrane domain, affect the hydrophobicity levels of the protein. Since two different pathological mutations of H-REEP1 change the localization of the protein from the ER to LDs, we wanted to investigate which region is necessary and sufficient for lipid droplets sorting.

For this purpose we used mutational analysis. We generated two truncated forms of H-REEP1 protein fused in frame with HA tag at the N-terminal. One truncated form was generated without the first transmembrane domanin, while in the second truncated form lacked the first transmembrane and the loop between two trans-membranes domain. The cDNA of truncated from was cloned in pcDNA3.1 plasmid and expressed in HeLa cells. Similarly to the H-REEP-P19R and H-REEP1-D56N, truncated forms localized on the lipid droplets surface of HeLa cells (Figure 24). Therefore, probably the second trans-membrane domain contains the necessary information for lipid droplet targeting, whereas the first tranmembrane domain contains information for ER targeting.

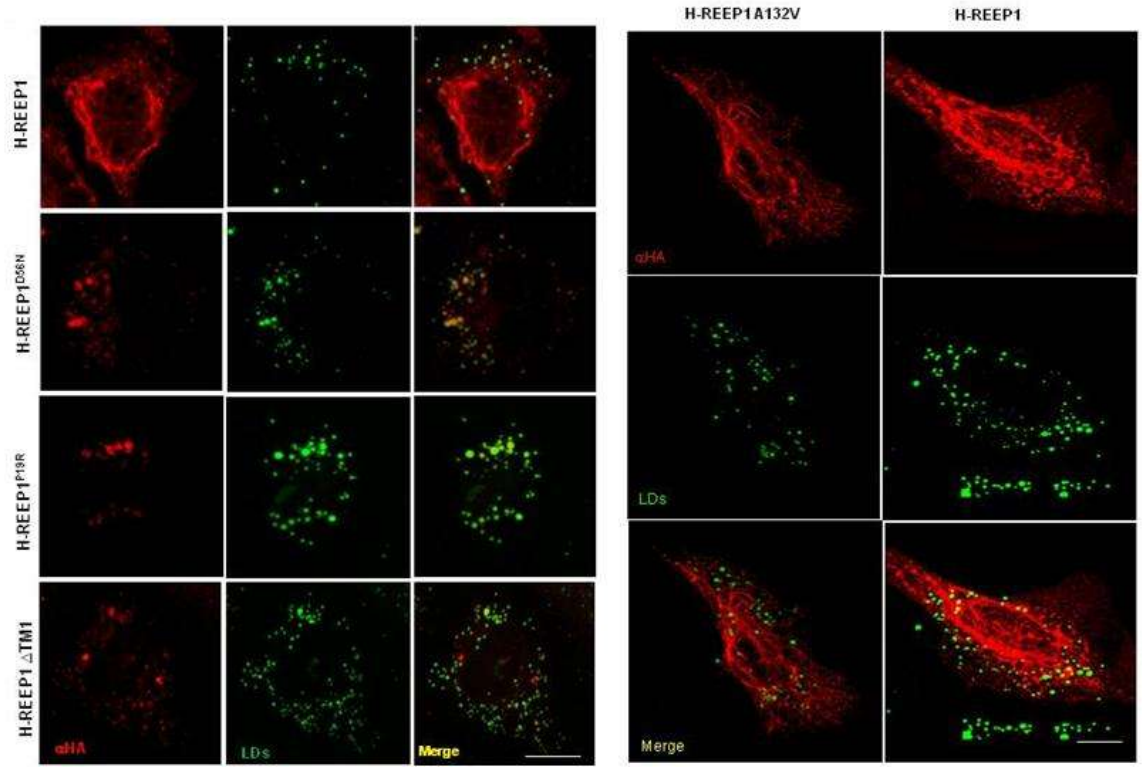

Figure 24. Subcellular localization changes of H-REEP1 in response to point mutations. HeLa cells were transfected with HA tagged human REEP1 and double labeled with BODIPY 493/503 to display lipid droplets (green) and anti HA tag to label REEP1 (red). Pathological mutation affecting the first (P19R) or the second transmembrane domain (D56N) causes a relocation of REEP1 around lipid droplets structures. In addition deletion of the first transmembrane domain (HREEP1 ΔTM1) has the same phenotype of point mutations P19R and D56N. Scale bar: 20 µm

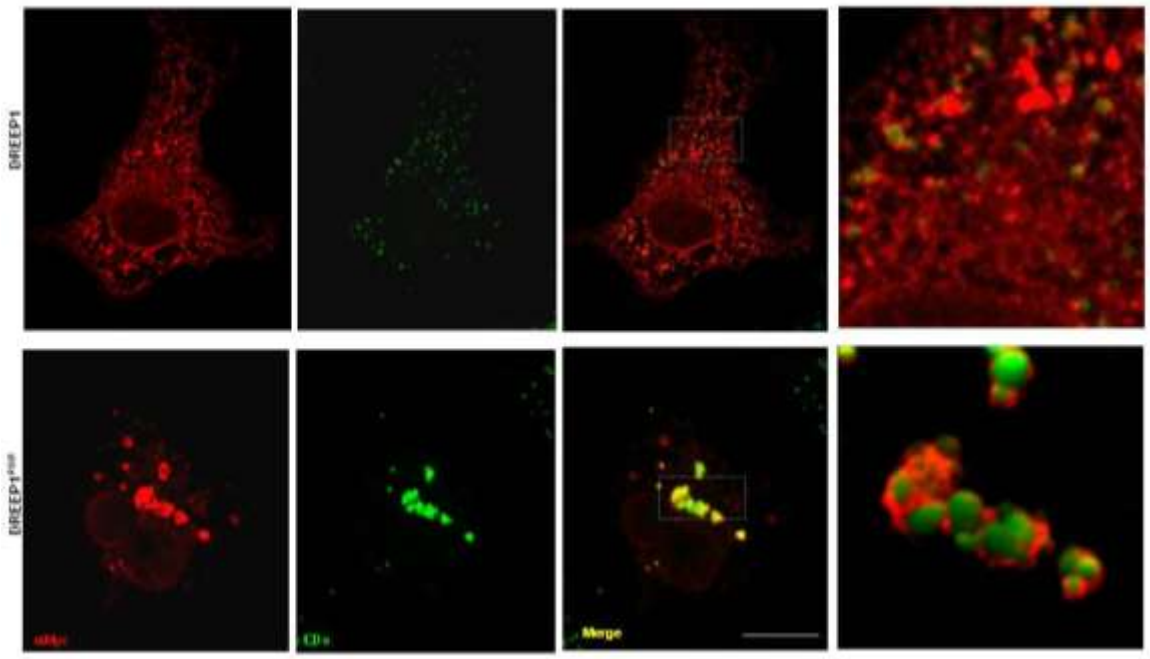

Figure 25. In vitro localization of D-REEP1 confirms the in vivo phenotype. HeLa cells were transfected with Myc tagged D-REEP1 and double labeled with BODIPY 493/503 to display lipid droplets (green) and anti Myc tag to label D-REEP1 (red). Scale bar: 20 µm. Inset shows higher-magnification images

4.10 H-REEP1 IS CAPABLE OF HOMO-OLIGOMERIZATION

Co-immunoprecipitation (co-IP) is a common technique used for the identification of protein interaction. An antibody for the protein of interest, linked to a support matrix, is incubated with a cell extract to allow the antibody to bind the protein in solution. The antibody/antigen complex will then be pulled out of the sample by precipitation: this will physically isolates, from the rest of the sample, the protein of interest and other proteins potentially bound to it (co-immunoprecipitation). Finally, components of the immunocomplex (antibody, antigen and co-immunprecipitated proteins) are analyzed by SDSPAGE and Western blot. To test if H-REEP1 could self-assemble, HeLa cells were co-transfected with H-REEP1-HA and H-REEP1-Myc constructs. Lysates prepared from these cells were immunoprecipitated using anti-Myc antibodies. The immunoprecipitate was analyzed by western blotting with both anti-Myc and anti-HA

antibodies. The presence of both Myc and HA signals in the immunoprecipitate (phase P) showed that immunoprecipitation of H-REEP1-Myc pulled down also H-REEP1-HA thus suggesting that H-REEP1 molecules are capable of homo-oligomerization (Figure 26).

To analyze if H-REEP1-P19R protein could oligomerize with the wild type protein HeLa cells were separately transfected with H-REEP1-P19R-HA and H-REEP1-Myc constructs and processed as described above for the wild type form. Myc signal was observed in the immunoprecipiate while the HA signal was detected at the supernatant phase suggesting that probably the mutated form of D-REEP1-P19R is not capable of holigomerization (Figure 26).

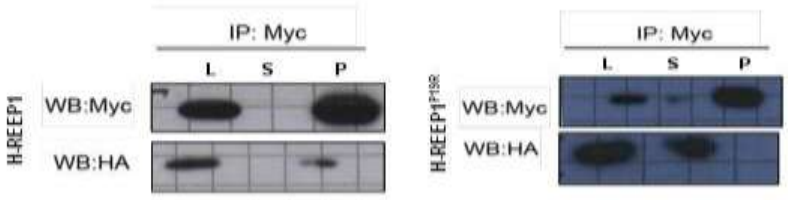

Figure 26. Wild type but not H-REEP1-P19R self-associates. Lysates from HeLa cells co-transfected with wild type DREEP1-Myc and DREEP1-HA or DREEP1^{P19R}-Myc and DREEP1^{P19R}-HA were immunoprecipitated and analyzed by western blot. L, lysate; S, supernatant; P, pellet

.

4.11 REEP1 MEMBRANE TOPOLOGY

H-REEP1 protein, belongs to the REEP/DP1/Yop1p superfamily, has two trans-membrane domains and a TB2/DP1/HAV22 or known as deleted in polyposis domain. The DP1/Yop1 family proteins members contain two hydrophobic segments. It has been proposed that each of these hydrophobic segments form a “wedge” shape within the lipid bilayer, while the hydrophilic segments are found in the cytoplasm. Previous studies have reported that the C-terminal part of H-REEP1 protein is oriented toward the cytosol. Based on this finding we wanted to verify the orientation of D-REEP1 protein as well as the orientation of the N-terminal part of H-REEP1. To test this hypothesis we used a protease protection assay. This technique entails the isolation of intact membrane vesicles from cellular fraction and the subsequent protease treatment of the sample. The vesicle membrane will shelter from proteases digestion the part of

the protein not exposed to the cytoplasm. Membrane vesicles were prepared from HeLa cells transfected with D-REEP1 and cells transfected with H-REEP1. Transfected cells were homogenized in the absence of detergent and fragmented membranes were vesiculated by sonication. Proteinase K was added to the intact vesiculated membranes which were then analyzed by western blotting. Loss of HA and Myc signals detection in western blots of membrane fraction treated with proteinase K (P2K) indicates that the amino- and carboxy-terminal parts of REEP1 are digested and therefore face the cytoplasm. calnexin was used as an internal control. The antibody used to recognize calnexin, binds the N-terminal of the protein that is located in the luminal part of the ER. Therefore after protease digestion the N-terminal of calnexin located inside the vesiculated membrane is protected, and the antibody signal can be detected by western blot analysis (Figure 27).

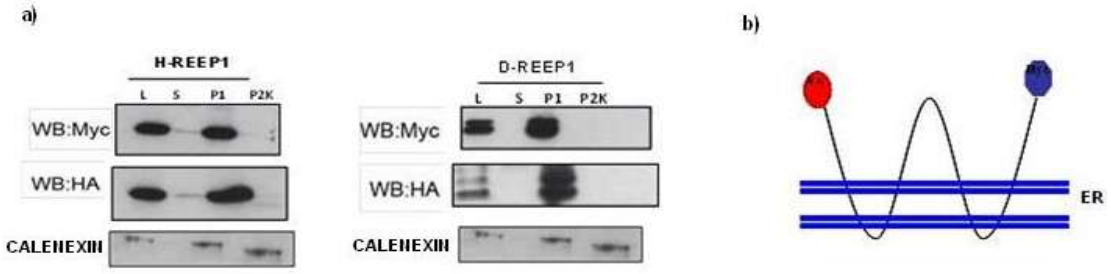

Figure 27. Membrane topology of human and *Drosphila* REEP1. (a) Western blot analysis of vesciculated membrane fractions from H-REEP1 and D-REEP1 expressing cell homogenates, treated with Proteinase K. L, lysate; S, supernatant; P1, pellet. P2K, pellet treated with proteasi. (b) Schematic presentation of the possible membrane insertion of H-REEP1 and D-REEP1

5. DISCUSSION

Mutations of SPG31 gene, which encodes REEP1 protein, are responsible for a dominant form of Hereditary Spastic Paraplegia (HSP), a clinically and genetically heterogeneous group of inherited disorders mainly characterized by progressive lower limb spasticity and weakness. The mechanisms by which REEP1 mutations produce dominant HSP in humans are controversial. The broad mutational spectrum observed (small frameshift mutations, but nonsense, missense, microRNA target site alterations and deletion) has suggested that the molecular mechanism is likely to be haploinsufficiency; however, other mechanisms have been postulated to be possible. The REEP1 gene encodes an ER integral membrane protein, with two transmembrane domains and a TB2/DP1/HVA22 domain with unknown function (Züchner et al. 2006). REEP1 protein belongs to the REEP/DP1/YOP1 superfamily of ER-shaping proteins and is thought to interact with other two HSP related proteins, atlastin-1 and spastin to coordinate ER shaping. However, the precise molecular function of REEP1 remain to be elucidated

We used *Drosophila melanogaster* as a model organism to study REEP1 function *in vivo*. The anatomy and development of *Drosophila* nervous system has been extensively characterized and many tools are available to study the neuronal functions (i.e. synaptic transmission). Although morphologically distinct and of lower complexity, the *D. melanogaster* CNS comprises the same basic building blocks as the mammalian CNS. These properties, apart from making the fruit fly a good model in neurobiological research, make *D. melanogaster* a powerful tool for the understanding of the genetic and molecular mechanisms of neural development and for the investigation of the neural basis of behavior. Flies also provide a platform for rapid drug discovery because it is easy to generate large numbers of genetically identical animals that can be tested. Therefore, fly models have been generated to understand the pathological mechanism of neurodegeneration. Our group has successfully generated *Drosophila* models for other two HSP-linked proteins, atlastin (SPG3) and spastin (SPG4). Creation of this *Drosophila* HSP models elucidated the cellular function of atlastin and spastin proteins. Moreover, the use of active compound, vimblastine, rescued the neuronal defects

caused by *Drosophila* spastin loss of function. Thus *Drosophila melanogaster* is a powerful genetic tool for studying HSP pathogenic mechanism.

We identified as the homolog of H-REEP1, the CG42678 gene (D-REEP1) in *Drosophila*. The presence in the *Drosophila* genome of a high conserved H-REEP1 ortholog combined with the wide array of experimental tools available makes *Drosophila* a valuable system to investigate the function of D-REEP1. Domain sequence analysis showed that all of the H-REEP1 protein domains are conserved in the *Drosophila* homolog.

Experiments we carried out *in vivo* and *in vitro* have shown that D-REEP1 modulates ER membrane morphology and affects the lipid droplets (LDs) size and number. D-REEP1 localizes in the ER membrane, consistent with the localization of the human ortholog. *In vitro* subcellular fractionation studies have shown that D-REEP1 associates with ER membranes. D-REEP1, as H-REEP1, includes two hydrophobic regions conferring a "wedge" shape to the protein that shallowly inserts into the outer lipid monolayer of the ER membrane. Both the N- and the C-terminus are hydrophilic and protrude into the cytoplasm. Protease protection studies employing proteinase K treatment of intact vesiculated membranes from HeLa cells overexpressing D-REEP1 demonstrated that the D-REEP1 C-terminus and N-terminus faces the cytoplasm. These data are consistent with membrane topology model proposed for the REEP1-4 subfamily (Park et al. 2010).

Loss of D-REEP1 *in vivo* resulted in an elongation of the ER profiles in *Drosophila* neurons. This data suggest an evolutionary conserved function of D-REEP1 with the role of REEP1-4 subfamily members in ER membrane shaping and network formation (Park *et al,* 2010).

Our *in vivo* data suggest an unexpected role for D-REEP1 in controlling lipid storage in *Drosophila.* Analysis of *Drosophila* D-REEP1 mutants showed reduced lipid storage in the fat body, the adipose tissue of *Drosophila*, and a reduced quantity of total triglycerides in third instar larvae compared to *wild type* controls. The lipid droplets storage defects of D-REEP1 loss of function *in vivo* are similar to those observed in *Drosophila dSeipin mutant* (SPG20) (Tian et al.2011). Seipin, an integral ER protein, has been established as an important factor in regulating LDs dynamics, particularly size and distribution.

Moreover we detected a decrease of lipid droplets number in the nervous system of D-REEP1 mutants, a phenotype that has not been reported previously. In eukaryotes, lipid droplets are believed to arise primarily from the ER, where the enzymes that synthesize neutral lipids reside, and in yeast it has been shown that they invariably arise from or close to the ER (Buhman et al. 2001). Alteration of ER profile length in D-REEP1 loss of function mutant could change the dynamics of ER network formation. Due to the strong connection between ER and LDs formation we suggest that loss of REEP1 may affect lipid droplets biogenesis, even though, further experimental data are needed to characterize in more detail this mechanism.

In vivo overexpression of D-REEP1 did not lead to obvious alterations of ER morphology but decreased the LDs size in the nervous system. DP1/Yop1p proteins deform the lipid bilayer into high-curvature tubules through hydrophobic insertion and scaffolding mechanisms by occupying more space in the outer than the inner leaflet of the ER lipid bilayer via their membrane-inserted, double-hairpin hydrophobic domains (Hu et al. 2009). Such "shaping" activity is found in all REEPs and in REEP1, it is determined by residues 37 to 76. This domain represents also an intramembrane site of interaction with numerous other ER-resident proteins. Based on protein family similarity and structure conservation the small size LDs phenotype can be due to higher curvature induced by the overexpression of D-REEP1.

To better clarify the pathological mechanism of REEP1 we generated transgenic lines expressing mutant forms of the protein. We over expressed *in vivo* the p.P19R mutation, a missense mutation that falls in a highly conserved region of REEP1 N-terminal region. The D-REEP1-P19R mutant form localized predominantly in the surface of LDs *in vivo.* There are two classes of proteins that can reside in the lipid droplets; the first class are proteins without integral hydrophobic domain that could be targeted to LDs from the cytosol, like Perilipin (Garcia et al. 2003). The second group is characterized by the presence of an integral hydrophobic domain that is most likely inserted in the ER, allowing the protein to laterally diffuse into forming droplets, like oleosin (Hope, Denis J Murphy, and McLauchlan 2002). Access to the LD surface is only possible because these proteins lack hydrophilic domains on the luminal side of the membrane, as such domains could not be accommodated in the hydrophobic LD core. Bioinformatics analysis of D-REEP1-P19R sequence suggested that this mutation

within the first transmembrane domain altered its hydrophobicity. Therefore this amino acid substitution could change the topology of REEP1 from two to one transmembrane domain and facilitate the insertion in the LDs membrane. In addition, because the second transmembrane domain is not affected by this mutation, it may contain the necessary information for LD targeting. The overexpression of D-REEP-P19R *in vivo* determined an increase of LDs size and a decrease of their number in *Drosophila* nervous system. Two hypotheses could explain the increase of lipid droplets size. According to the first one, LDs can locally synthesize the neutral lipids or the neutral lipids can be targeted and delivered from the ER through LD-ER contact sites (Moessinger et al. 2011). The second possibility is that increase of LDs size is caused by fusion of smaller, existing LDs. Therefore the D-REEP1-P19R may increase the LD-ER contact size or facilitates the LDs fusion. Additionally, an increase association of some proteins with LDs, can vary the concentration of proteins located on LDs membrane and affect the neutral lipids turnover and as consequence the LDs size. An analogous condition is verified when ADRP protein is expressed in HEK 293 cells. ADRP-mediated repression of TAG (triacylglycerol) hydrolysis in HEK293 cells correlated with a dramatic loss of ATGL from lipid droplets and caused an increase in TAG mass (Listenberger et al. 2007). The *in vivo* subcellular location of D-REEP1-P19R, almost exclusively in LDs surface, could modify the concentration of existing LDs proteins leading to a defective lipid droplet turnover. However, these hypothesises need to be confirmed by experimental data.

The p.P19R mutation cause an autosomal dominat form of HSP, with early onset associated to a severe phenotype. The haploinsufficiency mechanism is generally considered to give rise to HSP-causing REEP1 mutations (Beetz et al. 2008). Different subcellular localization of mutated protein could sustain the haploinsufficiency mechanism. However, based on the *in vivo* phenotypes of D-REEP1-P19R, an increase of LDs size and a reduction of LDs number in the nervous system, suggest that probably this mutation do not lead to haploinsufficiency but it rather leads to a dominat negative effect, interfering with the wild type protein function.

To understand the pathological mechanism of REEP1 mutations, we decided to analyze the phenotypes of humanized flies. Transgenic flies for H-REEP1-A132V pathological

mutation were generated. Expression of H-REEP-A132V, in *Drosophila* showed an association of the protein predominantly with the ER marker GFP-KDEL. *In vivo,* overexpression of H-REEP-A132V did not lead to obvious changes in the ER morphology. This difference observed between the severity of the phenotypes caused by REEP-A132V and that caused by REEP1-P19R could somehow reflect the weaker clinical phenotype of the patient carrying the D-REEP1-A132V. In fact, this patient displayed a non severe form of HSP with slight symptoms and late onset. Our ongoing work is focused on understanding if A132V pathological mutation can affect the lipid metabolism in *Drosophila* nervous system or the cytoskeleton dynamics *in vivo*.

To further confirm the involvement of REEP1 in lipid droplets regulation we evaluated the expression of both human and *Drosophila* REEP1 protein in mammalian cell culture. Expression of H-REEP1 in HeLa cells displayed a reticular pattern and tubular ER, in agreement with previous reports. In addition, expression of H-REEP1-D56N, a pathological mutation within the second transmembrane domain, showed a localization on LDs surface. Bioinformatics analysis showed that D56N mutation similarly to the P19R mutation changes the hydrophobicity profile, and increases the length of the hydrophilic loop between the transmembrane domains. In addition, expression in HeLa cells of H-REEP1 lacking the first transmembrane domain (ΔTM1 REEP1), showed a localization of the truncated protein with LDs membrane. The data obtained *in vivo* by the expression of D-REEP1-P19R and the expression of ΔTM1 REEP1support the idea that the second transmembrane domain has the necessary informations for LDs targeting. Moreover, these data imply that the alteration of aminoacid hydrophobicity could changes the membrane insertion of REEP1 protein leading to a different subcellular localization and produce a dysfunctional protein.

Our study demonstrated that the *Drosophila* ortholog D-REEP1, is also involved in coordinating the ER morphology. Moreover our data demonstrate that loss of function and missense mutations of REEP1 affect lipid droplets biogenesis and lipid droplets size. The fundamental link between ER and lipid droplets biogenesis imply that a dysfunction of the ER or a modification of ER morphology can directly affect LDs formation or metabolism. Nevertheless further studies will be necessary to analyze in more detail and to confirm the function D-REEP1 in order to establish its direct

involvement in the regulation of LDs size or biogenesis. Identification of the precise molecular mechanism of REEP1 function may contribute to a better understanding of neuronal degeneration in Hereditary Spastic Paraplegia.

Recently, other genes/proteins involved in HSP, erlin2 (SPG18), seipin (SPG17) and spartin (SPG20), have been implicated in alteration of synthesis and metabolism of lipids and sterols. (Eastman, Yassaee, and Bieniasz 2009; Edwards et al. 2009; Hooper et al. 2010).Within the last few years, genetic and functional data on HSP genes and proteins have opened an entirely novel perspective on the pathogenesis of this disease, strongly indicating that alterations in cholesterol, fatty acid, phospholipid, and sphingolipid metabolism play a relevant role in the pathogenesis of HSP. Lipid composition is important for the organization of neuronal membranes, affects crucial processes such as exocytosis and ion channel function, and contributes to the formation of membrane domains. Furthermore, there is increasing evidence that lipids provide an important role as signaling mediators and effectors (Piomelli, Astarita, and Rapaka 2007). Remarkably, disturbances in lipid metabolism offer the unprecedented opportunity to identify biomarkers for HSP and to design novel therapeutic strategies aiming at restoring the normal lipid profile.

6. REFERENCES

Allan, V J, and R D Vale. 1991. “Cell cycle control of microtubule-based membrane transport and tubule formation in vitro.” *The Journal of cell biology* 113(2): 347–59. http://www.pubmedcentral.nih.gov/articlerender.fcgi?artid=2288932&tool=pmcentrez&rendertype=abstract (January 21, 2013).

Andersson, Linda, Pontus Boström, Johanna Ericson, Mikael Rutberg, Björn Magnusson, Denis Marchesan, Michel Ruiz, Lennart Asp, Ping Huang, Michael A Frohman, Jan Borén, and Sven-Olof Olofsson. 2006. “PLD1 and ERK2 regulate cytosolic lipid droplet formation.” *Journal of cell science* 119(Pt 11): 2246–57. http://www.ncbi.nlm.nih.gov/pubmed/16723731 (November 21, 2012).

Bartz, René, Wen-Hong Li, Barney Venables, John K Zehmer, Mary R Roth, Ruth Welti, Richard G W Anderson, Pingsheng Liu, and Kent D Chapman. 2007. “Lipidomics reveals that adiposomes store ether lipids and mediate phospholipid traffic.” *Journal of lipid research* 48(4): 837–47. http://www.ncbi.nlm.nih.gov/pubmed/17210984 (October 26, 2012).

Baumann, O, and B Walz. 2001. “Endoplasmic reticulum of animal cells and its organization into structural and functional domains.” *International review of cytology* 205: 149–214. http://www.ncbi.nlm.nih.gov/pubmed/11336391 (November 1, 2012).

Beetz, Christian, Rebecca Schüle, Tine Deconinck, Khanh-Nhat Tran-Viet, Hui Zhu, Berry P H Kremer, Suzanna G M Frints, Wendy A G van Zelst-Stams, Paula Byrne, Susanne Otto, Anders O H Nygren, Jonathan Baets, Katrien Smets, Berten Ceulemans, Bernard Dan, Narasimhan Nagan, Jan Kassubek, Sven Klimpe, Thomas Klopstock, Henning Stolze, Hubert J M Smeets, Constance T R M Schrander-Stumpel, Michael Hutchinson, Bart P van de Warrenburg, Corey Braastad, Thomas Deufel, Margaret Pericak-Vance, Ludger Schöls, Peter de Jonghe, and Stephan Züchner. 2008. “REEP1 mutation spectrum and genotype/phenotype correlation in hereditary spastic paraplegia type 31.” *Brain□: a journal of neurology* 131(Pt 4): 1078–86. http://www.pubmedcentral.nih.gov/articlerender.fcgi?artid=2841798&tool=pmcentrez&rendertype=abstract (January 18, 2013).

Behan, W M, and M Maia. 1974. “Strümpell’s familial spastic paraplegia: genetics and neuropathology.” *Journal of neurology, neurosurgery, and psychiatry* 37(1): 8–20. http://www.pubmedcentral.nih.gov/articlerender.fcgi?artid=494557&tool=pmcentrez&rendertype=abstract (January 18, 2013).

Blaner, William S, Sheila M O’Byrne, Nuttaporn Wongsiriroj, Johannes Kluwe, Diana M D’Ambrosio, Hongfeng Jiang, Robert F Schwabe, Elizabeth M C Hillman, Roseann Piantedosi, and Jenny Libien. 2009. “Hepatic stellate cell lipid droplets: a specialized lipid droplet for retinoid storage.” *Biochimica et biophysica acta* 1791(6): 467–73. http://www.pubmedcentral.nih.gov/articlerender.fcgi?artid=2719539&tool=pmcentrez&rendertype=abstract (November 26, 2012).

Boström, Pontus, Linda Andersson, Mikael Rutberg, Jeanna Perman, Ulf Lidberg, Bengt R Johansson, Julia Fernandez-Rodriguez, Johanna Ericson, Tommy Nilsson, Jan Borén, and Sven-Olof Olofsson. 2007. “SNARE proteins mediate fusion between cytosolic lipid droplets and are implicated in insulin sensitivity.” *Nature cell biology* 9(11): 1286–93. http://www.ncbi.nlm.nih.gov/pubmed/17922004 (November 23, 2012).

6. REFERENCES

Bozza, Patricia T, and João P B Viola. "Lipid droplets in inflammation and cancer." *Prostaglandins, leukotrienes, and essential fatty acids* 82(4-6): 243–50. http://www.ncbi.nlm.nih.gov/pubmed/20206487 (December 1, 2012).

Brand, A H, and N Perrimon. 1993. "Targeted gene expression as a means of altering cell fates and generating dominant phenotypes." *Development (Cambridge, England)* 118(2): 401–15. http://www.ncbi.nlm.nih.gov/pubmed/8223268 (November 2, 2012).

Brasaemle, Dawn L. 2007. "Thematic review series: adipocyte biology. The perilipin family of structural lipid droplet proteins: stabilization of lipid droplets and control of lipolysis." *Journal of lipid research* 48(12): 2547–59. http://www.ncbi.nlm.nih.gov/pubmed/17878492 (November 9, 2012).

Brasaemle, Dawn L, Vidya Subramanian, Anne Garcia, Amy Marcinkiewicz, and Alexis Rothenberg. 2009. "Perilipin A and the control of triacylglycerol metabolism." *Molecular and cellular biochemistry* 326(1-2): 15–21. http://www.ncbi.nlm.nih.gov/pubmed/19116774 (November 11, 2012).

De Brito, Olga Martins, and Luca Scorrano. 2010. "An intimate liaison: spatial organization of the endoplasmic reticulum-mitochondria relationship." *The EMBO journal* 29(16): 2715–23. http://www.pubmedcentral.nih.gov/articlerender.fcgi?artid=2924651&tool=pmcentrez&rendertype=abstract (November 2, 2012).

Buhman, K K, H C Chen, and R V Farese. 2001. "The enzymes of neutral lipid synthesis." *The Journal of biological chemistry* 276(44): 40369–72. http://www.ncbi.nlm.nih.gov/pubmed/11544264 (January 21, 2013).

Castillon, Alicia, Hui Shen, and Enamul Huq. 2009. "Blue light induces degradation of the negative regulator phytochrome interacting factor 1 to promote photomorphogenic development of Arabidopsis seedlings." *Genetics* 182(1): 161–71. http://www.pubmedcentral.nih.gov/articlerender.fcgi?artid=2674814&tool=pmcentrez&rendertype=abstract (December 15, 2012).

Cermelli, Silvia, Yi Guo, Steven P Gross, and Michael A Welte. 2006. "The lipid-droplet proteome reveals that droplets are a protein-storage depot." *Current biology□: CB* 16(18): 1783–95. http://www.ncbi.nlm.nih.gov/pubmed/16979555 (November 5, 2012).

Cole, Nelson B, Diane D Murphy, Theresa Grider, Susan Rueter, Dawn Brasaemle, and Robert L Nussbaum. 2002. "Lipid droplet binding and oligomerization properties of the Parkinson's disease protein alpha-synuclein." *The Journal of biological chemistry* 277(8): 6344–52. http://www.ncbi.nlm.nih.gov/pubmed/11744721 (January 3, 2013).

Csordás, György, Christian Renken, Péter Várnai, Ludivine Walter, David Weaver, Karolyn F Buttle, Tamás Balla, Carmen A Mannella, and György Hajnóczky. 2006. "Structural and functional features and significance of the physical linkage between ER and mitochondria." *The Journal of cell biology* 174(7): 915–21. http://www.pubmedcentral.nih.gov/articlerender.fcgi?artid=2064383&tool=pmcentrez&rendertype=abstract (November 2, 2012).

Dreier, L, and T A Rapoport. 2000. "In vitro formation of the endoplasmic reticulum occurs independently of microtubules by a controlled fusion reaction." *The Journal of cell biology* 148(5): 883–98. http://www.pubmedcentral.nih.gov/articlerender.fcgi?artid=2174540&tool=pmcentrez&rendertype=abstract (January 21, 2013).

Dubé, M P, M A Mlodzienski, Z Kibar, M R Farlow, G Ebers, P Harper, E H Kolodny, G A Rouleau, and D A Figlewicz. 1997. “Hereditary spastic paraplegia: LOD-score considerations for confirmation of linkage in a heterogeneous trait.” *American journal of human genetics* 60(3): 625–9. http://www.pubmedcentral.nih.gov/articlerender.fcgi?artid=1712512&tool=pmcentrez&rendertype=abstract (January 18, 2013).

Eastman, Scott W, Mina Yassaee, and Paul D Bieniasz. 2009. “A role for ubiquitin ligases and Spartin/SPG20 in lipid droplet turnover.” *The Journal of cell biology* 184(6): 881–94. http://www.pubmedcentral.nih.gov/articlerender.fcgi?artid=2699154&tool=pmcentrez&rendertype=abstract (January 3, 2013).

Eden, Emily R, Ian J White, Anna Tsapara, and Clare E Futter. 2010. “Membrane contacts between endosomes and ER provide sites for PTP1B-epidermal growth factor receptor interaction.” *Nature cell biology* 12(3): 267–72. http://www.ncbi.nlm.nih.gov/pubmed/20118922 (October 26, 2012).

Edwards, Thomas L, Virginia E Clowes, Hilda T H Tsang, James W Connell, Christopher M Sanderson, J Paul Luzio, and Evan Reid. 2009. “Endogenous spartin (SPG20) is recruited to endosomes and lipid droplets and interacts with the ubiquitin E3 ligases AIP4 and AIP5.” *The Biochemical journal* 423(1): 31–9. http://www.pubmedcentral.nih.gov/articlerender.fcgi?artid=2762690&tool=pmcentrez&rendertype=abstract (January 18, 2013).

Ehehalt, Robert, Joachim Füllekrug, Jürgen Pohl, Axel Ring, Thomas Herrmann, and Wolfgang Stremmel. 2006. “Translocation of long chain fatty acids across the plasma membrane--lipid rafts and fatty acid transport proteins.” *Molecular and cellular biochemistry* 284(1-2): 135–40. http://www.ncbi.nlm.nih.gov/pubmed/16477381 (January 21, 2013).

Errico, Alessia, Andrea Ballabio, and Elena I Rugarli. 2002. “Spastin, the protein mutated in autosomal dominant hereditary spastic paraplegia, is involved in microtubule dynamics.” *Human molecular genetics* 11(2): 153–63. http://www.ncbi.nlm.nih.gov/pubmed/11809724 (January 18, 2013).

Fink, John K. 2003. “Advances in the hereditary spastic paraplegias.” *Experimental neurology* 184 Suppl : S106–10. http://www.ncbi.nlm.nih.gov/pubmed/14597333 (January 18, 2013).

Fischer, Judith, Caroline Lefèvre, Eva Morava, Jean-Marie Mussini, Pascal Laforêt, Anne Negre-Salvayre, Mark Lathrop, and Robert Salvayre. 2007. “The gene encoding adipose triglyceride lipase (PNPLA2) is mutated in neutral lipid storage disease with myopathy.” *Nature genetics* 39(1): 28–30. http://www.ncbi.nlm.nih.gov/pubmed/17187067 (November 28, 2012).

Fortini, M E, M P Skupski, M S Boguski, and I K Hariharan. 2000. “A survey of human disease gene counterparts in the Drosophila genome.” *The Journal of cell biology* 150(2): F23–30. http://www.pubmedcentral.nih.gov/articlerender.fcgi?artid=2180233&tool=pmcentrez&rendertype=abstract (January 21, 2013).

Friedman, Jonathan R, Brant M Webster, David N Mastronarde, Kristen J Verhey, and Gia K Voeltz. 2010. “ER sliding dynamics and ER-mitochondrial contacts occur on acetylated microtubules.” *The Journal of cell biology* 190(3): 363–75. http://www.pubmedcentral.nih.gov/articlerender.fcgi?artid=2922647&tool=pmcentrez&rendertype=abstract (November 2, 2012).

Garcia, Anne, Anna Sekowski, Vidya Subramanian, and Dawn L Brasaemle. 2003. “The central domain is required to target and anchor perilipin A to lipid droplets.” *The Journal of biological chemistry* 278(1): 625–35. http://www.ncbi.nlm.nih.gov/pubmed/12407111 (January 28, 2013).

Goizet, Cyril, Christel Depienne, Giovanni Benard, Amir Boukhris, Emeline Mundwiller, Guilhem Solé, Isabelle Coupry, Julie Pilliod, Marie-Laure Martin-Négrier, Estelle Fedirko, Sylvie Forlani, Cécile Cazeneuve, Didier Hannequin, Perrine Charles, Imed Feki, Jean-François Pinel, Anne-Marie Ouvrard-Hernandez, Stanislas Lyonnet, Elisabeth Ollagnon-Roman, Jacqueline Yaouanq, Annick Toutain, Christelle Dussert, Bertrand Fontaine, Eric Leguern, Didier Lacombe, Alexandra Durr, Rodrigue Rossignol, Alexis Brice, and Giovanni Stevanin. 2011. "REEP1 mutations in SPG31: frequency, mutational spectrum, and potential association with mitochondrial morpho-functional dysfunction." *Human mutation* 32(10): 1118–27. http://www.ncbi.nlm.nih.gov/pubmed/21618648 (January 29, 2013).

Gong, Jingyi, Zhiqi Sun, and Peng Li. 2009. "CIDE proteins and metabolic disorders." *Current opinion in lipidology* 20(2): 121–6. http://www.ncbi.nlm.nih.gov/pubmed/19276890 (January 3, 2013).

Grigoriev, Ilya, Susana Montenegro Gouveia, Babet van der Vaart, Jeroen Demmers, Jeremy T Smyth, Srinivas Honnappa, Daniël Splinter, Michel O Steinmetz, James W Putney, Casper C Hoogenraad, and Anna Akhmanova. 2008. "STIM1 is a MT-plus-end-tracking protein involved in remodeling of the ER." *Current biology : CB* 18(3): 177–82. http://www.pubmedcentral.nih.gov/articlerender.fcgi?artid=2600655&tool=pmcentrez&rendertype=abstract (October 26, 2012).

Gross, S P, M A Welte, S M Block, and E F Wieschaus. 2000. "Dynein-mediated cargo transport in vivo. A switch controls travel distance." *The Journal of cell biology* 148(5): 945–56. http://www.pubmedcentral.nih.gov/articlerender.fcgi?artid=2174539&tool=pmcentrez&rendertype=abstract (January 21, 2013).

Guo, Yi, Tobias C Walther, Meghana Rao, Nico Stuurman, Gohta Goshima, Koji Terayama, Jinny S Wong, Ronald D Vale, Peter Walter, and Robert V Farese. 2008. "Functional genomic screen reveals genes involved in lipid-droplet formation and utilization." *Nature* 453(7195): 657–61. http://www.pubmedcentral.nih.gov/articlerender.fcgi?artid=2734507&tool=pmcentrez&rendertype=abstract (October 26, 2012).

Haemmerle, Guenter, Robert Zimmermann, Marianne Hayn, Christian Theussl, Georg Waeg, Elke Wagner, Wolfgang Sattler, Thomas M Magin, Erwin F Wagner, and Rudolf Zechner. 2002. "Hormone-sensitive lipase deficiency in mice causes diglyceride accumulation in adipose tissue, muscle, and testis." *The Journal of biological chemistry* 277(7): 4806–15. http://www.ncbi.nlm.nih.gov/pubmed/11717312 (November 23, 2012).

Hansen, Jens Jacob, Alexandra Dürr, Isabelle Cournu-Rebeix, Costa Georgopoulos, Debbie Ang, Marit Nyholm Nielsen, Claire-Sophie Davoine, Alexis Brice, Bertrand Fontaine, Niels Gregersen, and Peter Bross. 2002. "Hereditary spastic paraplegia SPG13 is associated with a mutation in the gene encoding the mitochondrial chaperonin Hsp60." *American journal of human genetics* 70(5): 1328–32. http://www.pubmedcentral.nih.gov/articlerender.fcgi?artid=447607&tool=pmcentrez&rendertype=abstract (January 18, 2013).

Harding, A E. 1993. "Hereditary spastic paraplegias." *Seminars in neurology* 13(4): 333–6. http://www.ncbi.nlm.nih.gov/pubmed/8146482 (January 18, 2013).

Hetzer, Martin W, Tobias C Walther, and Iain W Mattaj. 2005. "Pushing the envelope: structure, function, and dynamics of the nuclear periphery." *Annual review of cell and developmental biology* 21: 347–80. http://www.ncbi.nlm.nih.gov/pubmed/16212499 (November 1, 2012).

Hooper, Christopher, Swamy S Puttamadappa, Zak Loring, Alexander Shekhtman, and Joanna C Bakowska. 2010. "Spartin activates atrophin-1-interacting protein 4 (AIP4) E3 ubiquitin ligase and promotes ubiquitination of adipophilin on lipid droplets." *BMC biology* 8: 72.

http://www.pubmedcentral.nih.gov/articlerender.fcgi?artid=2887783&tool=pmcentrez&rendertype=abstract (January 18, 2013).

Hope, R Graham, Denis J Murphy, and John McLauchlan. 2002. "The domains required to direct core proteins of hepatitis C virus and GB virus-B to lipid droplets share common features with plant oleosin proteins." *The Journal of biological chemistry* 277(6): 4261–70. http://www.ncbi.nlm.nih.gov/pubmed/11706032 (January 29, 2013).

Hu, Junjie, Yoko Shibata, Christiane Voss, Tom Shemesh, Zongli Li, Margaret Coughlin, Michael M Kozlov, Tom A Rapoport, and William A Prinz. 2008. "Membrane proteins of the endoplasmic reticulum induce high-curvature tubules." *Science (New York, N.Y.)* 319(5867): 1247–50. http://www.ncbi.nlm.nih.gov/pubmed/18309084 (November 2, 2012).

Hu, Junjie, Yoko Shibata, Peng-Peng Zhu, Christiane Voss, Neggy Rismanchi, William A Prinz, Tom A Rapoport, and Craig Blackstone. 2009. "A class of dynamin-like GTPases involved in the generation of the tubular ER network." *Cell* 138(3): 549–61. http://www.pubmedcentral.nih.gov/articlerender.fcgi?artid=2746359&tool=pmcentrez&rendertype=abstract (November 2, 2012).

Jacquier, Nicolas, Vineet Choudhary, Muriel Mari, Alexandre Toulmay, Fulvio Reggiori, and Roger Schneiter. 2011. "Lipid droplets are functionally connected to the endoplasmic reticulum in Saccharomyces cerevisiae." *Journal of cell science* 124(Pt 14): 2424–37. http://www.ncbi.nlm.nih.gov/pubmed/21693588 (November 2, 2012).

Kenwrick, S, A Watkins, and E De Angelis. 2000. "Neural cell recognition molecule L1: relating biological complexity to human disease mutations." *Human molecular genetics* 9(6): 879–86. http://www.ncbi.nlm.nih.gov/pubmed/10767310 (January 18, 2013).

Kiseleva, Elena, Ksenia N Morozova, Gia K Voeltz, Terrence D Allen, and Martin W Goldberg. 2007. "Reticulon 4a/NogoA locates to regions of high membrane curvature and may have a role in nuclear envelope growth." *Journal of structural biology* 160(2): 224–35. http://www.pubmedcentral.nih.gov/articlerender.fcgi?artid=2048824&tool=pmcentrez&rendertype=abstract (November 2, 2012).

Krahmer, Natalie, Yi Guo, Florian Wilfling, Maximiliane Hilger, Susanne Lingrell, Klaus Heger, Heather W Newman, Marc Schmidt-Supprian, Dennis E Vance, Matthias Mann, Robert V Farese, and Tobias C Walther. 2011. "Phosphatidylcholine synthesis for lipid droplet expansion is mediated by localized activation of CTP:phosphocholine cytidylyltransferase." *Cell metabolism* 14(4): 504–15. http://www.ncbi.nlm.nih.gov/pubmed/21982710 (November 28, 2012).

Kuerschner, Lars, Christine Moessinger, and Christoph Thiele. 2008. "Imaging of lipid biosynthesis: how a neutral lipid enters lipid droplets." *Traffic (Copenhagen, Denmark)* 9(3): 338–52. http://www.ncbi.nlm.nih.gov/pubmed/18088320 (November 14, 2012).

Lee, C, M Ferguson, and L B Chen. 1989. "Construction of the endoplasmic reticulum." *The Journal of cell biology* 109(5): 2045–55. http://www.pubmedcentral.nih.gov/articlerender.fcgi?artid=2115887&tool=pmcentrez&rendertype=abstract (January 21, 2013).

Levine, Tim, and Chris Loewen. 2006. "Inter-organelle membrane contact sites: through a glass, darkly." *Current opinion in cell biology* 18(4): 371–8. http://www.ncbi.nlm.nih.gov/pubmed/16806880 (November 2, 2012).

Lin, Pengfei, Jianwei Li, Qiji Liu, Fei Mao, Jisheng Li, Rongfang Qiu, Huili Hu, Yang Song, Yang Yang, Guimin Gao, Chuanzhu Yan, Wanling Yang, Changshun Shao, and Yaoqin Gong. 2008. "A

missense mutation in SLC33A1, which encodes the acetyl-CoA transporter, causes autosomal-dominant spastic paraplegia (SPG42)." *American journal of human genetics* 83(6): 752–9. http://www.pubmedcentral.nih.gov/articlerender.fcgi?artid=2668077&tool=pmcentrez&rendertype=abstract (January 21, 2013).

Listenberger, Laura L, Anne G Ostermeyer-Fay, Elysa B Goldberg, William J Brown, and Deborah A Brown. 2007. "Adipocyte differentiation-related protein reduces the lipid droplet association of adipose triglyceride lipase and slows triacylglycerol turnover." *Journal of lipid research* 48(12): 2751–61. http://www.ncbi.nlm.nih.gov/pubmed/17872589 (January 29, 2013).

Marsh, J Lawrence, and Leslie Michels Thompson. 2004. "Can flies help humans treat neurodegenerative diseases?" *BioEssays : news and reviews in molecular, cellular and developmental biology* 26(5): 485–96. http://www.ncbi.nlm.nih.gov/pubmed/15112229 (January 21, 2013).

Martinez-Botas, J, J B Anderson, D Tessier, A Lapillonne, B H Chang, M J Quast, D Gorenstein, K H Chen, and L Chan. 2000. "Absence of perilipin results in leanness and reverses obesity in Lepr(db/db) mice." *Nature genetics* 26(4): 474–9. http://www.ncbi.nlm.nih.gov/pubmed/11101849 (January 21, 2013).

McDermott, C, K White, K Bushby, and P Shaw. 2000. "Hereditary spastic paraparesis: a review of new developments." *Journal of neurology, neurosurgery, and psychiatry* 69(2): 150–60. http://www.pubmedcentral.nih.gov/articlerender.fcgi?artid=1737070&tool=pmcentrez&rendertype=abstract (January 18, 2013).

McMonagle, P, S Webb, and M Hutchinson. 2002. "The prevalence of 'pure' autosomal dominant hereditary spastic paraparesis in the island of Ireland." *Journal of neurology, neurosurgery, and psychiatry* 72(1): 43–6. http://www.pubmedcentral.nih.gov/articlerender.fcgi?artid=1737699&tool=pmcentrez&rendertype=abstract (January 18, 2013).

Melo, Rossana C N, Heloisa D'Avila, Hsiao-Ching Wan, Patrícia T Bozza, Ann M Dvorak, and Peter F Weller. 2011. "Lipid bodies in inflammatory cells: structure, function, and current imaging techniques." *The journal of histochemistry and cytochemistry : official journal of the Histochemistry Society* 59(5): 540–56. http://www.pubmedcentral.nih.gov/articlerender.fcgi?artid=3201176&tool=pmcentrez&rendertype=abstract (November 14, 2012).

Moessinger, Christine, Lars Kuerschner, Johanna Spandl, Andrej Shevchenko, and Christoph Thiele. 2011. "Human lysophosphatidylcholine acyltransferases 1 and 2 are located in lipid droplets where they catalyze the formation of phosphatidylcholine." *The Journal of biological chemistry* 286(24): 21330–9. http://www.pubmedcentral.nih.gov/articlerender.fcgi?artid=3122193&tool=pmcentrez&rendertype=abstract (January 21, 2013).

Montenegro, Gladys, Adriana P Rebelo, James Connell, Rachel Allison, Carla Babalini, Michela D'Aloia, Pasqua Montieri, Rebecca Schüle, Hiroyuki Ishiura, Justin Price, Alleene Strickland, Michael A Gonzalez, Lisa Baumbach-Reardon, Tine Deconinck, Jia Huang, Giorgio Bernardi, Jeffery M Vance, Mark T Rogers, Shoji Tsuji, Peter De Jonghe, Margaret A Pericak-Vance, Ludger Schöls, Antonio Orlacchio, Evan Reid, and Stephan Züchner. 2012. "Mutations in the ER-shaping protein reticulon 2 cause the axon-degenerative disorder hereditary spastic paraplegia type 12." *The Journal of clinical investigation* 122(2): 538–44. http://www.pubmedcentral.nih.gov/articlerender.fcgi?artid=3266795&tool=pmcentrez&rendertype=abstract (January 18, 2013).

Muqit, Miratul M K, and Mel B Feany. 2002. "Modelling neurodegenerative diseases in Drosophila: a fruitful approach?" *Nature reviews. Neuroscience* 3(3): 237–43. http://www.ncbi.nlm.nih.gov/pubmed/11994755 (January 21, 2013).

Murphy, D J. 2001. "The biogenesis and functions of lipid bodies in animals, plants and microorganisms." *Progress in lipid research* 40(5): 325–438. http://www.ncbi.nlm.nih.gov/pubmed/11470496 (January 21, 2013).

Murphy, Samantha, Sally Martin, and Robert G Parton. 2010. "Quantitative analysis of lipid droplet fusion: inefficient steady state fusion but rapid stimulation by chemical fusogens." *PloS one* 5(12): e15030. http://www.pubmedcentral.nih.gov/articlerender.fcgi?artid=3009727&tool=pmcentrez&rendertype=abstract (January 3, 2013).

Nishino, Naonobu, Yoshikazu Tamori, Sanshiro Tateya, Takayuki Kawaguchi, Tetsuro Shibakusa, Wataru Mizunoya, Kazuo Inoue, Riko Kitazawa, Sohei Kitazawa, Yasushi Matsuki, Ryuji Hiramatsu, Satoru Masubuchi, Asako Omachi, Kazuhiro Kimura, Masayuki Saito, Taku Amo, Shigeo Ohta, Tomohiro Yamaguchi, Takashi Osumi, Jinglei Cheng, Toyoshi Fujimoto, Harumi Nakao, Kazuki Nakao, Atsu Aiba, Hitoshi Okamura, Tohru Fushiki, and Masato Kasuga. 2008. "FSP27 contributes to efficient energy storage in murine white adipocytes by promoting the formation of unilocular lipid droplets." *The Journal of clinical investigation* 118(8): 2808–21. http://www.pubmedcentral.nih.gov/articlerender.fcgi?artid=2483680&tool=pmcentrez&rendertype=abstract (January 3, 2013).

Oelkers, Peter, Debra Cromley, Mahajabeen Padamsee, Jeffrey T Billheimer, and Stephen L Sturley. 2002. "The DGA1 gene determines a second triglyceride synthetic pathway in yeast." *The Journal of biological chemistry* 277(11): 8877–81. http://www.ncbi.nlm.nih.gov/pubmed/11751875 (December 10, 2012).

Orso, Genny, Diana Pendin, Song Liu, Jessica Tosetto, Tyler J Moss, Joseph E Faust, Massimo Micaroni, Anastasia Egorova, Andrea Martinuzzi, James A McNew, and Andrea Daga. 2009. "Homotypic fusion of ER membranes requires the dynamin-like GTPase atlastin." *Nature* 460(7258): 978–83. http://www.ncbi.nlm.nih.gov/pubmed/19633650 (November 2, 2012).

Ostermeyer, Anne G, Lynne T Ramcharan, Youchun Zeng, Douglas M Lublin, and Deborah A Brown. 2004. "Role of the hydrophobic domain in targeting caveolin-1 to lipid droplets." *The Journal of cell biology* 164(1): 69–78. http://www.pubmedcentral.nih.gov/articlerender.fcgi?artid=2171963&tool=pmcentrez&rendertype=abstract (November 28, 2012).

Park, Seong H, Peng-Peng Zhu, Rell L Parker, and Craig Blackstone. 2010. "Hereditary spastic paraplegia proteins REEP1, spastin, and atlastin-1 coordinate microtubule interactions with the tubular ER network." *The Journal of clinical investigation* 120(4): 1097–110. http://www.pubmedcentral.nih.gov/articlerender.fcgi?artid=2846052&tool=pmcentrez&rendertype=abstract (November 2, 2012).

Piomelli, Daniele, Giuseppe Astarita, and Rao Rapaka. 2007. "A neuroscientist's guide to lipidomics." *Nature reviews. Neuroscience* 8(10): 743–54. http://www.ncbi.nlm.nih.gov/pubmed/17882252 (January 29, 2013).

Prinz, W A, L Grzyb, M Veenhuis, J A Kahana, P A Silver, and T A Rapoport. 2000. "Mutants affecting the structure of the cortical endoplasmic reticulum in Saccharomyces cerevisiae." *The Journal of cell biology* 150(3): 461–74. http://www.pubmedcentral.nih.gov/articlerender.fcgi?artid=2175198&tool=pmcentrez&rendertype=abstract (January 21, 2013).

6. REFERENCES

Raychaudhuri, Sumana, and William A Prinz. 2008. "Nonvesicular phospholipid transfer between peroxisomes and the endoplasmic reticulum." *Proceedings of the National Academy of Sciences of the United States of America* 105(41): 15785–90. http://www.pubmedcentral.nih.gov/articlerender.fcgi?artid=2572964&tool=pmcentrez&rendertype=abstract (November 2, 2012).

Reid, E. 1997. "Pure hereditary spastic paraplegia." *Journal of medical genetics* 34(6): 499–503. http://www.pubmedcentral.nih.gov/articlerender.fcgi?artid=1050975&tool=pmcentrez&rendertype=abstract (January 18, 2013).

Reid, Evan, Mark Kloos, Allison Ashley-Koch, Lori Hughes, Simon Bevan, Ingrid K Svenson, Felicia Lennon Graham, Perry C Gaskell, Andrew Dearlove, Margaret A Pericak-Vance, David C Rubinsztein, and Douglas A Marchuk. 2002. "A kinesin heavy chain (KIF5A) mutation in hereditary spastic paraplegia (SPG10)." *American journal of human genetics* 71(5): 1189–94. http://www.pubmedcentral.nih.gov/articlerender.fcgi?artid=385095&tool=pmcentrez&rendertype=abstract (November 15, 2012).

Reiter, L T, L Potocki, S Chien, M Gribskov, and E Bier. 2001. "A systematic analysis of human disease-associated gene sequences in Drosophila melanogaster." *Genome research* 11(6): 1114–25. http://www.pubmedcentral.nih.gov/articlerender.fcgi?artid=311089&tool=pmcentrez&rendertype=abstract (November 7, 2012).

Robenek, Horst, Oliver Hofnagel, Insa Buers, Mirko J Robenek, David Troyer, and Nicholas J Severs. 2006. "Adipophilin-enriched domains in the ER membrane are sites of lipid droplet biogenesis." *Journal of cell science* 119(Pt 20): 4215–24. http://www.ncbi.nlm.nih.gov/pubmed/16984971 (November 28, 2012).

Rost, B, P Fariselli, and R Casadio. 1996. "Topology prediction for helical transmembrane proteins at 86% accuracy." *Protein science□: a publication of the Protein Society* 5(8): 1704–18. http://www.pubmedcentral.nih.gov/articlerender.fcgi?artid=2143485&tool=pmcentrez&rendertype=abstract (January 29, 2013).

Saito, Harumi, Momoka Kubota, Richard W Roberts, Qiuyi Chi, and Hiroaki Matsunami. 2004. "RTP family members induce functional expression of mammalian odorant receptors." *Cell* 119(5): 679–91. http://www.ncbi.nlm.nih.gov/pubmed/15550249 (December 10, 2012).

Savage, M J, D J Goldberg, and S Schacher. 1987. "Absolute specificity for retrograde fast axonal transport displayed by lipid droplets originating in the axon of an identified Aplysia neuron in vitro." *Brain research* 406(1-2): 215–23. http://www.ncbi.nlm.nih.gov/pubmed/2436714 (January 21, 2013).

SCHWARZ, G A, and C N LIU. 1956. "Hereditary (familial) spastic paraplegia; further clinical and pathologic observations." *A.M.A. archives of neurology and psychiatry* 75(2): 144–62. http://www.ncbi.nlm.nih.gov/pubmed/13282534 (January 18, 2013).

Schweiger, Martina, Achim Lass, Robert Zimmermann, Thomas O Eichmann, and Rudolf Zechner. 2009. "Neutral lipid storage disease: genetic disorders caused by mutations in adipose triglyceride lipase/PNPLA2 or CGI-58/ABHD5." *American journal of physiology. Endocrinology and metabolism* 297(2): E289–96. http://www.ncbi.nlm.nih.gov/pubmed/19401457 (November 28, 2012).

Silva, M C, P Coutinho, C D Pinheiro, J M Neves, and P Serrano. 1997. "Hereditary ataxias and spastic paraplegias: methodological aspects of a prevalence study in Portugal." *Journal of clinical epidemiology* 50(12): 1377–84. http://www.ncbi.nlm.nih.gov/pubmed/9449941 (January 18, 2013).

Soni, Krishnakant G, Gonzalo A Mardones, Rachid Sougrat, Elena Smirnova, Catherine L Jackson, and Juan S Bonifacino. 2009. "Coatomer-dependent protein delivery to lipid droplets." *Journal of cell science* 122(Pt 11): 1834–41. http://www.pubmedcentral.nih.gov/articlerender.fcgi?artid=2684835&tool=pmcentrez&rendertype=abstract (November 28, 2012).

Sparkes, Imogen, Nicholas Tolley, Isabel Aller, Julia Svozil, Anne Osterrieder, Stanley Botchway, Christopher Mueller, Lorenzo Frigerio, and Chris Hawes. 2010. "Five Arabidopsis reticulon isoforms share endoplasmic reticulum location, topology, and membrane-shaping properties." *The Plant cell* 22(4): 1333–43. http://www.pubmedcentral.nih.gov/articlerender.fcgi?artid=2879755&tool=pmcentrez&rendertype=abstract (November 2, 2012).

De Stefani, Diego, Anna Raffaello, Enrico Teardo, Ildikò Szabò, and Rosario Rizzuto. 2011. "A forty-kilodalton protein of the inner membrane is the mitochondrial calcium uniporter." *Nature* 476(7360): 336–40. http://www.ncbi.nlm.nih.gov/pubmed/21685888 (November 5, 2012).

Sturley, Stephen L, and M Mahmood Hussain. 2012. "Lipid droplet formation on opposing sides of the endoplasmic reticulum." *Journal of lipid research* 53(9): 1800–10. http://www.ncbi.nlm.nih.gov/pubmed/22701043 (November 26, 2012).

Suzuki, Michitaka, Yuki Shinohara, Yuki Ohsaki, and Toyoshi Fujimoto. 2011. "Lipid droplets: size matters." *Journal of electron microscopy* 60 Suppl 1: S101–16. http://www.ncbi.nlm.nih.gov/pubmed/21844583 (November 1, 2012).

Suzuki, T, A Hiroki, T Watanabe, T Yamashita, I Takei, and K Umezawa. 2001. "Potentiation of insulin-related signal transduction by a novel protein-tyrosine phosphatase inhibitor, Et-3,4-dephostatin, on cultured 3T3-L1 adipocytes." *The Journal of biological chemistry* 276(29): 27511–8. http://www.ncbi.nlm.nih.gov/pubmed/11342532 (January 21, 2013).

Targett-Adams, Paul, Doreen Chambers, Sarah Gledhill, R Graham Hope, Johannes F Coy, Andreas Girod, and John McLauchlan. 2003. "Live cell analysis and targeting of the lipid droplet-binding adipocyte differentiation-related protein." *The Journal of biological chemistry* 278(18): 15998–6007. http://www.ncbi.nlm.nih.gov/pubmed/12591929 (November 28, 2012).

Terasaki, M, L B Chen, and K Fujiwara. 1986. "Microtubules and the endoplasmic reticulum are highly interdependent structures." *The Journal of cell biology* 103(4): 1557–68. http://www.pubmedcentral.nih.gov/articlerender.fcgi?artid=2114338&tool=pmcentrez&rendertype=abstract (January 21, 2013).

Terasaki, M, and L A Jaffe. 1991. "Organization of the sea urchin egg endoplasmic reticulum and its reorganization at fertilization." *The Journal of cell biology* 114(5): 929–40. http://www.pubmedcentral.nih.gov/articlerender.fcgi?artid=2289104&tool=pmcentrez&rendertype=abstract (January 21, 2013).

Terasaki, M, N T Slater, A Fein, A Schmidek, and T S Reese. 1994. "Continuous network of endoplasmic reticulum in cerebellar Purkinje neurons." *Proceedings of the National Academy of Sciences of the United States of America* 91(16): 7510–4. http://www.pubmedcentral.nih.gov/articlerender.fcgi?artid=44431&tool=pmcentrez&rendertype=abstract (January 21, 2013).

Tian, Yuan, Junfeng Bi, Guanghou Shui, Zhonghua Liu, Yanhui Xiang, Yuan Liu, Markus R Wenk, Hongyuan Yang, and Xun Huang. 2011. "Tissue-autonomous function of Drosophila seipin in preventing ectopic lipid droplet formation." *PLoS genetics* 7(4): e1001364.

http://www.pubmedcentral.nih.gov/articlerender.fcgi?artid=3077376&tool=pmcentrez&rendertype=abstract (December 11, 2012).

Tsaousidou, Maria K, Karim Ouahchi, Tom T Warner, Yi Yang, Michael A Simpson, Nigel G Laing, Philip A Wilkinson, Ricardo E Madrid, Heema Patel, Faycal Hentati, Michael A Patton, Afif Hentati, Philippa J Lamont, Teepu Siddique, and Andrew H Crosby. 2008. "Sequence alterations within CYP7B1 implicate defective cholesterol homeostasis in motor-neuron degeneration." *American journal of human genetics* 82(2): 510–5. http://www.pubmedcentral.nih.gov/articlerender.fcgi?artid=2426914&tool=pmcentrez&rendertype=abstract (January 6, 2013).

Turró, Silvia, Mercedes Ingelmo-Torres, Josep M Estanyol, Francesc Tebar, Manuel A Fernández, Cecilia V Albor, Katharina Gaus, Thomas Grewal, Carlos Enrich, and Albert Pol. 2006. "Identification and characterization of associated with lipid droplet protein 1: A novel membrane-associated protein that resides on hepatic lipid droplets." *Traffic (Copenhagen, Denmark)* 7(9): 1254–69. http://www.ncbi.nlm.nih.gov/pubmed/17004324 (January 21, 2013).

Tusnády, G E, and I Simon. 1998. "Principles governing amino acid composition of integral membrane proteins: application to topology prediction." *Journal of molecular biology* 283(2): 489–506. http://www.ncbi.nlm.nih.gov/pubmed/9769220 (January 29, 2013).

Waterman-Storer, C M, and E D Salmon. 1998. "Endoplasmic reticulum membrane tubules are distributed by microtubules in living cells using three distinct mechanisms." *Current biology□: CB* 8(14): 798–806. http://www.ncbi.nlm.nih.gov/pubmed/9663388 (November 2, 2012).

Welte, M A, S P Gross, M Postner, S M Block, and E F Wieschaus. 1998. "Developmental regulation of vesicle transport in Drosophila embryos: forces and kinetics." *Cell* 92(4): 547–57. http://www.ncbi.nlm.nih.gov/pubmed/9491895 (January 21, 2013).

Welte, Michael A. 2009. "Fat on the move: intracellular motion of lipid droplets." *Biochemical Society transactions* 37(Pt 5): 991–6. http://www.ncbi.nlm.nih.gov/pubmed/19754438 (October 26, 2012).

West, Matt, Nesia Zurek, Andreas Hoenger, and Gia K Voeltz. 2011. "A 3D analysis of yeast ER structure reveals how ER domains are organized by membrane curvature." *The Journal of cell biology* 193(2): 333–46. http://www.pubmedcentral.nih.gov/articlerender.fcgi?artid=3080256&tool=pmcentrez&rendertype=abstract (November 1, 2012).

Wu, C C, K E Howell, M C Neville, J R Yates, and J L McManaman. 2000. "Proteomics reveal a link between the endoplasmic reticulum and lipid secretory mechanisms in mammary epithelial cells." *Electrophoresis* 21(16): 3470–82. http://www.ncbi.nlm.nih.gov/pubmed/11079566 (January 21, 2013).

Wältermann, Marc, Andreas Hinz, Horst Robenek, David Troyer, Rudolf Reichelt, Ursula Malkus, Hans-Joachim Galla, Rainer Kalscheuer, Tim Stöveken, Philipp von Landenberg, and Alexander Steinbüchel. 2005. "Mechanism of lipid-body formation in prokaryotes: how bacteria fatten up." *Molecular microbiology* 55(3): 750–63. http://www.ncbi.nlm.nih.gov/pubmed/15661001 (December 6, 2012).

Zhao, X, D Alvarado, S Rainier, R Lemons, P Hedera, C H Weber, T Tukel, M Apak, T Heiman-Patterson, L Ming, M Bui, and J K Fink. 2001. "Mutations in a newly identified GTPase gene cause autosomal dominant hereditary spastic paraplegia." *Nature genetics* 29(3): 326–31. http://www.ncbi.nlm.nih.gov/pubmed/11685207 (November 20, 2012).

Zhou, Linkang, Li Xu, Jing Ye, De Li, Wenshan Wang, Xuanhe Li, Lizhen Wu, Hui Wang, Feifei Guan, and Peng Li. 2012. "Cidea promotes hepatic steatosis by sensing dietary fatty acids." *Hepatology (Baltimore, Md.)* 56(1): 95–107. http://www.ncbi.nlm.nih.gov/pubmed/22278400 (January 21, 2013).

Züchner, Stephan, Gaofeng Wang, Khanh-Nhat Tran-Viet, Martha A Nance, Perry C Gaskell, Jeffery M Vance, Allison E Ashley-Koch, and Margaret A Pericak-Vance. 2006. "Mutations in the novel mitochondrial protein REEP1 cause hereditary spastic paraplegia type 31." *American journal of human genetics* 79(2): 365–9. http://www.pubmedcentral.nih.gov/articlerender.fcgi?artid=1559498&tool=pmcentrez&rendertype=abstract (January 18, 2013).

ACKNOWLEDGEMENTS:

My warm thanks are due to Prof. M.L.MOSTACCIUOLO for her support and guidance during this three years. I owe my most sincere gratitude to my co-supervisor Genny Orso who gave me the opportunity to work with her. Thanks to Andrea Daga for his valuable advices and friendly help

Thanks to Andrea Daga's laboratory; I wish to extend my warmest thanks to all those who have helped me with my work, in particularly to Mariagiulia Battaglia.

I owe my loving thanks to my family (my father and mother, Namik and Haneme, my brothers and sisters Migert, Anita, Sonila, Nestor) for their encouragement and support.